Instytut Podstawowych Problemów Techniki

Polska Akademia Nauk

Marta Gruca

Motion of regular systems of many particles interacting hydrodynamically under gravity

rozprawa doktorska

Promotor rozprawy

prof. dr hab. Maria Ekiel-Jeżewska

Instytut Podstawowych Problemów Techniki

Polskiej Akademii Nauk

Warszawa 2016

Oświadczenie autora rozprawy

Oświadczam, że niniejsza rozprawa została napisana przeze mnie samodzielnie.

data   podpis autora rozprawy

Oświadczenie promotora rozprawy

Niniejsza rozprawa jest gotowa do oceny przez recenzentów.

data   podpis promotora rozprawy

Praca ta jest dla mnie szczególnie ważna.
W całości dedykuję ją mojej Mamie.

Parts of the results presented in this thesis have been published in:

M. Gruca, M. Bukowicki, M. L. Ekiel-Jeżewska, "Periodic and quasiperiodic motions of many particles falling in a viscous fluid", *Physical Review E*, **92**, p.023026 (2015).

Streszczenie

Cząstki opadające w płynie oddziałują między sobą hydrodynamicznie, co prowadzi do złożonych i nieliniowych efektów nawet przy znacznie mniejszej od jedności liczbie Reynoldsa, gdy równania ruchu płynu są liniowe. W przypadku opadającej kropli zawiesiny cząstki cyrkulują po orbitach kwaziperiodycznych, a grupa pozostaje stabilna przez długi czas, zanim ulegnie deformacji i rozpadowi.

Przedmiotem tej rozprawy jest pogłębiona analiza ruchów periodycznych regularnych układów cząstek, opadających grawitacyjnie w lepkim płynie, które przejawiają pewne właściwości ruchów kwaziperiodycznych występujących w opadającej kropli zawiesiny. Dla układów chaotycznych składających się z mniejszej liczby cząstek zostało udowodnione, że długotrwałe interakcje pomiędzy cząstkami są związane z istnieniem stabilnych lub niestabilnych rozwiązań periodycznych. To, czy podobnie jest w przypadku opadającej kropli zawiesiny (układ chaotyczny) jest obecnie przedmiotem dyskusji. Istotnym wkładem do tej dyskusji jest identyfikacja i analiza rozwiązań periodycznych dla dużych grup cząstek, której podjęto się w tej rozprawie. Ważną przyczyną zainteresowania tym aspektem dynamiki również jest fakt, że rozwiązania okresowe stanowią układy modelowe, pozwalając na skuteczną analizę teoretyczną zjawisk zachodzących w rzeczywistych, bardziej złożonych układach.

W rozprawie przedstawiono dwa układy wykonujące ruchy periodyczne: układ dwóch pierścieni cząstek i układ czterech pierścieni. Pierścienie umieszczone się w płaszczyznach poziomych, a ich środki znajdują się nad sobą. Układy określone są przez liczbę cząstek oraz odpowiednio 1 i 3 zmienne opisujące konfigurację początkową. Główna część wyników dotyczy bardziej złożonego, 4-pierścieniowego układu. Zostały dla niego znalezione 3 główne typy ruchów periodycznych, z czego dwa typy nie mają odpowiednika w znanych wcześniej rozwiązaniach periodycznych w układzie dwóch pierścieni. Cechą szczególną układu czterech pierścieni jest bogata dynamika kwaziperidyczna, z szerokim spektrum parametrów, dla których grupa cząstek pozostaje razem przez długi czas. Jest to element wspólny z dynamiką opadającej kropli zawiesiny. W

niniejszej rozprawie pokazano, że układ jest bardzo wrażliwy na warunki początkowe, zarówno pod względem czasu rozpadu grupy cząstek, jak i typu tego rozpadu - mamy do czynienia ze zjawiskiem chaotycznego rozpraszania. Badanie czasu rozpadu grupy wymagało wprowadzenia nowego kryterium rozpadu, które wydaje się być bardziej adekwatne niż często stosowane w literaturze kryterium oparte na odległości. Nowe kryterium może być stosowane w różnych typach układów, w których obserwujemy względne oscylacje cząstek. Układy dwóch oraz czterech pierścieni zostały kompleksowo przebadane dla różnych liczb cząstek oraz geometrii układu (stopnia „spłaszczenia"), co pozwoliło stwierdzić ogólność otrzymanych wyników, a także określić zależność otrzymanych wyników od warunków początkowych. Rozwiązania periodyczne zostały znalezione dla szerokiego zakresu warunków początkowych. Dla układów zbyt płaskich, zbyt rozciągniętych w pionie lub ze zbyt małą liczbą cząstek ruchy periodyczne nie są obserwowane. Efekt ten idzie w parze ze zmniejszającym się zakresem parametrów, dla których obserwowane są ruchy kwaziperiodyczne.

Oprócz zbadania dynamiki cząstek w płynie Stokesa, rozprawa zawiera również analizę ruchów periodycznych w ośrodku przepuszczalnym (płyn z wtrąceniami stałymi). Dynamika płynu w takim ośrodku opisywana jest za pomocą równań Brinkmana-Debye–Büche. W pracy pokazano, że przy dużym współczynniku przepuszczalności istnieją ruchy periodyczne, zaś mała wartość współczynnika przepuszczalności jakościowo zmienia dynamikę układu - grupa cząstek może opadać wolniej niż pojedyncza cząstka. Mała wartość współczynnika przepuszczalności prowadzi do braku rozwiązań periodycznych zarówno w układzie czterech, jak i dwóch pierścieni. W przypadku układu czterech pierścieni wraz ze zmniejszaniem się współczynnika przepuszczalności długotrwałe ruchy kwaziperiodyczne są obecne dla zawężającego się zakresu parametrów początkowych.

Wyniki rozszerzono o analizę ruchu płynu wokół cząstek wykonujących ruchy periodyczne, zarówno w płynie Stokesa, jak i w ośrodku przepuszczalnym. Określono przy jakich warunkach płyn cyrkuluje wewnątrz opadającej grupy cząstek, a w jakich przepływa przez jej środek. Wykazano, że układ czterech pierścieni lepiej oddaje dynamikę opadającej kropli zawiesiny niż układ dwóch pierścieni.

Abstract

Particles settling in the fluid interact hydrodynamically what leads to complex, non-linear effects, even at Reynolds number much smaller than unity, when equations of fluid motion are linear. In case of settling suspension drop, particles circulate quasi-periodically and the group stays together for a long time before it deforms and destabilises.

The aim of this dissertation is an in-depth analysis of periodic motions in regular systems of particles, falling under gravity in a viscous fluid, which exhibit some properties analogous to quasipriodic motions in suspension drop. In chaotic systems consisting of a few particles, it is known that long-lasting interactions between particles are associated with existence of stable or unstable periodic solutions. The question if this association is valid also for drop of suspension (chaotic system) is currently discussed. A significant contribution to this discussion is identification and analysis of periodic motions of larger numbers of particles, what is the subject of this dissertation. An important reason for focusing on this aspect of dynamics is also the fact that periodic solutions are used as model systems, allowing for effective theoretical analysis of behaviour of more complex systems.

In this dissertation two configurations preforming periodic motions are introduced: system of two rings of particles and system of four rings, with 2 and 4 parameters, respectively. The rings are oriented horizontally and their centres are placed one above the other. The main part of results concerns more complex, 4-rings system. In this work three main types of periodic solutions were found, and two of them do not have an analogue in already known solution in the system of two rings. Specific feature of 4-rings system is rich quasiperiodic dynamics with broad spectrum of parameters for which particles stay together for a long time. Similar behaviour is observed for a settling drop of suspension. In this dissertation it is shown that the dynamics of presented system is very sensitive to initial configuration, both in terms of time and type of decay: chaotic scattering is observed. Investigation of time of decay required developing new criterion

of decay which seems to be more adequate than often used distance-based criterion. New criterion can be used in various types of systems where relative oscillations of particles take place. Systems of 2 and 4 rings had been comprehensively studied for different number of particles and different geometry of the configuration what allowed to confirm generality of obtained results and to specify their dependence on initial conditions. For wide range of initial conditions periodic motions were discovered. In too flat systems, or those too wide, periodic motions are not observed. This effect is accompanied by shrinking range of initial parameters for which quasiperiodic motions are observed.

Apart from analysis of dynamics in Stokes fluid, the dissertation includes also study of dynamics in permeable medium, where the fluid motion is described by Brinkman-Debye–Büche (BDB) equations. In the dissertation is shown that at high permeability periodic motions exist, while at low permeability coefficient there is a qualitative change of dynamics: group of particles can settle slower than a single one. Small value of permeability coefficient leads to lack of periodic solutions, both in systems of 2 and 4 rings. In case of 4-rings system, long-lasting quasiperiodic motions can be observed in shrinking range of initial parameters when the permeability coefficient is reduced.

Results described above were supplemented with analysis of fluid dynamics around the particles performing periodic motions, both in Stokes fluid and in permeable medium. It was determined under what conditions fluid circulates inside a group of particles and when does it stream through the middle of the group. It was shown that system of 4 rings better reflects dynamics of suspension drop than does the system of 2 rings.

Contents

Chapter 1

Introduction

1.1 Background and motivation

Dynamics of fluid is described with nonlinear Navier-Stokes equations [1]. When the value of Reynolds number is very low ($Re << 1$) and the fluid is incompressible, equations simplify to linear Stokes equations. Their features are: instantaneous relaxation of fluid velocity and time-reversibility of the flow [1–3]. Very small Reynolds number means that characteristic time scale of particle velocity relaxation is much smaller than the characteristic advective time scale (given by the ratio of particle velocity to its size). Additionally, particles considered in this dissertation do not perform Brownian motions [1] what means that the Péclet number is much greater than unity ($Pe >> 1$, Péclet number is given by the ratio of time scale related to Brownian motions and the advective time scale). Assumptions described above apply to the whole thesis.

In Stokes fluid, when a particle exerts force on the fluid, it effects in influence on velocities of other particles (present in the fluid). This mechanism is called hydrodynamic interactions. Hydrodynamic interactions are nonlinear and long-rage: in bulk they decay with distance r between particles positions as $1/r$. In general hydrodynamic interactions do not follow superposition principle. In case of point model of particles (which accurately describes dynamics of particles of arbitrary shape if they are separated widely enough) the superposition principle holds.

Since Reynolds number can be small for different size scales, the Stokes equations describe fluid dynamics in various size scales. In macro-scale they describe fluid in such

systems as e. g motion of bubbles in magma [4, 5] and millimetre-size beads in silicon oil or glycerine[6, 7]; in mezoscale micrometer objects moving in water [8, 9]. They can be also applied to fluid with Brownian particles, such as dynamics of nanomechanisms [10] as well as in interactions between proteins [11] and parts of a single protein [12, 13]. In the last three examples Brownian motions contribute significantly to the dynamics.

An important system, where hydrodynamic interactions play a crucial role, is sedimentation of groups of particles or suspensions [14–17]. In medicine many-particle dynamics is present e.g. in the erythrocyte sedimentation rate (ESR) assay [18, 19], [20], where the settling time of red blood cells is measured. Sedimentation of solid impurities and ascent of bubbles are common problems in many industrial processes [21–25]. In nature similar properties are observed e.g. in group of microorganisms [26–28] and already mentioned bubbles in magma [4, 5].

An interesting system is sedimentation of a suspension drop. Dynamics of this system has been studied numerically and experimentally [29–33]. During the settlement of such drop, particles of suspension circulate along quasiperiodic orbits over a long time [29, 30]. Trajectories of particles closely resemble streamlines inside settling drop of a heavier fluid [30]. During the settlement some of the particles detach from the rest of the group and form characteristic 'tail' above the drop. Over time the drop gradually deforms from initially spherical shape and it becomes more and more flat. In effect it forms an expanding torus which subsequently destabilises and decays into two or three subgroups of particles. Although the process of expansion of settling group of particles could be caused by non-negligible inertia [34–36] this mechanism was proved to not be the only factor responsible for observed behaviour, since the expansion of a suspension drop can be restored in simulations with non-inertial particles at $Re = 0$. Investigations of evolution of settling suspension drop have shown, that the process of formation of torus and subsequent destabilisation of the group is very sensitive to initial conditions, i. e. random configuration of particles at the beginning of the simulation [33, 37]. Different initial configurations result in decay into 2 or 3 subgroups, while differences in destabilisation time can by of the orders of magnitude [37]. Some authors [33] claim, that destabilisation of torus coincides with the moment when fluid starts to flow up through the middle of the torus. Another explanation of the drop break-up [38] is related to existence of periodic and quasiperiodic orbits: if the particles are close to the periodic orbits, they stay together for a longer time and the drop does not break up. This idea [38] is a starting point of this thesis.

A reference point for many studies on hydrodynamically interacting particles is the article by Janosi et. al [39], where authors investigated motion of three settling point

particles located in a vertical plane ($y = 0$). Despite of conceptually simple system, this study allowed for deeper understanding of dynamics of hydrodynamically interacting particles, where interesting, complex collective effects are observed [40–46]. In their study [39], authors analysed dynamics of a system, where initial positions of two particles are established, while initial position of the third particle is changed. It allowed to create 2-dimensional maps, where for each initial position of the third particle given properties of dynamics were indicated. The studied quantities were: interaction time of the whole group and label of particle which lags behind after decay of the triplet, what is shown in Figure 1.1 reprinted from [39]. It turned out that regions where dynamics is similar (similar time of decay in Fig. 1.1B or the same type of decay in Fig. 1.1A) have fractal form. For some regions behaviour of the system is deterministic - group of particles decays in a certain way, low sensitivity to change of initial conditions is observed - but for many parameters particles interact for a long time and exact time and type of decay is very sensitive to initial conditions: chaotic scattering is observed. Authors suggest that: '[irregularity in time and type of decay] is due to an underlying invariant chaotic saddle which is a globally non-attracting set, and cannot be reached exactly. Particles, however, can come arbitrarily close to it and exhibit chaotic motion before escaping' [39]. Authors explain that observed chaotic saddle contains infinite number bounded trajectories among which it is generally believed that infinite number of unstable periodic orbits exist [39, 47]. Analysis performed in the discussed study shows, that the dynamics of even small group of sedimenting particles leads to complex chaotic effects.

Periodic solutions are studied in many areas of micro-hydrodynamics (not only in gravitational field). Classic example are Jefferys's orbits [48]: periodic solutions for rigid, axisymmetric ellipsoid in shear flow. Later it was shown, that the solution is valid for any axisymmetric shape with fore-aft symmetry [49]. Jeffery's orbits were starting point for investigation of dynamics in modified systems: slightly broken axisymmetry [50–52], curvature of the rod [53] or non-negligible inertia leads to quasiperiodic motions, related to Jeffery's orbits. Another important application of Jeffery's orbits is dynamics of an elastic fibre in flow [54–59] which has great application potential due to rapid development and promising perspectives for microfluidic devices [60, 61]. Due to their importance in understanding of the dynamics, periodic and close to periodic motions are commonly studied in various system, such as interactions between particles in micro-channel [62], pair of micro-rotors [63] or particles in a rotating drum [64]. The phenomena of periodic motions is often discussed in context of self-assembly of particles [10, 62, 65] which is an intensively studied issue because of its importance in

nanotechnology [66] and medicine [67].

Periodic motions in groups of particles settling under gravity were investigated theoretically and experimentally. The smallest system which exhibit nontrivial behaviour is system of three particles. Hocking [68], Caflisch [69] and Jayaweera et al.[34] have shown, that initially configuration where three particles are placed at vertexes of isosceles triangle leads to periodic motions - in special case of equilateral triangle particles settle down without change of configuration. For system of three particles a conservation law was recognised [68]: given that gravity acts along z axis, the area of a triangle obtained by projection of particles positions on xy plane, remains constant. It was a starting point for theoretical analysis of stability [70] which revealed existence of infinite number of periodic solutions and stability of periodic orbits, what confirmed prior numerical [69] and experimental [34, 71] studies.

In systems of 4 particles three types of periodic solutions have been found. In the first one, particles initially are placed in vertexes of horizontal rhombus [72]. The second type may be considered as a generalisation of the first one: initial configuration is a horizontal kite [73]. In case of kite configuration, period of the motion can be very long because it consists of large number of oscillations (defined as crossing up of i-th particle through the horizontal plane containing centre of mass of the system). For rhombus configuration period consists of only one oscillation. Research conducted by Bargieł et al. [73] have shown that periodic solutions may have long and complex trajectory. The same conclusion was postulated by Janosi et al. [39] although in the latter system periodic solutions, if exist, are unstable and thus could not be observed. In case of 4 particles in kite configurations periodic solutions were captured in numerical simulations. The third type of periodic motions of 4 particles was described by Hocking [68]: in the initial configuration particles are placed at vertexes of a vertical rectangle.

The results for periodic or close to periodic motions have been extended to the system consisting of larger number of particles, analogous to those described above. To obtain such systems, in place of single particles (in systems of triangle, rhombus and deltoid) a pair of sticking particles was set. These systems perform quasiperiodic motions with complex trajectories [74].

As a separate case one can consider a system consisting of particles placed in vertexes of horizontal polygon. Such systems were experimentally investigated by Jayaweera et. al [34]. This configuration settles under gravity in the Stokes fluid without change of shape - polygon expansion may occur due to nonzero inertia of particles in the system [34]. Experimental studies [34] as well as analytical calculations [75]
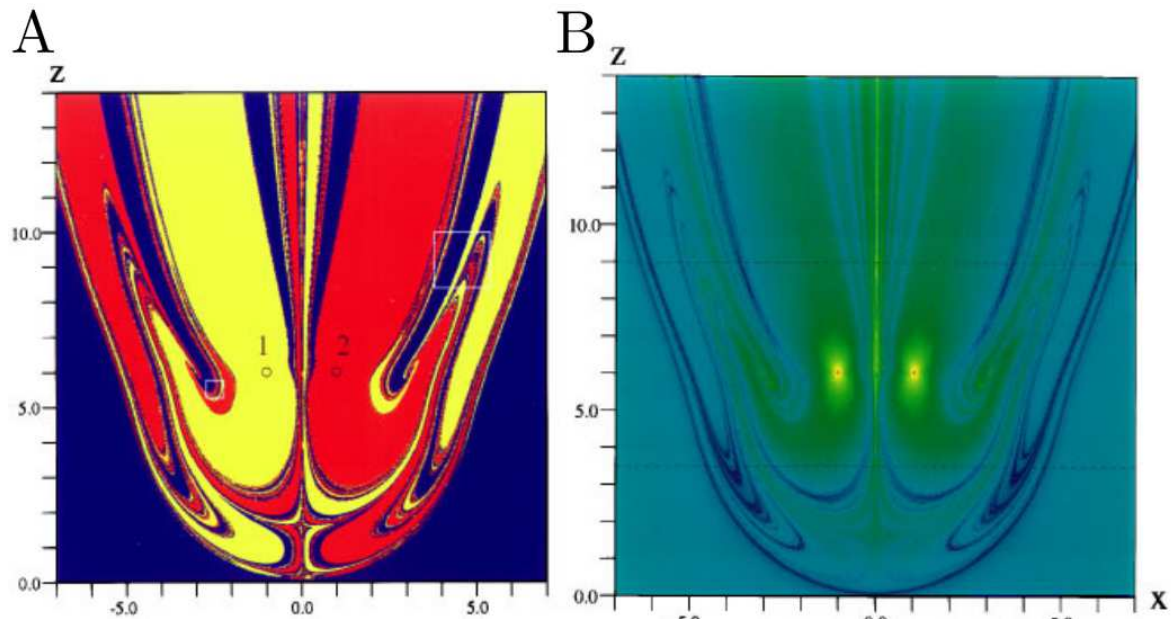
Figure 1.1: The system of 3 point-particles settling under gravity; initial positions of two particles are denoted in the left. Colours represent features of dynamics observed for different (x, z) initial positions of the third particle. A) Colour indicates which particle lags behind the other two after the decay: red - first particle, yellow - second particle and blue - third particle. B) Interaction time, colour scale from red by yellow, green, blue to violet indicate increasing interaction time, with the maximum reaching maximal simulation time. Reprinted from [39].

show, that the system is stable for the number of particles not larger than 6. In case of larger number of particles the system destabilises and breaks up due to non-symmetric perturbations.

The periodic dynamics of particles initially placed at the vertexes of a cube was first studied by Durlofsky and Brady [76]. More general case of initial configuration at vertexes of a prism was investigated by Ekiel-Jeżewska [38]. Numerical simulations and theoretical analysis revealed the existence of unstable periodic solutions and long phase of quasi-periodic motion after the breakage of symmetric configuration. Similar periodic dynamics has also been found (both theoretically and experimentally) in the system of rigid elongated particles, placed initially at the vertical edges of a prism [77].

Although the dynamics of system consisting of a low number of particles under constant external force has been already analysed theoretically [78], in the case with a large number of particles many questions appear. Do systems of large number of particles (of the order of thousands, tens of thousands) in regular configurations perform periodic motion? What classes of periodic motions can be found for more complex

initial configurations? How does the presence of additional particles influence the periodic dynamics and evolution of such system? Do the decay times of regular and irregular groups depend on the existence or lack of periodic and quasi periodic orbits? The mechanism of decay and the influence of periodic solution on the decay time still remain unknown. Also the questions about transition to chaos remain open in the problem of many-particle, regular systems, as described in previous paragraphs.

The first approach to answer these key questions was the article by Ekiel-Jeżewska [38]. In this paper the dynamics of a system of a small number of particles initially placed at the vertexes of a prism (the system of 2 'rings'), settling under gravity was analysed. The results showed that for such cluster there occurs relative periodic motion of particles, induced by the hydrodynamic interactions between them. The introduced system of 2 rings is interesting also because of the fact, that exhibits a certain properties of the settling drop of suspension. In both system we observe circulation of particles, destabilisation and sensitivity to small change of initial conditions. One may hypothesise, that in case of suspension drop the particles are left behind and form a 'tail', while moving away too much from periodic orbits, e.g. as a result of random perturbations [38]. In [38] it has been shown, that additional particles above the main group of particles (analogue of a tail in suspension drop) lead to extension and flattening of the main group of particles (analogue of deformations of spherical suspension drop). In this thesis the problem of analysis of modified system of 2 rings was raised, in order to obtain fluid motion around periodic orbits more similar to fluid motion around sedimenting suspension drop (the system is described in Chapter 2).

Another important issue linked to the dynamics of a settling group of particles is the motion of the fluid surrounding the particles [32, 33]. We know that in case of suspension drop relatively large amount of fluid is dragged inside it together with particles: to what extent does it happen in regular configurations of particles? Do we observe similar pattern or rather the fluid would stream through the group, without circulation?

This problem is important due to its significance for exchange between fluid circulating inside group of particles and fluid from outside the group. If fluid circulates together with particles (closed streamlines in centre of mass reference frame) its exchange with fluid outside the drop is reduced. This may lead to long-range transport of some amount of fluid inside the settling group of particles, without mixing with external fluid. Potentially this mechanism can provide exchange of small, yet concentrated portions of fluid between layers of fluid, e. g. of different composition. Shape

of streamlines in centre of mass reference frame may be also interesting due to the fact that according to some authors [33] in suspension drop fluid starts to stream up through the group of particles when the destabilisation of the group of particles occurs. The analysis of fluid motion around the settling group of particles will be the other aspect of this thesis.

Because of increasing interest in dynamics of groups of particles in permeable medium [79–84], this thesis will also contain analysis of regular groups of sedimenting particles in permeable medium. A model of such a medium is the fluid dynamics is described by Brinkman-Debye-Bueche equations (BDB) [76, 85]. In this dissertation an influence of medium permeability on the existence of periodic motions and shape of periodic trajectories has been studied, both in the system of 2 rings and its modification. Additionally, fluid motion around the particles has been investigated.

1.2 Outline of the thesis

This thesis has been divided and reported in 10 chapters and 3 appendices. The outline of the thesis is as follows:

Chapter 1 presents the background and motivation of this work. The literature review in topic of sedimentation at low Reynolds number and its applications are presented. Also the state of art in periodic motions is described. The main open questions which were the motivation of this thesis are formulated.

Chapter 2 introduces the theoretical background: dynamics of point-particles in a viscous fluid including numerical method and basic solution of fluid motion for Hadamard-Rybczyński drop. We also discuss other models of particle dynamics, and justify the selected model. Additionally the comparison between regular polygon made of point-particles and continuous ring is presented.

Chapter 3 presents the symmetrized dynamics of 2-ring system (system of 2 identical regular polygons placed in two horizontal planes) with detailed introduction of the system, initial configuration and parameters. Conditions required for periodic motions are discussed. Dependence of trajectory shape and period time on system parameters is presented.

In Chapter 4 dynamics of fluid around periodic solutions from Chapter 3 is analysed. Shape of fluid drop dragged with particles is discussed. Analysis includes evolution of fluid motion during the period and results for the systems with different parameters.

Chapter 5 presents dynamics of 2-rings system in permeable medium. Equations of motion for point-particles in the Brinkmana-Debye–Büche medium are introduced, differences with respect to the Stokes fluid are discussed. Analysis of a single ring of particles is analysed. Influence of permeability of the medium on existence of periodic motions and trajectory shape is presented. Additionally, fluid motion around particles is shown.

In Chapter 6 dynamics of 4-rings system is analysed. Using large number of simulations, maps showing features of system dynamics for different initial configurations are created. Interaction time and type of decay of the group are determined. Signs of chaotic scattering in 4-rings system dynamics are described. The thickness of quasiperiodic trajectories is analysed quantitatively and periodic solutions are found. Dependence of periodic solutions on system parameters is investigated.

Chapter 7 presents dynamics of fluid around periodic solutions in 4-rings system. Similarly as in Chapter 4, special attention is paid to size and shape of fluid drop dragged with particles.

In Chapter 8 dynamics of 4-rings system in permeable medium is analysed. Existence of periodic solutions for different permeability coefficient is investigated. Fluid motion around the particles is analysed.

Chapter 9 presents comparison between dynamics with- and without reduction of number of degrees of freedom owing to system symmetries. Destabilisation time in non-symmetrized dynamics is discussed.

Chapter 10 contains summary of main results presented in the dissertation. Original elements of the thesis are emphasised and directions of future studies are proposed.

Three appendices contain supplement, in-depth analysis of the following topics:

- Appendix A: Fluid motion around periodic orbits of the particles in the system of 2 and 4 rings.

- Appendix B: Periodic solutions with complex trajectories.

- Appendix C: Detailed comparison of symmetrized and non-symmetrized dynamics.

Chapter 2

The system of many particles falling under gravity in a viscous fluid

2.1 Particles motion

2.1.1 Point-particle dynamics

In this work, the model system is a regular group of particles settling under gravity in low-Reynolds number regime. The model analysed here was presented in an article by Gruca et. al [86]. The total external force acting in the system is gravity $\boldsymbol{G}$. The system consists of a group of M particles settling under identical gravitational forces $\frac{\boldsymbol{G}}{M}$ in a fluid of viscosity η. Since the size of particles is assumed to be small, point-particle approximation is used. The fluid velocity $\boldsymbol{v}$ and pressure p satisfy the Stokes equations,

$$\eta\nabla^2\boldsymbol{v}(\boldsymbol{r}) - \nabla p(\boldsymbol{r}) = -\frac{1}{M}\sum_{i=1}^{M}\boldsymbol{G}\,\delta(\boldsymbol{r}-\tilde{\boldsymbol{r}}_i), \tag{2.1}$$

$$\nabla\cdot\boldsymbol{v}(\boldsymbol{r}) = 0. \tag{2.2}$$

where M is the number of particles, $\tilde{\boldsymbol{r}}_i$ denotes the position of the particle with label i, and the z-axis is chosen along gravity, with $\boldsymbol{G} = -G\hat{\boldsymbol{z}}$ where $G > 0$ and $\hat{\boldsymbol{z}}$ is the unit vector along the z-axis. The equations are written in the laboratory frame of reference.

The fluid velocity $\boldsymbol{v}(\boldsymbol{r})$ and pressure $p(\boldsymbol{r})$ are given by

$$\tilde{\boldsymbol{v}}(\boldsymbol{r}) = \frac{1}{M}\sum_{i=1}^{M}\boldsymbol{T}(\boldsymbol{r}-\tilde{\boldsymbol{r}}_i)\cdot\boldsymbol{G}, \tag{2.3}$$

$$\tilde{p}(\boldsymbol{r}) = \frac{1}{M}\sum_{i=1}^{M}\boldsymbol{P}(\boldsymbol{r}-\tilde{\boldsymbol{r}}_i)\cdot\boldsymbol{G}, \tag{2.4}$$

with the Green tensors,

$$\boldsymbol{T}(\boldsymbol{R}) = \frac{1}{8\pi\eta R} \left(\boldsymbol{I} + \frac{\boldsymbol{R} \otimes \boldsymbol{R}}{R^2} \right), \tag{2.5}$$

$$\boldsymbol{P}(\boldsymbol{R}) = \frac{\boldsymbol{R}}{4\pi R^3}, \tag{2.6}$$

where $R = |\boldsymbol{R}|$.

The equations of motion of the particles are given by

$$\frac{d\tilde{\boldsymbol{r}}_i}{dt} = \frac{1}{M} \sum_{j \neq i}^{M} \boldsymbol{T}(\tilde{\boldsymbol{r}}_{ij}) \cdot \boldsymbol{G} + \mathbf{u}_0 \tag{2.7}$$

where $\tilde{\boldsymbol{r}}_{ij} = \tilde{\boldsymbol{r}}_i - \tilde{\boldsymbol{r}}_j$, and

$$\mathbf{u}_0 = \boldsymbol{G}/(6M\pi\eta a_p) \tag{2.8}$$

is the Stokes velocity of the isolated particle, with a_p equal to the radius of a single particle. It is convenient to choose the inertial frame of reference moving with the velocity $\mathbf{u}_0$. The benefit is that in this frame the dynamics is independent of the additional length scale a_p. From now on, we use dimensionless variables, based on an initial size of the group d as the length unit, and $G/(8\pi\eta d)$ as the velocity unit. Therefore, $8\pi\eta d^2/G$ is the time unit. From now on, $\boldsymbol{r}_i = \tilde{\boldsymbol{r}}_i/d$ denotes the dimensionless position of a particle i. Later on all dimensionless quantities we will denote without tilde.

After normalisation presented above the fluid velocity (2.3) around particles takes the form:

$$\boldsymbol{v}(\boldsymbol{r}, t) = -\frac{1}{M} \sum_{i=1}^{M} \frac{1}{(r - r_i(t))} \left(\boldsymbol{I} + \frac{(\boldsymbol{r} - \boldsymbol{r}_i(t)) \otimes (\boldsymbol{r} - \boldsymbol{r}_i(t))}{(r - r_i(t))^2} \right) \hat{\boldsymbol{z}} \tag{2.9}$$

2.1.2   System and dynamics of many particles

Following Gruca et al. [86] let us consider the systems consisting of two or four horizontally placed regular polygons, with a particle at each vertex (for the scheme of the systems see Figs. 3.1 and 6.1). From now on the polygons will be referred as 'rings' due to their shape. Each of K rings consists of equal number of particles N, so that the total number of particles in the system $M = KN$.

Because of the system symmetry, the cylindrical coordinates will be used, as the most convenient. The position of particle i is denoted as $\boldsymbol{r}_i = (\rho_i, \phi_i, z_i)$.

Previous studies have shown [38], that even initially axially-symmetric group of particles can be quickly destabilised and destroyed by non-symmetric numerical perturbations, what provides difficulties in determining the period. To avoid these difficulties, the symmetrization of the dynamics is introduced. More precisely, in terms of constraints it implies that the azimuthal components of the particle velocities are forced to vanish, with $\phi_i = \mathrm{const}(t)$ for $i = 1, ..., M$.

We use the labelling $i = K(n - 1) + k$, with $n = 1, ..., N$ denoting the number of particle in the ring, and $k = 1, ..., K$ denoting number of the ring. Then the azimuthal coordinate of i-th particle is given by:

$$\phi_{K(n-1)+k} = \frac{2\pi(n - 1)}{N},\tag{2.10}$$

and both radial and vertical coordinates of the particles from the same ring k are the same:

$$\rho_{K(n-1)+k} = \rho_k,\tag{2.11}$$

$$z_{K(n-1)+k} = z_k,\tag{2.12}$$

for $n = 1, ..., N$ and $k = 1, ..., K$.

Due to symmetrization we reduce the system of $3M$ equations (2.7) to the system of $2K$ equations for ρ_l and z_l, with $l = 1, ..., K$. As in the published study [86] the system of equations takes the form,

$$\frac{d\rho_l}{dt} = -\frac{1}{M} \sum_{k=1}^{K} \sum_{n=1}^{N} (1 - \delta_{kl}\delta_{n1}) \frac{(z_k - z_l) \left[\rho_k \cos\left(\frac{2\pi(n-1)}{N} \right) - \rho_l \right]}{R_{lkn}^3},\tag{2.13}$$

$$\frac{dz_l}{dt} = -\frac{1}{M} \sum_{k=1}^{K} \sum_{n=1}^{N} (1 - \delta_{kl}\delta_{n1}) \left(\frac{1}{R_{lkn}} + \frac{(z_k - z_l)^2}{R_{lkn}^3} \right),\tag{2.14}$$

$$R_{kln}^2 = (z_k - z_l)^2 + \rho_l^2 + \rho_k^2 - 2\rho_l\rho_k \cos\left(\frac{2\pi(n - 1)}{N} \right).\tag{2.15}$$

In Section 3 and 4 we consider evolution of configuration for $K = 2$, what means with two rings. Configuration with $K = 4$ rings has been investigated in study of Gruca *et al.* [86] and in Section 6.

2.1.3   Numerical implementation of the model

Identically as in the work by Gruca *et al.* [86] the numerical integration of Eqs. (2.13)-(2.15) is based on two methods: the fourth-order adaptive Runge-Kutta for

non-stiff problems and backward differentiation formula (BDF) for stiff problems. The system of ordinary differential equations is solved using lsoda from the FORTRAN library odepack. Initially the calculations start with non-stiff solver. Depending on number of time steps and accuracy the solver switches between method appropriate for stiff or non-stiff problem. This procedure is a standard and commonly used method for solving differential equations. The numerical calculations were performed with double precision and the error per each time step is not greater than 10^{-12}.

Since the main goal of this study is the analysis of relative motion of particles, it is convenient to trace their positions in the centre-of-mass frame of reference, located at the symmetry axis, $\boldsymbol{r}_{CM} = (0, 0, z_{CM})$ with

$$z_{CM} = \frac{1}{M} \sum_{i=1}^{M} z_i \qquad (2.16)$$

In this frame, ρ_i and ϕ_i are the same as in the laboratory frame, and particle vertical coordinates are $Z_i = z_i - z_{CM}$.

2.2 Fluid motion

2.2.1 Streamlines and fluid velocity field for the Hadamard-Rybczyński solution

The motion of fluid around sedimenting group of particles has great significance for transport and fluid mixing: portions of fluid may travel long distances circulating within the drop, with limited mixing with external fluid. It this subsection we present brief summary of Hadamard-Rybczyński solution for sedimenting drop of fluid. Later, it will serve as a reference point in analysis of fluid dynamics around sedimenting group of particles, performing periodic oscillations (discussed in Sections 3 and 6). The existing analogy between streamlines and velocity field will be discussed in Sections 4 and 7.

Now, let us follow Kim & Karrila[3] and consider a spherical drop of fluid with radius a and fluid viscosity μ_{in} which is moving with velocity U in infinite fluid of viscosity μ_{out}. Such a drop moves if $\rho_{in} \neq \rho_{out}$, where ρ_{in} is the fluid density inside the drop, and ρ_{out} fluid density outside the drop. There are no external forces except of gravity:

$$\boldsymbol{F} = \frac{4}{3}\pi a^3 \boldsymbol{g}(\rho_{in} - \rho_{out}), \qquad (2.17)$$

where $\boldsymbol{g}$ is the gravitational acceleration. We will denote: $F = |\boldsymbol{F}|$. It is assumed that the Reynolds number satisfies: $Re \ll 1$.

For the spherical drop of fluid the Stokes equations for the fluid velocity field $\boldsymbol{u}$ and pressure π take the form:

$$\eta \nabla^2 \boldsymbol{u}(\boldsymbol{r}) - \nabla \pi(\boldsymbol{r}) = 0, \tag{2.18}$$

$$\nabla \cdot \boldsymbol{u}(\boldsymbol{r}) = 0, \tag{2.19}$$

with boundary conditions in the spherical system of coordinates (such that $-\hat{z} \cdot \hat{r} = \cos\theta$):

$u_r(r = a) = U\cos\theta$, u_θ is continuous, $\boldsymbol{u} \to 0$ and $\pi \to$ constant when $\boldsymbol{r} \to \infty$. Here and later on u_r, u_θ are components of velocity in spherical system of coordinates. Then the Hadamard - Rybczyński exterior solution for velocity field takes the form [3]:

$$\left.\begin{array}{l} u_r = \left[A_1\left(\frac{a}{r}\right) - 2B_1\left(\frac{a}{r}\right)^3\right] U\cos\theta \\[2mm] u_\theta = -\left[\frac{A_1}{2}\left(\frac{a}{r}\right) + B_1\left(\frac{a}{r}\right)^3\right] U\sin\theta \end{array}\right\} \quad \text{for} \quad r \geq a \tag{2.20}$$

The interior solution for velocity field has the form:

$$\left.\begin{array}{l} u_r = \left[\frac{a_1}{10}\left(\frac{r}{a}\right)^2 + b_1\right] U\cos\theta \\[2mm] u_\theta = -\left[\frac{a_1}{5}\left(\frac{r}{a}\right)^2 + b_1\right] U\sin\theta \end{array}\right\} \quad \text{for} \quad r \leq a \tag{2.21}$$

Where: u_r, u_θ are components of velocity in spherical system of coordinates. The coefficients A_1, B_1, a_1, b_1 are expressed by the formulas:

$$A_1 = \frac{2 + 3\lambda}{2(1 + \lambda)}, \quad B_1 = \frac{\lambda}{4(1 + \lambda)}, \quad a_1 = -\frac{5}{1 + \lambda}, \quad b_1 = \frac{3 + 2\lambda}{2(1 + \lambda)} \tag{2.22}$$

where: $\lambda = \mu_{in}/\mu_{out}$.

The velocity of the drop is equal to [3]:

$$\boldsymbol{U} = \frac{\boldsymbol{F}}{2\pi\mu_0 a}\frac{1 + \lambda}{2 + 3\lambda} \tag{2.23}$$

The velocity $\boldsymbol{U}$ is related to the force $\boldsymbol{F}$ by the relation presented above (2.23) and we denote: $\boldsymbol{U} = (0, 0, U)$ and $U = |\boldsymbol{U}|$.

Let's now consider a drop of fluid with viscosity μ settling under gravity in a fluid with the same viscosity μ. For $\lambda = 1$ the coefficients are: $A_1 = \frac{5}{4}, B_1 = \frac{1}{8}, a_1 = -\frac{5}{2}, b_1 = \frac{5}{4}$, and the velocity of the drop is equal to:

$$U = \frac{F}{5\pi\eta\tilde{a}} \quad \text{for} \quad \lambda = 1, \tag{2.24}$$

later on we will denote $a = \frac{\tilde{a}}{d}$. Such a spherical drop of fluid with $\rho_{in} > \rho_{out}$, $\mu_{in} = \mu_{out} = \mu$ we will call the ideal drop. It is convenient to analyse the streamlines and field of fluid velocity value in the frame moving with the velocity of the drop. Thus we will denote:

$$w(r) := u(r) - U, \tag{2.25}$$

and $w(r) = |w(r)|$.
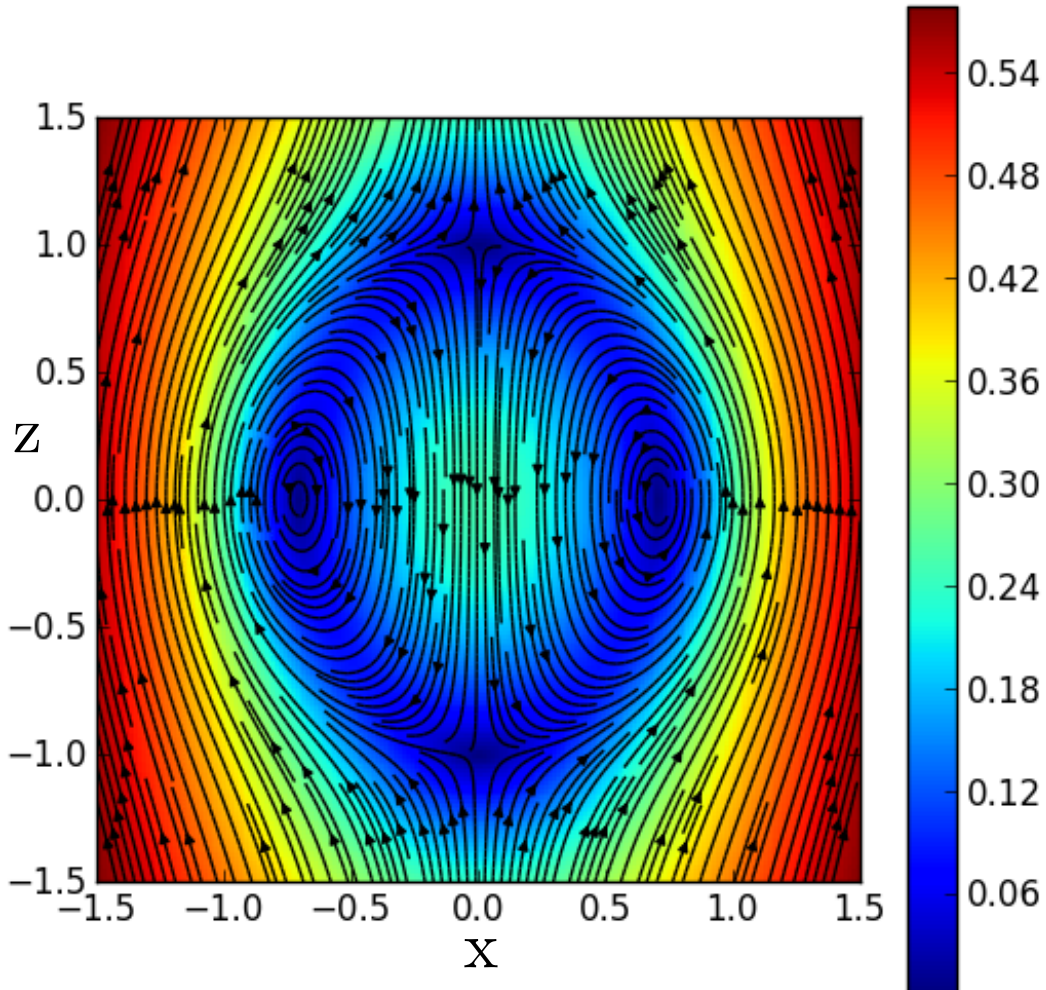

Figure 2.1: The settling spherical fluid drop with $\rho_{in} > \rho_{out}$, $a = 1$. Fluid streamlines and the value of velocity, $w(r,t)/U$, are presented in the frame moving with U. Here the velocity is normalised by U, the drop settling speed.

The velocity of fluid inside and around such a drop is shown in Figure 2.1 in the frame of reference moving with $\boldsymbol{U}$. The plot is based on the Hadamard-Rybczyński formula (2.20)-(2.21). The streamlines are closed inside the drop and stationary. The shape is exactly spherical. One can observe that there are symmetric vortexes (circulations of the fluid) inside the drop. Streamlines outside the fluid drop reflect the intuition: the further from the centre of the drop, the more vertical the streamlines are. With $\boldsymbol{r} \to \infty$, we obtain $\boldsymbol{w}(\boldsymbol{r}) \to -\boldsymbol{U}$.
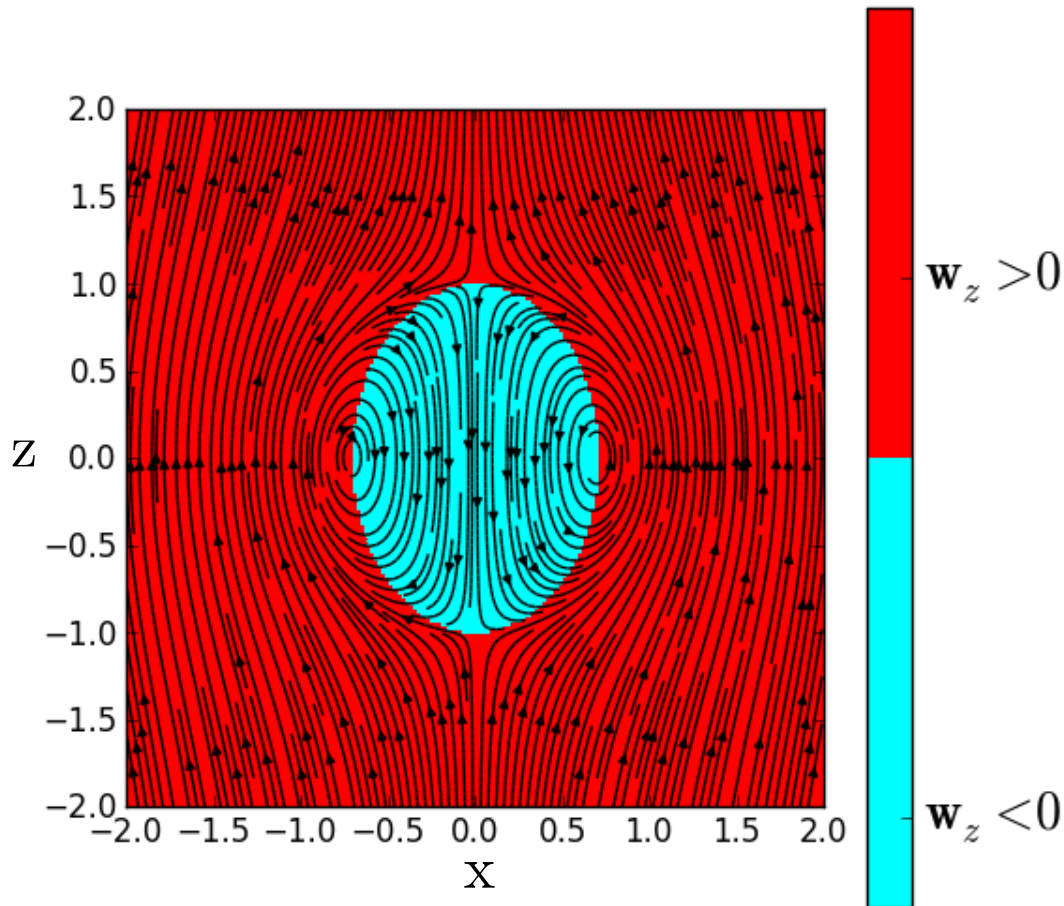

Figure 2.2: Regions, where the the fluid moves down faster than the droplet (cyan, $w_z(\boldsymbol{r}) < 0$) or slower (red, $w_z(\boldsymbol{r}) > 0$). Arrows indicate the streamlines in the reference frame comoving with U.

Another aspect we should closely look at is value of velocity of the fluid inside and around the drop (also shown in Fig. 2.1). It is convenient to analyse it in the reference frame moving with the drop (as it was done with streamlines) and normalised by drop settling velocity $U = |\boldsymbol{U}|$. Near the centre of the drop the value of the fluid velocity $w(\boldsymbol{r})/U$ is noticeably greater than 0 - here the circulation of the fluid is the fastest. In the Eq. 2.21 and Fig. 2.1 we can observe that there are 4 points, where $w(\boldsymbol{r}) = 0$: at $r = a, \theta \in \{0, \pi\}$ (on the top and at the bottom of the drop), $r = a/\sqrt{2}, \theta = \in \{\frac{\pi}{2}, -\frac{\pi}{2}\}$

(in the centres of vertexes).

In Figure 2.2 there are marked regions where the fluid moves down slower or faster than the whole drop. The ellipsoidal-shaped region in the middle of the drop corresponds to values of settling velocity greater than the settling velocity of the drop, U.

In Section 4 fluid velocity calculated for the case of ideal drop (presented above) will be compared with the one observed around sedimenting groups of particles. The dynamics of the particles will be presented and discussed in Sections 3 and 7.
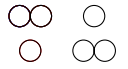
2.3   Discussion of selected particles models

Solution for the dynamics of spherical particles in viscous fluid subjected to forces has the form of multipole expansion [3, 87]. For two interacting particles in a fluid it has the form of an infinite series with subsequent terms of the order r^{-n} with increasing n, where r is the distance from centre of the sphere. In general good convergence can be obtained by taking a few initial terms of multiple expansion [88] together with lubrication correction in case of very close particles [89, 90]. The solution for many particles requires the multipole matrix determining and will not be discussed in this work (described e.g. in [3, 87, 91]). This method was implemented in software packages as described in [89] and [90].

Since multipole method is computationally expensive, an approximation is often used with only a few terms of the multipole expansion taken into account [3, 39, 69, 92]. In Rotne-Prager approximation [92] terms containing $\left(\frac{a_p}{r}\right)^3$ and $\left(\frac{a_p}{r}\right)$ are taken into account, while in point-particle approximation only $\left(\frac{a_p}{r}\right)$. The point model, used also in this study, has the advantage that the dynamics of particles does not require specifying particle size (we analyse identical point-particles) - the self-term can be extracted explicitly. The dynamics of particles is investigated in the reference frame moving with a settling velocity of a single particle. Results obtained in simulations may be applied for different values of radii of particles a_p after being corrected for a_p-dependent settling speed of isolated particle, the same for all particles. This property allows for presenting majority of the results without specifying a_p.

When particles are widely spaced the higher terms of multiple expansion and lubrication do not contribute much to their velocities. In case of close particles there are

Table 2.1: Settling velocities of three-particles system in different configurations, for multipole and point model. Reprinted from [93].

	Rod F	Rod $\perp F$	Vertical chain	Star F	Star $\perp F$	Kissing	Ring
Spheres	1.95	1.63	1.63–1.90	1.90	1.74	1.75	1.74–1.79–1
Point-particle approximation	2.00	1.61	1.61–2.04	2.04	1.75	1.81	1.75–1.74–1
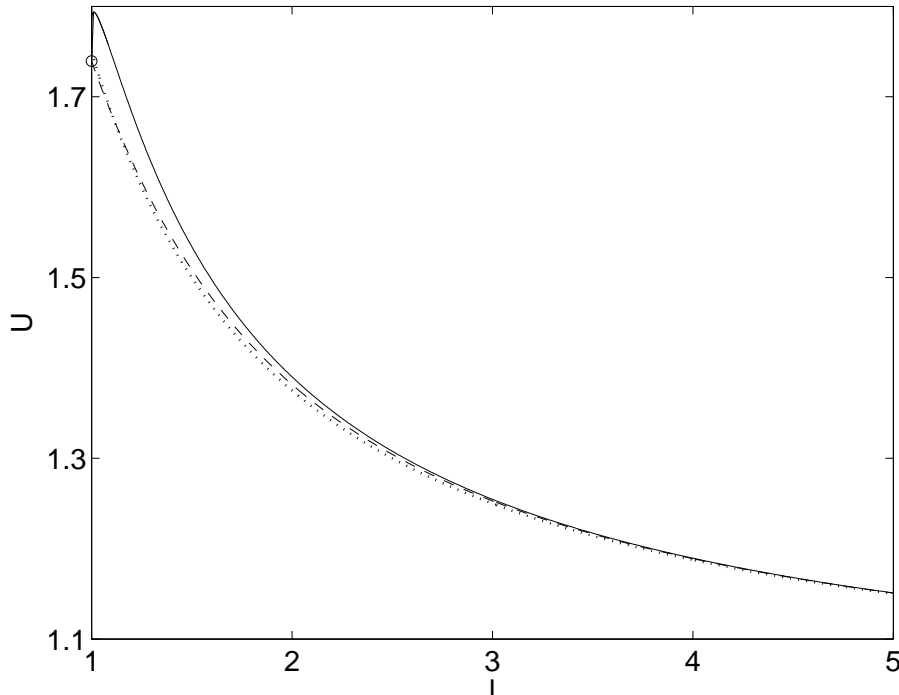
Figure 2.3: Settling velocity of three particles in the 'ring' configuration (Tab. 2.1) plotted versus distance between centres of particles, measured in particle diameters. Results for multipole method are marked with solid line, point-particle method with dotted line and multipole method without particle rotation with dashed line. Reprinted from [93].

some qualitative changes: centres of particles can not approach each other closer than $2a_p$ and when particles almost touch each other there is no relative motion of fluid and particle surface. In point-particle model the particles can rotate as in multipole method, but their angular velocities are usually not considered. These properties may lead to a different behaviour, e.g. in system of three particles new periodic solutions (absent in point-particle approximation) [94] and new equilibrium configurations [95] were found.

In case when the distances between particles are large, the dynamics is accurately described with the point model, e.g. in [69] dynamics for spheres is similar to the point-particles dynamics presented in [68]. Most of results for periodic motions were

obtained with point-particle model. Quantitative differences between the point model and accurate multipole model were studied by Ekiel-Jeżewska and Wajnryb [93]. They compared settling velocities of a three particle system in different configurations, calculated with point model and multipole method. The results reprinted from [93] are recapitulated in Table 2.1. For each configuration the difference between these two models is of the order of a few percent. In Figure 2.3 reprinted after [93] it is shown, how settling velocity depends on the distance between particles initially placed in the vertexes of a horizontal equilateral triangle ('ring' configuration from Tab.2.1). Dynamics of such a single ring but for larger number of particles was discussed in Section 2.4. In the whole presented range the difference between two models (multipole model - solid line, point model - dotted line) is smaller than 4%. For larger distances between particles this difference decreases with distance. We can observe that even for touching particles the difference between results for two alternative models is small and point-particle approximation can describe with good accuracy the dynamics of particles settling in the 'ring' configuration.

The difference in settling velocity in two alternative models are caused mainly by spinning of the particles surfaces. When rotation of particles in multipole method was blocked (dashed line in Figure 2.3) the settling velocity is almost identical to point model (dotted line) even for close distances between particles.

In our study the distances between rings are significantly larger than a_p. Distances between particles from the same ring can be regulated by changing a_p. For these reasons, heaving the trade-off between higher precision and computational speed, the latter was chosen. It has allowed to analyse behaviour of the system for very wide spectrum of parameters and initial configurations.

2.4 Dynamics of a single ring: comparison to continuous model

System of particles that will be studied in this work consists of a few horizontal rings of particles. First, let us discuss the dynamics of a single ring in comparison to a torus of the same size and mass (it will be discussed in details later). It may be expected that with growing number of particles in the ring its dynamics should be more and more similar to the dynamics of the torus, because particles in the ring are closer and closer to each other resembling continuous ring.
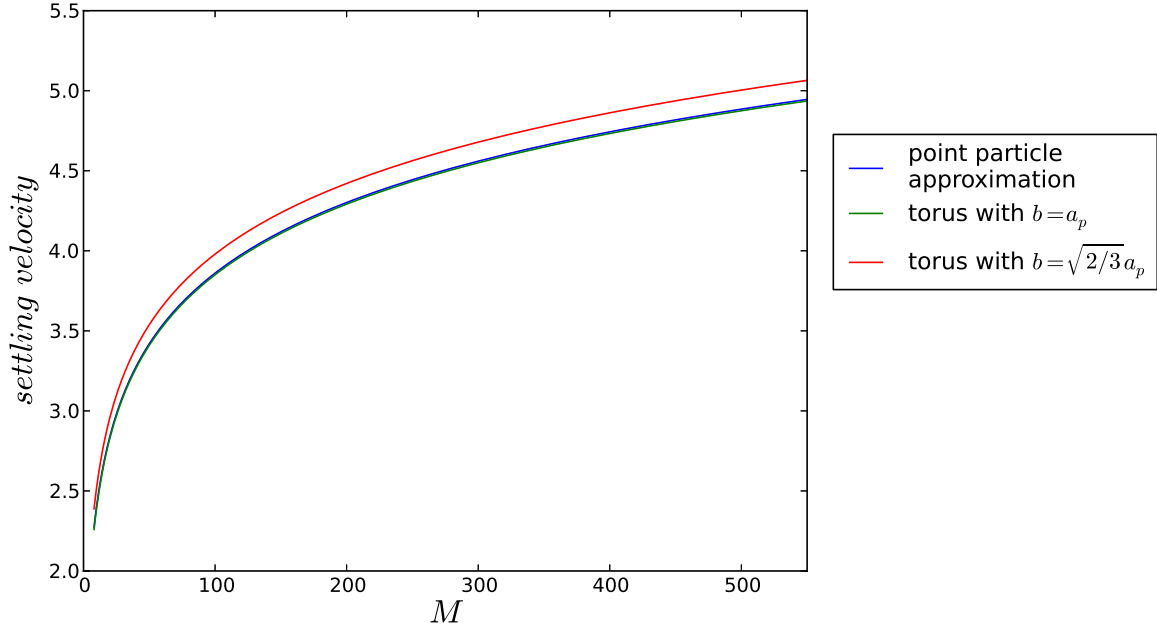
Figure 2.4: Settling velocity of a ring of M particles (blue line) in comparison to settling velocities torus with cross-sectional radius $b = a_p$ (green line) and $b = \sqrt{2/3}a_p$ (red line). Radius of ring of particles is set to $1/2$.

The friction coefficient for torus-shaped particle was first analytically calculated by Tchen [96]. We are interested in friction coefficient for a tangential motion. Here we present a formula in convenient form used by Adamczyk [97]. The friction coefficient of a torus $\tilde{\xi}$ is given by:

$$\tilde{\xi} = \frac{4\pi\eta\tilde{l}}{\ln(\tilde{l}/\tilde{b}) + 0.75} \tag{2.26}$$

where: η is a fluid viscosity, $l/2\pi$ is a centre-line radius and b is a cross-sectional radius. In our normalisation the formula takes the form:

$$\xi = \frac{l}{2(\ln(l/b) + 0.75)} \tag{2.27}$$

where ξ, l, b are dimensionless parameters. Velocity of a horizontal torus dragged with force $\boldsymbol{F} = (F_x, F_y, F_z)$ in tangential direction is equal to:

$$v_z = \frac{2F_z(\ln(l/b) + 0.75)}{l}. \tag{2.28}$$

In order to compare the continuous model with the system of M touching particles, b will be identified with particle radius a_p, l will be put equal to $2\pi\rho_1$, where ρ_1 is radius of the ring of particles, and $\boldsymbol{F}$ is the unit force, equal to the total weight of all particles. Since the particles are touching each other $2a_p M = l$, and consequently $a_p = \frac{l}{2M}$. Taking these assumptions into account we obtain:

$$v_z = \frac{2}{\pi}\left(\ln(2M) + 0.75\right) \tag{2.29}$$

The results presented in Figure 2.4 show that settling velocity of ring consisting of M touching particles (blue line) is almost identical to the velocity of a corresponding torus (green line). Good concordance between results for these two models is kept even for relatively small number of particles, such as $M = 8$. For greater number of particles velocities are more and more similar. The red line in Figure 2.4 denotes settling velocity of a torus with volume identical to the volume of M spherical particles, what is an alternative method to compare torus with ring of particles, used sometimes in the literature [97]. In this approach cross-sectional radius of the torus b is given by $b = \sqrt{2/3}a_p$. As shown in Figure 2.4 settling velocity of ring of particles is better approximated by a torus with $b = a_p$.

In summary it was shown here that settling velocity of ring of particles which touch each other have almost identical settling velocity as a torus of corresponding size. The concordance is better for larger number of particles M, although even for relatively small values of M the difference is less than 1%. When comparing ring of particles to the torus we should consider a torus with cross-sectional radius equal to the radius of particles rather than a torus with the same volume as M particles.

Chapter 3

Dynamics of 2 rings of many particles in a viscous fluid

In this section we will consider system consisting of $M = 2N$ particles, placed in two identical, horizontal rings, similarly as in works by Ekiel-Jeżewska [38] and Gruca *et al.* [86]. The ratio of the vertical distance between the rings to the rings diameter in this configuration is denoted as C. It has been shown [38] that periodic motions occur only when C is greater than the critical value C_0, which depends exclusively on the number of particles in the system. When the initial distance between rings is smaller, $C < C_0$, both rings infinitely expand, rather than performing periodic motions.

The dependence of the critical value C_0 on the number of particles was studied by Ekiel-Jeżewska [38]. In Table 3.1 the predicted values fo C_0 for different number of particles are presented, based on analytical approximation derived in the referred study [38]. One may notice that the value of C_0 decreases with the increasing number of particles, reaching very low values for large M.

M	4	16	32	64	128	256	20000	100000
C_0	0.5	0.0446	0.0169	0.00683	0.00286	0.00123	0.00000841	0.00000144

Table 3.1: The limit value of $C = C_0$ depending on the number of particles M in the system of 2 rings. Values calculated with analytic formula for approximated dynamics [38].

For $C > C_0$ there exist periodic motions and the following two cases may occur: the first one is when two particles placed one above the other, from different rings, interact stronger with each other than with neighbouring particles form the same ring. The

second case is when the interaction between the adjacent particles from the same ring is dominant. In this work the regime where $C \gg C_0$ will be considered, what means that the interactions between particles from the same ring dominate (note, that this notation by no means implies that $C > 1$; in fact also values $C < 1$ will be studied).

3.1   One-parameter family of initial configurations

In the initial configuration, two rings of particles are placed one above each other. For convenience, the diameter of each ring $d = 1$. The initial vertical distance between the rings is equal to C. The scheme of the system is shown in Fig.3.1.
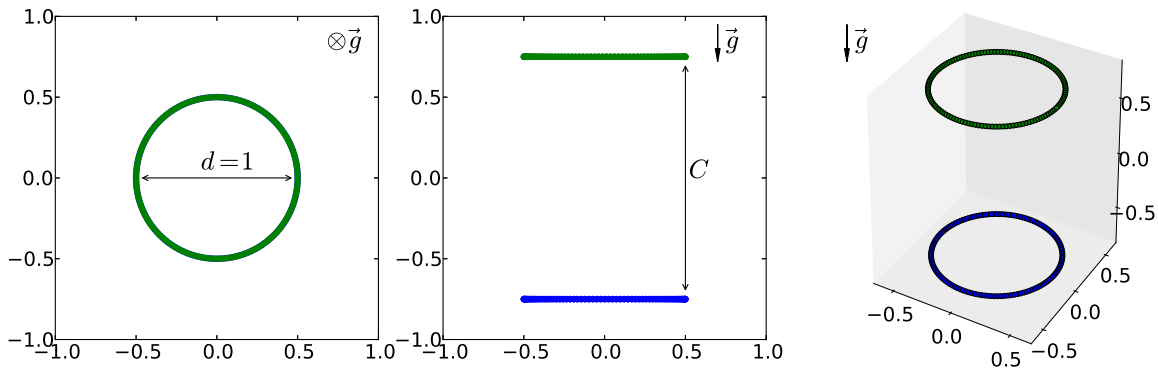
Figure 3.1: Initial configuration of the system of $M = 256$ particles and $C = 1.5$. The coordinates are given by Eqs.(3.1) - (3.2). Top, side and 3D views presented.

The initial positions $\boldsymbol{r}_i = (\rho_i, \phi_i, z_i)$ of the particles $i = 1, ..., M$ are given by,

$$\boldsymbol{r}_{2n-1} = \left(\frac{1}{2}, \frac{2\pi(n-1)}{N}, \frac{C}{2} \right), \tag{3.1}$$

$$\boldsymbol{r}_{2n} = \left(\frac{1}{2}, \frac{2\pi(n-1)}{N}, -\frac{C}{2} \right), \tag{3.2}$$

with $n = 1, ..., N$ and $N = \frac{M}{2}$.

3.2   Numerical analysis of particles motion for different initial conditions

The dynamics has been investigated by conducting over 10000 numerical simulations for different number of particles, $M = 4, 16, 32, 64, 128, 256, 500, 1000, 3000,$

$5000, 10000, 20000, 100000$, and initial values of $C \in [0.05, 2.5]$. For these values of the parameters periodic motion of particles is observed, given that $C > C_0$. No signs of destabilisation are present during the whole simulation time (typically equal to $t = 5000$), corresponding to 300-2700 periods. The examples of particle trajectories for different values of C are shown in Fig.3.2.
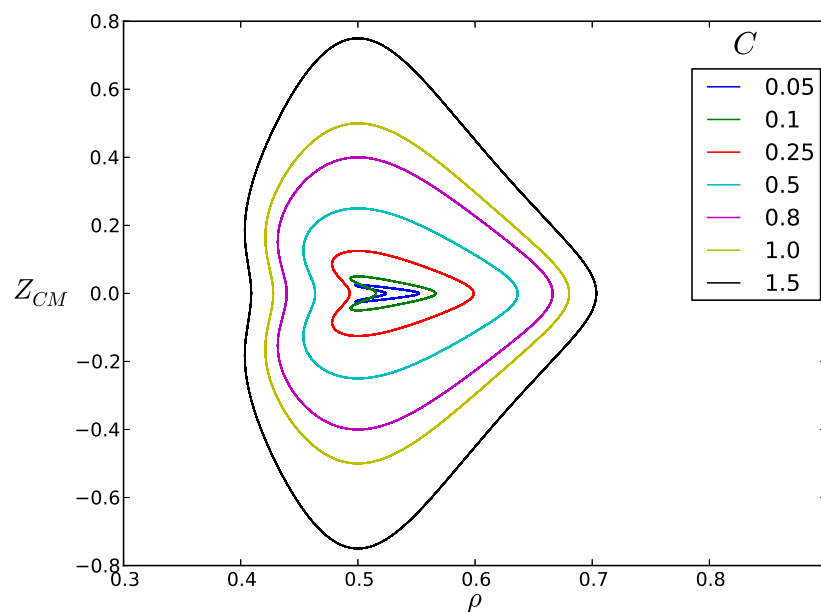
Figure 3.2: The trajectories of particles in the centre-of-mass reference frame ($M = 100000$). The trajectory $Z_{CM}(\rho)$ of each particle has the same shape. Different shapes (and colours) correspond to the values of C indicated in the legend.

Each two particles from different rings, but with equal angular coordinates, move along the same trajectory in the centre-of-mass reference frame. The shape of this trajectory is identical for all particles, but depends on the values of C and M. Later on in this subsection the results for $C = 1.2$ will be presented. Similar periodic trajectories have been found for different numbers of particles M [38, 86], and the their shapes are qualitatively similar.

The dependence of trajectory shape on the number of particles in the system is shown in Figure 3.3 ($C = 1.2$). Larger number of particles leads to thinner and shorter trajectories.

Together with the horizontal size of trajectory, also the period changes with different numbers of particles, as summarised in Table 3.2. The period becomes shorter when the number of particles in the system is larger. This corresponds to shorter trajectories,
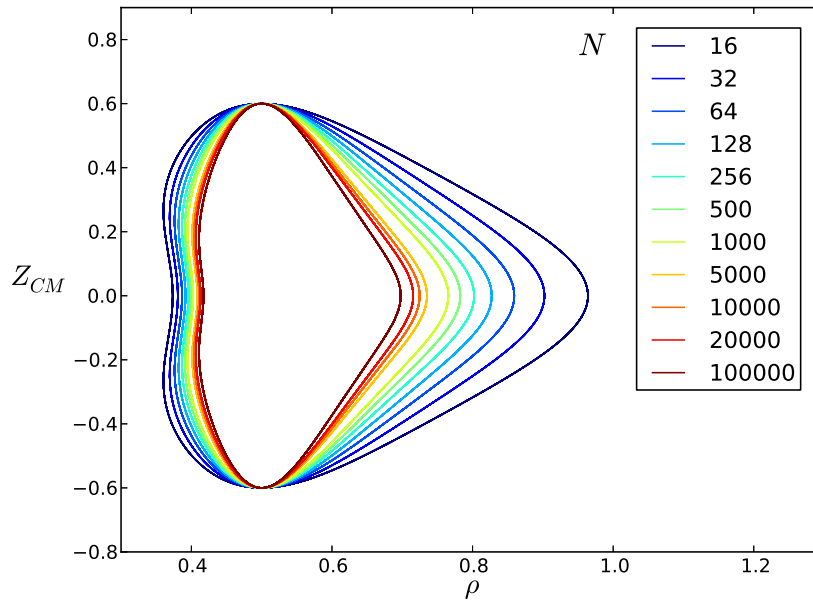
Figure 3.3: The trajectories of particles in the centre-of-mass reference frame for different numbers of particles M and constant $C = 1.2$.

M	T	$|\langle V_z(t)\rangle_T|$
4	48.761	0.669
16	12.662	1.348
32	10.784	1.590
64	9.538	1.826
128	8.635	2.058
256	7.943	2.287
500	7.409	2.508
1000	6.954	2.734
3000	6.376	3.092
5000	6.151	3.258
10000	5.881	3.482
20000	5.643	3.706
100000	5.185	4.225

Table 3.2: Period T and the absolute value of settling velocity $|\langle V_z(t)\rangle_T|$ for different number of particles M in the system of 2 rings. Results for $C = 1.2$.

but the differences in times of the periods are larger than the ones in the trajectories length. Clearly, apart from the effect of trajectory length, different speed of movement along the trajectory contribute significantly to the period length. Dependence of the
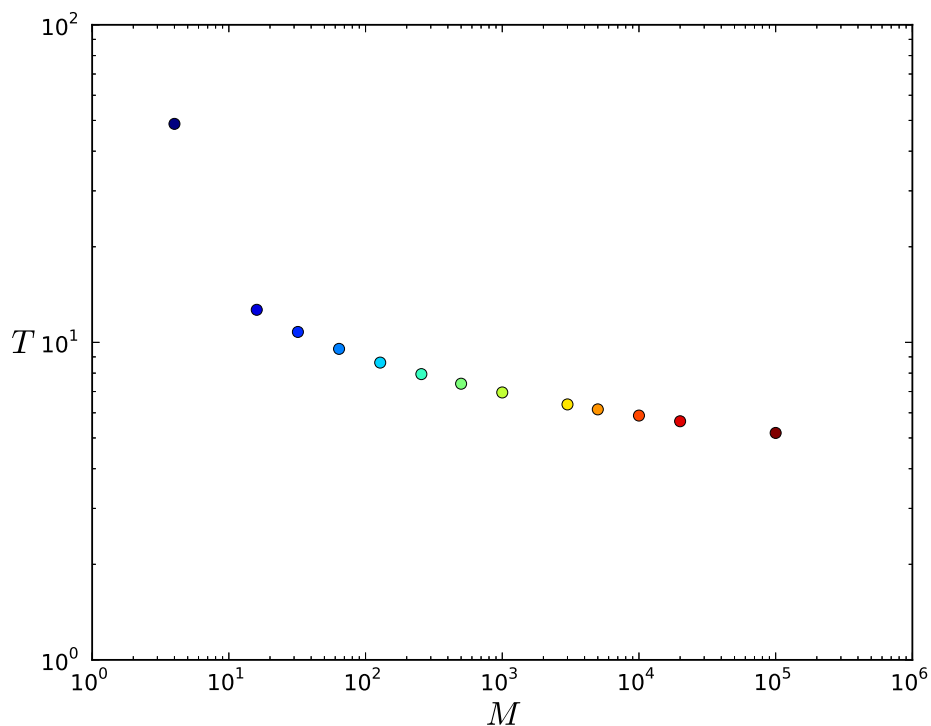
Figure 3.4: The dependence of the period T on the number of particles M for $C = 1.2$ (log-log scale).

period T on the number of particles is plotted in Figure 3.4.

Another important characteristic of the studied system is settling velocity of the whole group of particles, defined as the vertical velocity of the centre of mass:

$$V_z(t) = \frac{dz_{CM}}{dt}. \tag{3.3}$$

Since the configuration of particles varies periodically, also the settling velocity $V_z(t)$ fluctuates, as shown in Figure 3.5B for the case of $M = 32$ particles. For wide range of C, including shown $C = 0.5$, the cluster settles with the minimal speed when two rings are in the same horizontal plane (Figure 3.5A and B).

The cluster velocity averaged over the period will be denoted as $\langle V_z(t) \rangle_T$. In Table 3.1 and Figure 3.6 such an averaged velocity is shown, for different numbers of particles M. Clusters consisting of larger numbers of particles settle down faster.
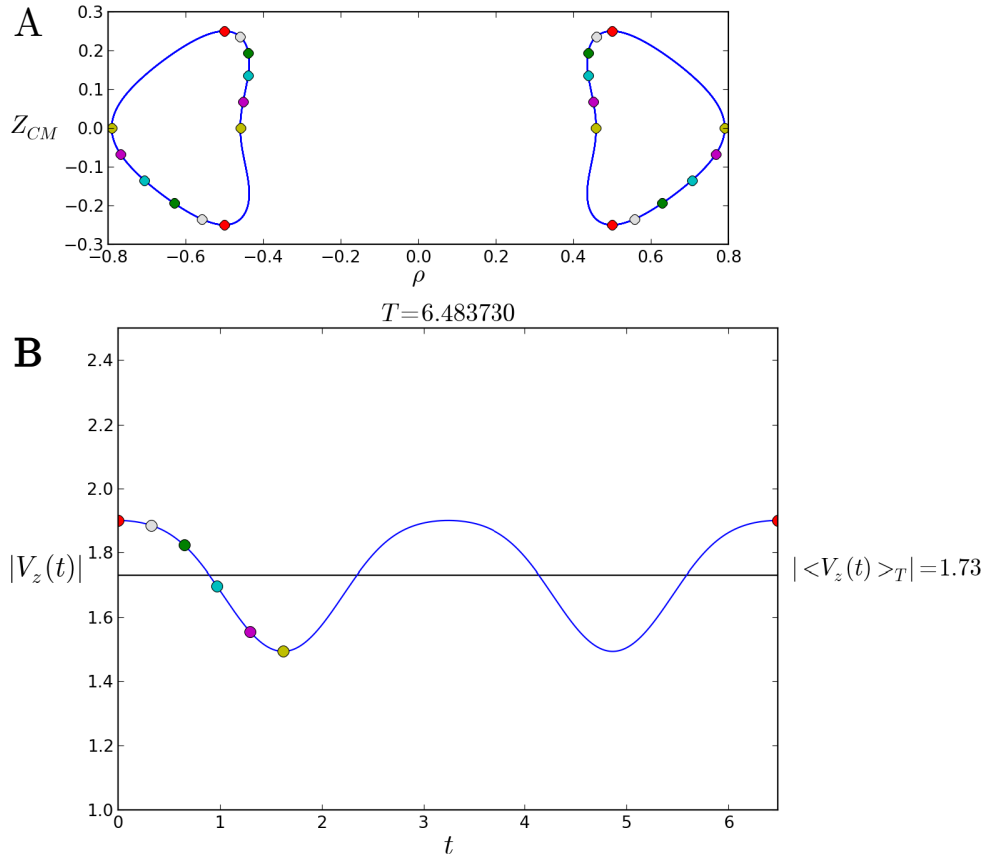
Figure 3.5: A) The trajectories of 4 point-particles in the centre-of-mass reference frame for $C = 0.5, M = 32$, cross-section $\phi = 0$ and $\phi = \pi$. The positions of particles at different time-points $(0, T/20, 2T/20, 3T/20, 4T/20, 5T/20$ are denoted, starting from $\rho = 0.5)$ are denoted with dots with distinguish colours (starting with red ones for $t = 0$ at $\rho = -0.5)$. B) The value of settling velocity $|V_z(t)|$ during one period. With colour dots different time-points are marked, consistently with colour code in plot (A)
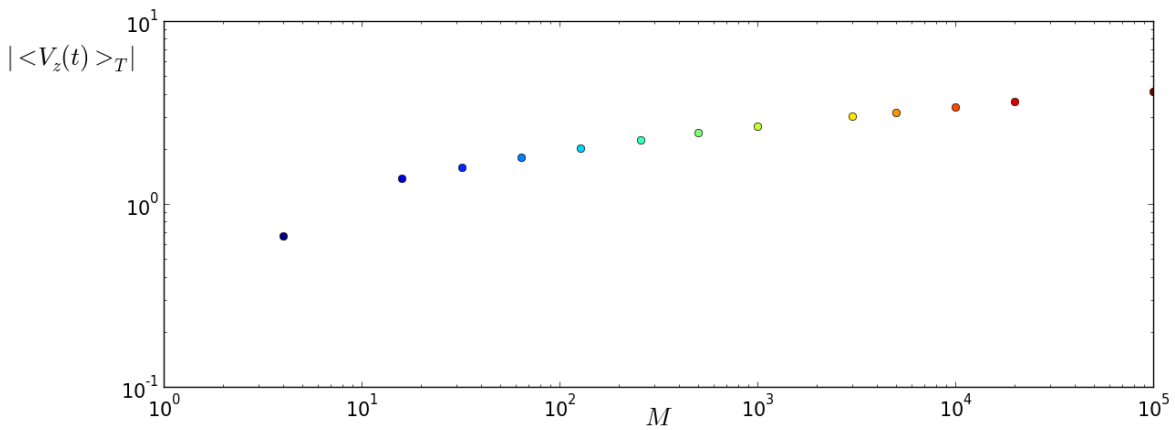
Figure 3.6: The dependence of the averaged cluster velocity $|\langle V_z(t)\rangle_T|$ on the number of particles M for $C = 1.2$.

3.3   Conclusions

In this section was conducted the analysis of relative periodic motions in sedimenting cluster consisting of two regular polygons (rings) of particles. Using numerical simulation it was shown, that periodic motions exist even for very large numbers of particles (e.g. $20000, 100000$), and in this way previous results ([38],[86]) were generalised. The main features of the periodic dynamics were determined for the wide range of two parameters that fully characterise the initial configuration of the cluster: number of particles M and the ratio of initial distance between rings to the rings diameter C. The dependence of trajectory shape on the value of C and M was shown in figures 3.2 and 3.3, respectively. Lower value of C and greater value of M lead to wider trajectories. Additionally, the period and average settling velocity were analysed (Table 3.2, Figs 3.4,3.6). For the increasing number of particles the period decreases, and the average settling velocity increases.

Chapter 4

Streamlines and fluid velocity field in the system of 2 rings in Stokes fluid

In the previous section we analysed dynamics of particles which settle down in a fluid of viscosity μ. Here the fluid motion around the clusters of the particles will be investigated. As before, we will consider system of two rings of particles, presented in Section 3, with the initial configuration given by the equations (3.1) - (3.2). This section is intended to answer the following questions: are the streamlines around particles similar to those for Hadamard-Rybczyński drop (see Figure 2.1)? What are the similarities and differences between them? Are the streamlines closed in the frame of reference moving with particles? How does the velocity field look like outside and inside the regular cluster of particles? To address these questions systematic analysis of the fluid velocity has been performed.

The solution for the Hadamard-Rybczyński drop of fluid, reviewed in the subsection 2.2.1, is the natural reference for the fluid velocity field around the particles. To compare both fields we assume that the total forces exerted on the 'drop' of particles $\boldsymbol{G}$ and the ideal fluid drop $\boldsymbol{F}$ (see Eq. 2.17) are the same: $F = G$. The settling speed U of the corresponding ideal drop is chosen as the z - component of the velocity of the 'drop' of settling particles averaged over the period (see Fig.4.1):

$$U = \langle V_z(t) \rangle_T + u_0. \tag{4.1}$$

To effectively compare these two cases it is useful to define the 'effective' radius of the 'drop' of fluid around the sedimenting cluster of particles. The definition of such 'radius' is not straightforward. We can introduce 'effective radius' as the radius of the
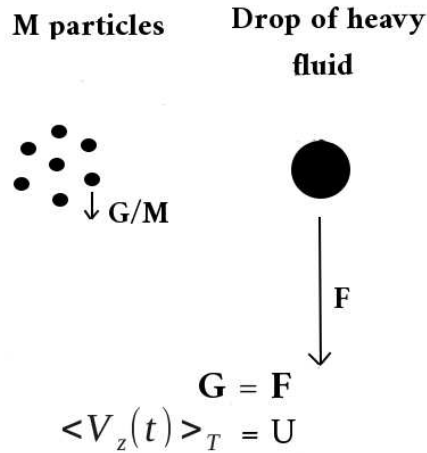
Figure 4.1: The scheme of comparison between Hadamard-Rybczyński drop and 'drop' of particles.

ideal drop defined above, i.e. dragged with the same force $F = G$ and moving with the same speed as group of particles. Eq. (2.24) for the velocity of the ideal drop, dragged with force F, in our normalisation has the form:

$$-U = \frac{8}{5}a_p. \tag{4.2}$$

This leads to the equation for the effective radius:

$$a = \frac{8}{5}\frac{1}{|U|} = \frac{8}{5}\frac{1}{|\langle V_z(t)\rangle_T + u_0|} \tag{4.3}$$

We will compare the field of fluid velocity in the frame of reference comoving with $U = \langle V_z(t)\rangle_T + u_0$. In this frame the fluid velocity field for ideal drop is given by Eqs. (2.20), (2.21) and (2.25):

$$\boldsymbol{w}(\boldsymbol{r}) := \boldsymbol{u}(\boldsymbol{r}) - \boldsymbol{U}, \tag{4.4}$$

and the analogical one for the fluid velocity of 'drop' of particles has the form:

$$\boldsymbol{W}(\boldsymbol{r}, t) = \boldsymbol{v}(\boldsymbol{r}, t) - \langle V_z(t)\rangle_T \hat{\boldsymbol{z}} - \boldsymbol{u}_0, \tag{4.5}$$

where $\boldsymbol{v}(\boldsymbol{r}, t)$ expressed by Eq. (2.9), depends on particle positions $\tilde{\boldsymbol{r}}_i$ at time t. We follow the convention that $W(\boldsymbol{r}, t) = |\boldsymbol{W}(\boldsymbol{r}, t)|$.

As we can see in Eq. (4.5), the relative velocity of the fluid around the cluster $\boldsymbol{W}(\boldsymbol{r}, t)$ depends on the chosen radius of the single particle a_p, what determines its self-term u_0, given by:

$$-u_0 = \frac{4}{3} \frac{1}{M a_p} \tag{4.6}$$

When the radius is very small, $a_p \to 0$, u_0 goes to infinity and the fluid streams through the cluster with little interference. The upper estimation of particle size is given by:

$$a_{p,max} = \min_t \left(\rho_1 \left(t \right) \right) \sin \left(\frac{2\pi}{M} \right), \tag{4.7}$$

what implies that the particles from one ring touch each other, when the ring is the smallest during the period. Note, that it is enough here to consider the minimum of $\rho_1 \left(t \right)$ since $\rho_2 \left(t \right) = \rho_1 \left(\frac{T}{2} + t \right)$.

We are interested in this amount of fluid, which is dragged together with the particles, what may contribute to the long-range fluid transport. This is the volume of fluid where we observe closed streamlines in the reference frame comoving with the particles: the larger and more stable this region is (denoted later as 'droplet'), the larger amount of fluid is dragged with particles. In the case, when the volume is large enough, more fluid can be lifted with the particles. Otherwise, when the fluid streams up through the middle of the cluster, the volume of dragged fluid radically decreases. In order to distinguish between these two cases we will need to examine the fluid velocity along the system symmetry axis z. Below I will show that the vertical velocity of the fluid $\boldsymbol{v} \left(\boldsymbol{r}, t \right)$ (in laboratory reference frame) along the symmetry axis of the system, does not depend on the number of particles and the mass distribution between them. Without the lost of generality, we can calculate the vertical velocity of the fluid v_z at the point O at $\boldsymbol{r}_O = (0, 0, 0)$ in the cylindrical coordinate system, $v_z(0, 0, 0)$. First let us consider the $v_z(0, 0, 0)$ in the presence of point mass m at point A, $\boldsymbol{r}_A = (\rho_A, \theta_A, z_A)$ in non-normalised variables. In this case, with notation $l = \sqrt{\rho_A{}^2 + z_A{}^2}$ and $\boldsymbol{r}_{OA} = \boldsymbol{r}_O - \boldsymbol{r}_A$ we can write as following:

$$v_z = \frac{mg}{8\pi\eta l} \left(\boldsymbol{I} + \frac{\boldsymbol{r}_{OA} \otimes \boldsymbol{r}_{OA}}{r_{OA}{}^2} \right) \hat{\boldsymbol{z}} = -\frac{mg}{8\pi\eta l} \left(1 + \frac{z_A^2}{l^2} \right), \tag{4.8}$$

Next we consider an analogous case, but this time with N point masses $m_1, m_2, \ldots, m_N$ distributed along a circle, parametrized with the angle θ. The circle we will consider next has the coordinates $\{ (\rho, \theta, z) : \rho = \rho_A; 0 \le \theta < 2\pi; z = z_A \}$ Using the equation (4.8) we obtain:

$$v_z = \sum_{i=1}^{N} \frac{-g m_i}{8\pi\eta l} \left(1 + \frac{z_A^2}{l^2} \right) = \frac{-g}{8\pi\eta l} \left(1 + \frac{z_A^2}{l^2} \right) \sum_{i=1}^{N} m_i = \frac{-mg}{8\pi\eta l} \left(1 + \frac{z_A^2}{l^2} \right). \tag{4.9}$$

This result is clearly valid for also for the rings studied in this dissertation, consisting of uniformly spaced $\frac{M}{2}$ point particles with equal masses. In consequence fluid velocity along z axis does not depend on number of particles.

In our system, using dimensionless variables, the vertical velocity of the fluid in the centre of mass of the cluster $(0, 0, z_{CM})$ can be calculated with the following formula:

$$v_c = \frac{1}{l_1^3}\left(\rho_1^2 + 2(z_1 - z_{CM})^2\right) + \frac{1}{l_2^3}\left(\rho_2^2 + 2(z_2 - z_{CM})^2\right) \tag{4.10}$$

$$l_1^2 = \rho_1^2 + (z_1 - z_{CM})^2 \tag{4.11}$$

$$l_2^2 = \rho_2^2 + (z_2 - z_{CM})^2 \tag{4.12}$$

Although the fluid velocity v_c at the particles centre of mass does not depend on the number of particles, the relative fluid motion around the cluster may be different for different M due to the changes of $\langle V_z(t) \rangle_T$ and $\boldsymbol{u_0}$. This dependence, together with the influence of parameter C, is presented in Figure 4.2, where particles settling velocity and the fluid velocity in the centre of the cluster are shown. We can observe, that the fluid streams through the middle of the system. The opposite situation (compact drop, fluid flow only around the droplet and not through the middle) is found only in some cases with low number of particles (e.g. $M = 8$) and with particle radius close to the maximal (see Appendix section A.1). Analogous analysis will be conducted for the system with four rings in Section 6.

The streamlines around the system of two rings are shown in Figure 4.3. The direction of streamlines does not change significantly, because the particles move faster than the fluid. However substantial changes in the velocity value are visible. The effective radius of the cluster a_p is much smaller than the size of the rings.

For larger numbers of particles (e.g. starting from $M = 32$) the particles velocity value is greater than the velocity of the fluid in the middle of the cluster, what implies that the fluid is not dragged with the particles. This behaviour is different than the one observed for random drop of particles [33].
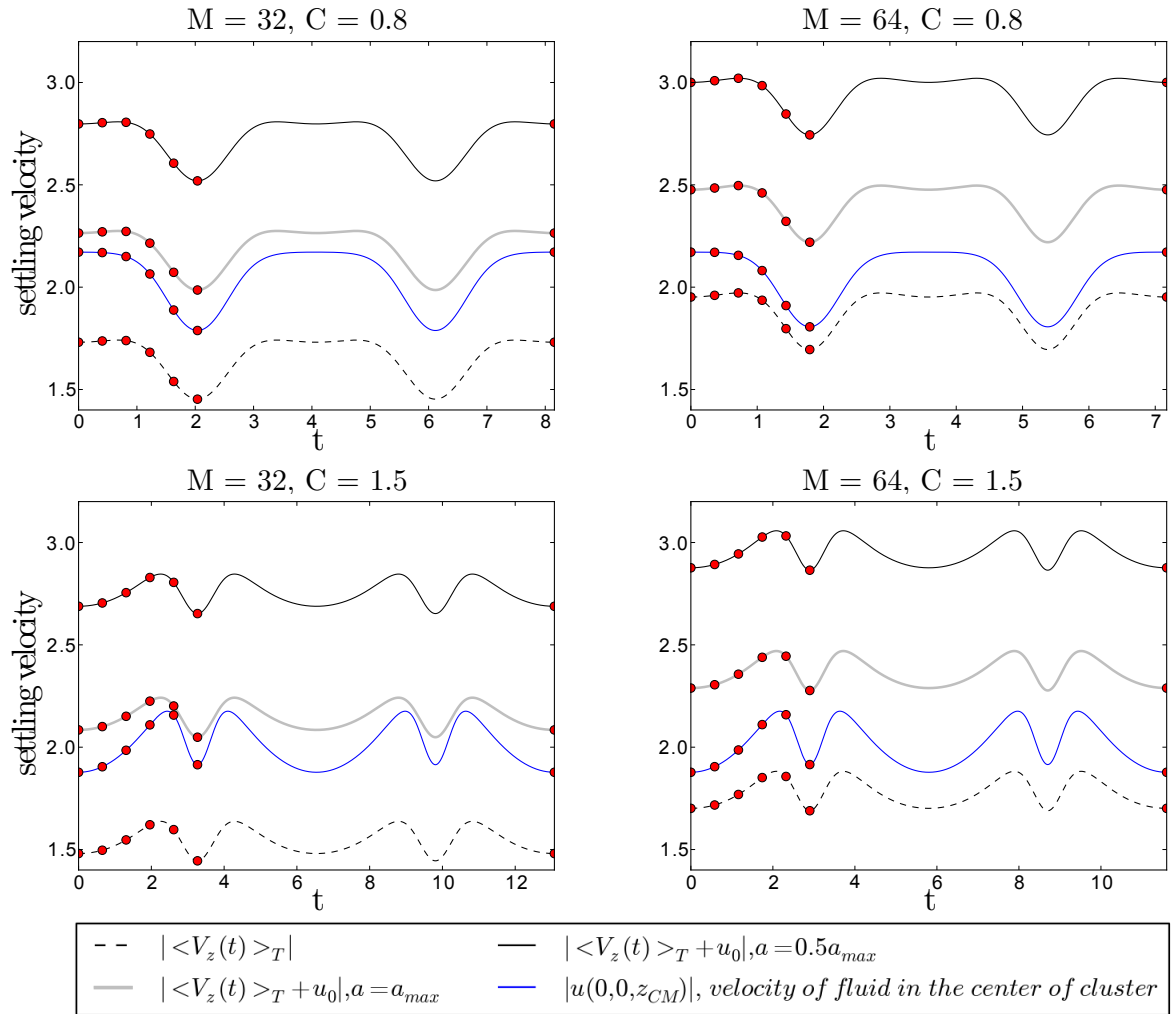
Figure 4.2: Velocity of the fluid (blue line), velocity of the particles without self-term u_0 (dashed line) and velocity of the particles for two different radii: $a = a_{max}$ (grey line) and $a = a_{max}/2$ (black solid line); plots for two different values of M and C. Chosen timepoints are marked with red dots: $t = 0$, $t = T/20$, $t = T/10$, $t = 3T/20$, $t = T/5$, $t = T/4$ and $t = T$. In all cases the fluid flows up through the middle of the group during whole period. This stream is faster for smaller radii of particles.

Figure 4.3: A) The streamlines and fluid velocity value $W(\boldsymbol{r}, t)/|\langle V_z(t)\rangle_T + u_0|$ around $M = 32$ point-forces (positions of particles marked with dots) for $C = 0.8$. Particles size is half of the maximal value, when they would touch each other. B) Streamlines and fluid velocity value around and inside ideal drop of fluid, which has the same effective radius.

Chapter 5

Dynamics of two rings and fluid motion in permeable medium

The dynamics of fluid in permeable media is described with the Brinkman-Debye–Büche (BDB) equations. For the system of M identical point particles, the sa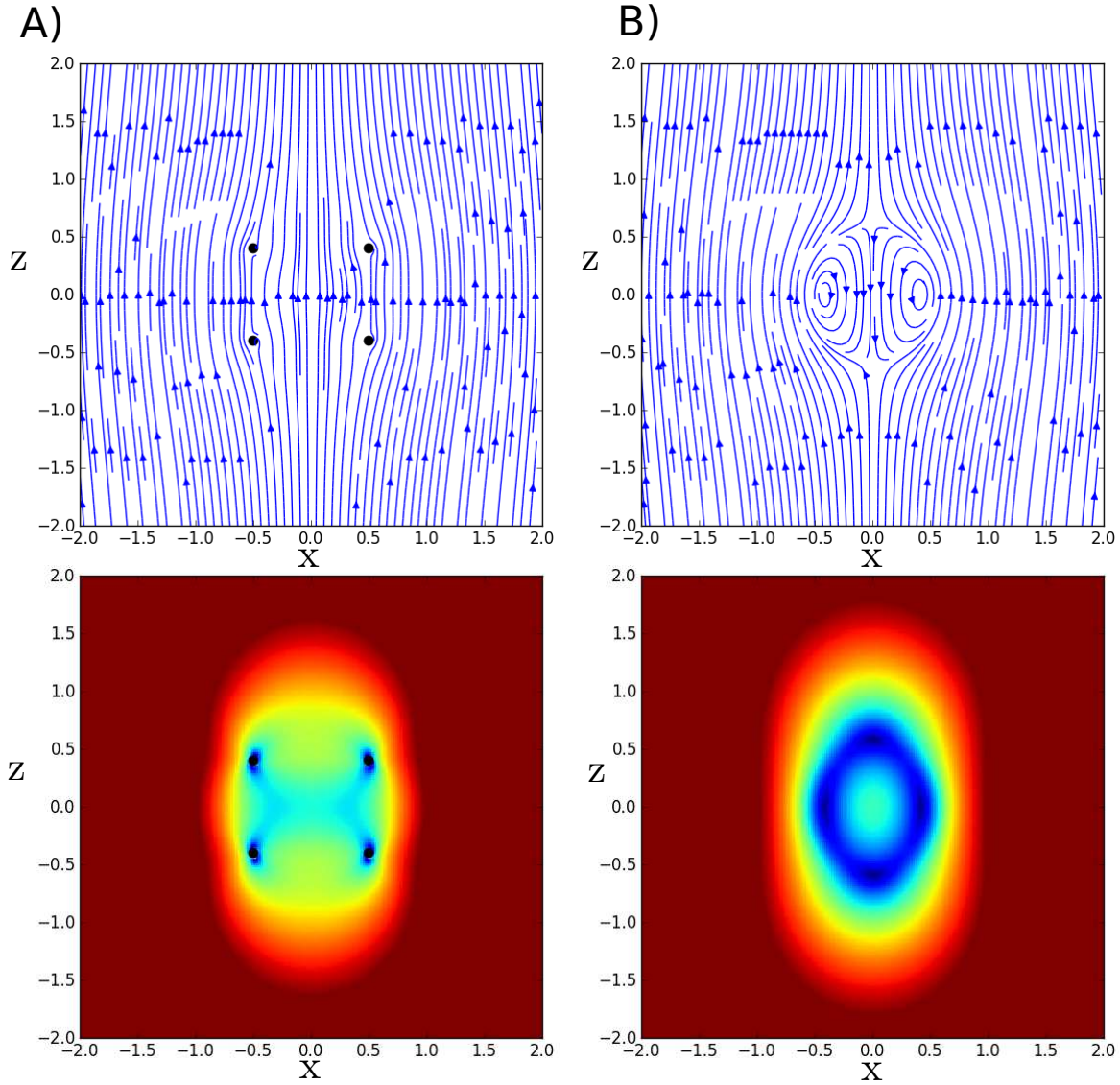me as in Section 2.1.1 but this time in permeable medium rather than in a viscous fluid, these equations are as follows:

$$\eta \left(\nabla^2 \tilde{\boldsymbol{v}}(\boldsymbol{r}) - \kappa^2 \tilde{\boldsymbol{v}}(\boldsymbol{r}) \right) - \nabla \tilde{p}(\boldsymbol{r}) \;=\; -\frac{1}{M} \sum_{i=1}^{M} \boldsymbol{G}\, \delta(\boldsymbol{r} - \tilde{\boldsymbol{r}}_i), \tag{5.1}$$

$$\nabla \cdot \tilde{\boldsymbol{v}}(\boldsymbol{r}) \;=\; 0, \tag{5.2}$$

where $\frac{\boldsymbol{G}}{M}$ is the external force exerted on a single particle $(\boldsymbol{G} = -G\hat{\boldsymbol{z}})$, $\boldsymbol{v}(\boldsymbol{r})$ is the velocity of fluid inside the permeable medium, $1/\kappa^2$ is the permeability coefficient ($1/\kappa$ is the characteristic screening length), η is the fluid viscosity and $\tilde{\boldsymbol{r}}_i$ is the position of particle i.

The fluid velocity $\tilde{\boldsymbol{v}}(\boldsymbol{r})$ and pressure $\tilde{p}(\boldsymbol{r})$ are given by:

$$\tilde{\boldsymbol{v}}(\boldsymbol{r}) \;=\; \frac{1}{M} \sum_{i=1}^{M} \boldsymbol{T}(\boldsymbol{r} - \tilde{\boldsymbol{r}}_i) \cdot \boldsymbol{G}, \tag{5.3}$$

$$\tilde{p}(\boldsymbol{r}) \;=\; \frac{1}{M} \sum_{i=1}^{M} \boldsymbol{P}(\boldsymbol{r} - \tilde{\boldsymbol{r}}_i) \cdot \boldsymbol{G}, \tag{5.4}$$

with the Green tensors:

$$\boldsymbol{T}(\boldsymbol{R}) = \frac{1}{4\pi\eta R}\left(h_1(\kappa R)\boldsymbol{I} + h_2(\kappa R)\frac{\boldsymbol{R}\otimes\boldsymbol{R}}{R^2}\right), \tag{5.5}$$

$$\boldsymbol{P}(\boldsymbol{R}) = \frac{\boldsymbol{R}}{4\pi R^3}, \tag{5.6}$$

where

$$h_1(\kappa R) = -\frac{1}{(\kappa R)^2} + \left(1 + \frac{1}{\kappa R} + \frac{1}{(\kappa R)^2}\right)e^{-\kappa R}, \tag{5.7}$$

$$h_2(\kappa R) = \frac{3}{(\kappa R)^2} - \left(1 + \frac{3}{\kappa R} + \frac{3}{(\kappa R)^2}\right)e^{-\kappa R} \tag{5.8}$$

and $R = |\boldsymbol{R}|$.

The equations of motion of the particles are given by

$$\frac{d\tilde{\boldsymbol{r}}_i}{dt} = \frac{1}{M}\sum_{j\neq i}^{M}\boldsymbol{T}(\tilde{\boldsymbol{r}}_{ij})\cdot\boldsymbol{G} + \boldsymbol{u}_0 \tag{5.9}$$

where $\tilde{\boldsymbol{r}}_{ij} = \tilde{\boldsymbol{r}}_i - \tilde{\boldsymbol{r}}_j$, and

$$\boldsymbol{u}_0 = \frac{\boldsymbol{G}}{6\pi\eta a_p(1 + \kappa a_p + (\kappa a_p)^2/3)} \tag{5.10}$$

is the settling velocity of the isolated particle in permeable medium, with a_p equal to the radius of the single particle. As in Section 3.1 we will consider the motion in the reference frame comoving with velocity $\boldsymbol{u}_0$, so that the results do not depend on the size of particle.

From now on, we use dimensionless variables, based on an initial size of the group d as the length unit, and $G/(4\pi\eta d)$ as the velocity unit. Therefore, $4\pi\eta d^2/G$ is the time unit. From now on, $\boldsymbol{r}_i = \tilde{\boldsymbol{r}}_i/d$ denotes the dimensionless position of a particle i. Later on all dimensionless quantities will be denoted without tilde.

After normalisation presented above the fluid velocity (5.3) around the particles takes the form:

$$\begin{aligned}\boldsymbol{v}(\boldsymbol{r},t) = -\frac{1}{M}\sum_{i=1}^{M}\frac{1}{|\boldsymbol{r}-\boldsymbol{r}_i(t)|}\left(h_1(\kappa|\boldsymbol{r}-\boldsymbol{r}_i(t)|)\boldsymbol{I}+\right.\\\left.+\frac{(\boldsymbol{r}-\boldsymbol{r}_i(t))\otimes(\boldsymbol{r}-\boldsymbol{r}_i(t))}{|\boldsymbol{r}-\boldsymbol{r}_i(t)|^2}h_2(\kappa|\boldsymbol{r}-\boldsymbol{r}_i(t)|)\hat{\boldsymbol{z}}\right.\end{aligned} \tag{5.11}$$

We will analyse the system of equations for K rings in the reference frame moving with the velocity $\boldsymbol{u}_0$ (Eq. (5.10)). As in Section 3 we solve the symmetrical dynamics and

reduce the system of $3M$ equations (5.9) to the system of $2K$ equations for ρ_l and z_l, with $l = 1, ..., K$. The initial configuration is the same as described in Section 3.1. The system of equations takes the form,

$$\frac{d\rho_l}{dt} = -\frac{1}{M} \sum_{k=1}^{K} \sum_{n=1}^{N} (1 - \delta_{kl}\delta_{n1}) \frac{(z_k - z_l) \left[\rho_k \cos\left(\frac{2\pi(n-1)}{N}\right) - \rho_l \right]}{R_{lkn}^3} h_2(\kappa R_{lkn}), \quad (5.12)$$

$$\frac{dz_l}{dt} = -\frac{1}{M} \sum_{k=1}^{K} \sum_{n=1}^{N} (1 - \delta_{kl}\delta_{n1}) \left(h_1(\kappa R_{lkn}) \frac{1}{R_{lkn}} + h_2(\kappa R_{lkn}) \frac{(z_k - z_l)^2}{R_{lkn}^3} \right), \quad (5.13)$$

$$R_{kln}^2 = (z_k - z_l)^2 + \rho_l^2 + \rho_k^2 - 2\rho_l\rho_k \cos\left(\frac{2\pi(n-1)}{N}\right). \quad (5.14)$$

5.1   Dynamics of a single ring

Let us now discuss the contributions to the fluid velocity (Eq. (5.11)) from the terms containing h_1 and h_2 functions in case of 1 ring. We will begin with the term containing h_2. In Figure 5.1 we can see that $h_2(\kappa R)$ is greater than 0 for all values of κR and monotonically decreases. In the velocity Green tensor (Eq. (5.5)) h_2 function is multiplied by $\frac{\boldsymbol{R} \otimes \boldsymbol{R}}{R^2}$, so the magnitude of contribution from this term depends on angle between force $\boldsymbol{F}$ and $\boldsymbol{R}$. In the special case when $\boldsymbol{F} \perp \boldsymbol{R}$ the contribution is equal to 0. Since h_1 function is multiplied by identity matrix $\boldsymbol{I}$, the contribution from this term in Green tensor does not depend on the direction of $\boldsymbol{R}$, what indicates that in the plane where $\boldsymbol{R} \perp \boldsymbol{F}$ (and close to this plane) only the term with h_1 is important.
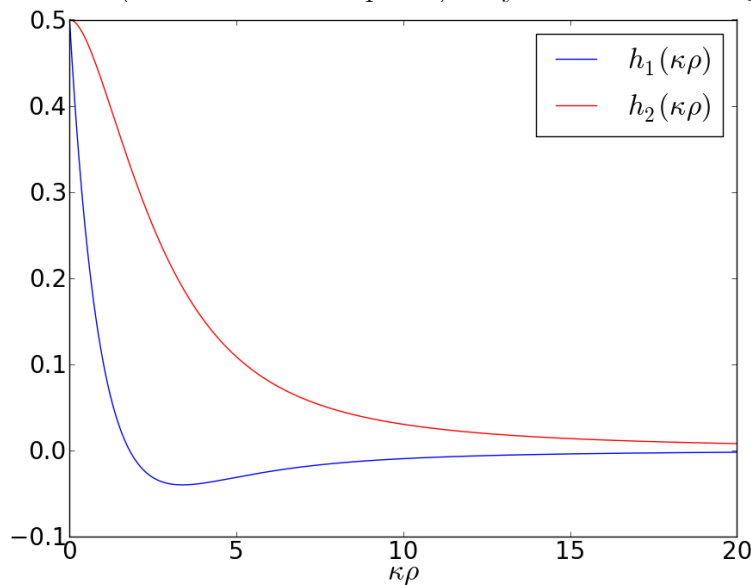

Figure 5.1: The dependence of h_1 and h_2 on κR given by Eq. (5.7) - (5.8).

Let's analyse the influence of the term in Green tensor containing h_1. Function h_1 (Fig. 5.1) has a single root and it returns values smaller than 0 for sufficiently large argument κR. The negative value of h_1 function for a given $\boldsymbol{R}$ indicates that the direction of fluid velocity in the plane of the ring in this point is opposite to the direction of the force that generates the flow. In our system of settling particles it means that in some regions the fluid velocity is pointing upward. As a consequence, for some configurations of particles the group settles down slower than an isolated single particle - e. g. a horizontal ring of particles may settle down slower than a single particle, what depends on number of particles M, permeability coefficient κ and the ring radius ρ, as it will be discussed in the next section. Another consequence is that smaller ring may settle down slower than a bigger one. This effect allows for a breakage of the system of several rings: due to the difference in settling velocities between the bottom bigger and upper smaller rings,the distance between them will increase. This type of decay is not possible in the Stokes fluid. The influence of parameters on the decay will be discussed in Section 5.2.

I will now discuss the case of a single ring of particles. This will be later a useful reference point for understanding the dynamics of two and more rings, especially their separation for some parameters.

The settling velocity of a single ring (Eq. (5.13)) is given by the equation:

$$V_z = -\frac{1}{M} \sum_{n=2}^{M} \frac{h_1(\kappa R_{1n})}{R_{1n}} \tag{5.15}$$

where $R_{1n} = \sqrt{2}\rho\sqrt{1 - \cos\left(\frac{2\pi(n-1)}{N}\right)}$. When only one ring is considered, h_2 does not appear in the equation and the only non-zero term includes h_1. As it was noticed in the previous subsection, function h_1 has a root in the range $(0, \infty)$, and for the arguments large enough, the value of h_1 is smaller than 0. At the same time we have: $\lim_{x\to\infty} h_1(x) = 0$. Function $\frac{h_1(\kappa R)}{R}$ reaches the minimum for a finite value of the argument, what is not the case for the Stokes fluid, when $\kappa = 0$.

In our system in the laboratory frame of reference the consequence is that for a given number of particles M and κ there exists a finite value $\rho = \rho_0$ for which the settling velocity of the ring is the smallest. For ρ smaller than ρ_0 the relation from Stokes fluid is kept: smaller rings settle faster than bigger ones. In the opposite situation, when ρ is greater than ρ_0, this relation is reversed: bigger rings settle down faster. In table 5.1 critical values of ρ_0 are presented, for which the settling velocity is the smallest.

	$M = 8$	$M = 16$	$M = 32$	$M = 64$	$M = 128$	$M = 256$	$M = 1000$
$\kappa\rho_0$	1.828	2.807	5.211	10.576	21.390	42.967	168.161

Table 5.1: The value of $\kappa\rho$ (dimensionless) for which the settling velocity of a single ring of particles reaches the minimum, for a given number of particles M.

Although the direction of $\boldsymbol{V}_z$ is opposite to gravity, but in the laboratory frame of reference (adding $\boldsymbol{u}_0$) the total velocity has the same direction as gravity. I examined wide range of $\kappa \in \{0.1, ..., 1000\}$ and $M \in \{4, 10000\}$ parameters and the settling velocity lower or equal to 0 would be possible (if ever) only for non-physically large radii of particles, bigger than approximately 1.6 (the number depends on parameters) of maximal radius when the particles touch each other.

5.2   Requirements for periodic motions of two rings.

The dynamics of a single ring described above has significant consequences for behaviour of our system with two rings. It implies the possibility of a new type of decay, when the vertical distance between rings grows. Since for some values of M and κ bigger rings settle down faster than smaller ones, it is possible that the smaller ring will be left behind. This mechanism is important during decay, because at the first

κ	$M = 8$	$M = 32$	$M = 64$	$M = 256$
0.5	43.6	28.8	25.2	20.8
1	57.2	34	29.6	24
2	154.4	52.8	43.6	34
5	decay	208.4	123.6	81.2
10	decay	decay	383.61	184.8
20	decay	decay	decay	454.81
50	decay	decay	decay	2043.64

Table 5.2: The period for clusters with different number of particles M in medium with permeability coefficient $1/\kappa^2$. Decay of the cluster takes place for smaller number of particles and smaller permeability coefficient (greater κ), $C = 1.5$.

moment of the dynamics the radius of upper ring is decreasing, while of the bottom one - increasing. The nature of the decay described here is different from the one mentioned in the Section 3, where the vertical distance between two rings does not
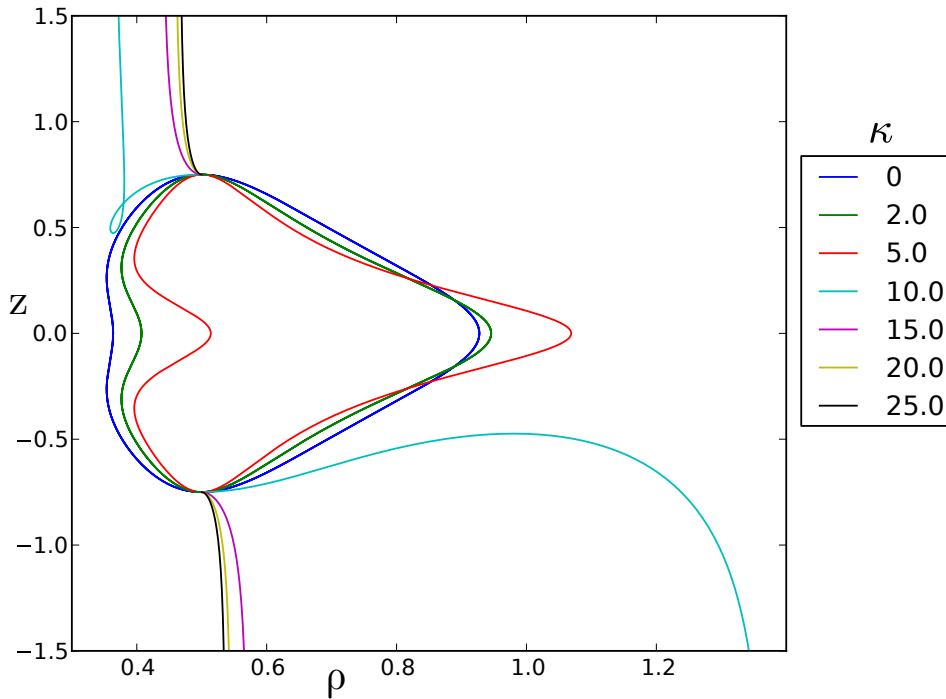
Figure 5.2: Trajectories of particles in the centre of mass reference frame of two rings for different values of permeability coefficient $1/\kappa^2$. For $\kappa \geq 10$ the two rings separate in the vertical direction.

increase. Similarly as in the Stokes fluid, in this work we will discuss only the case $C > C_0$.

In Table 5.2 the parameters that lead to periodic or non-periodic solutions are presented, for a chosen value of C. The values of κ for which we observe decay is greater for bigger number of particles M. The transition between periodic and non-periodic dynamics for increasing value of κ is shown in Figure 5.2. Bigger values of κ imply faster decay.

5.3   Analysis of periodic motions.

In the presented system, for a range of κ, M and C parameters, periodic motions are observed. In this section I will briefly present how the shape of the trajectory depends on values of these parameters. In Figure 5.4 the dependence on κ is presented.   Larger κ results in the trajectories which are more elongated in the horizontal direction. Apart from that, for larger κ the minimal ring radius is also larger a bit. These observations stay also for values of κ outside the range presented in the figure.
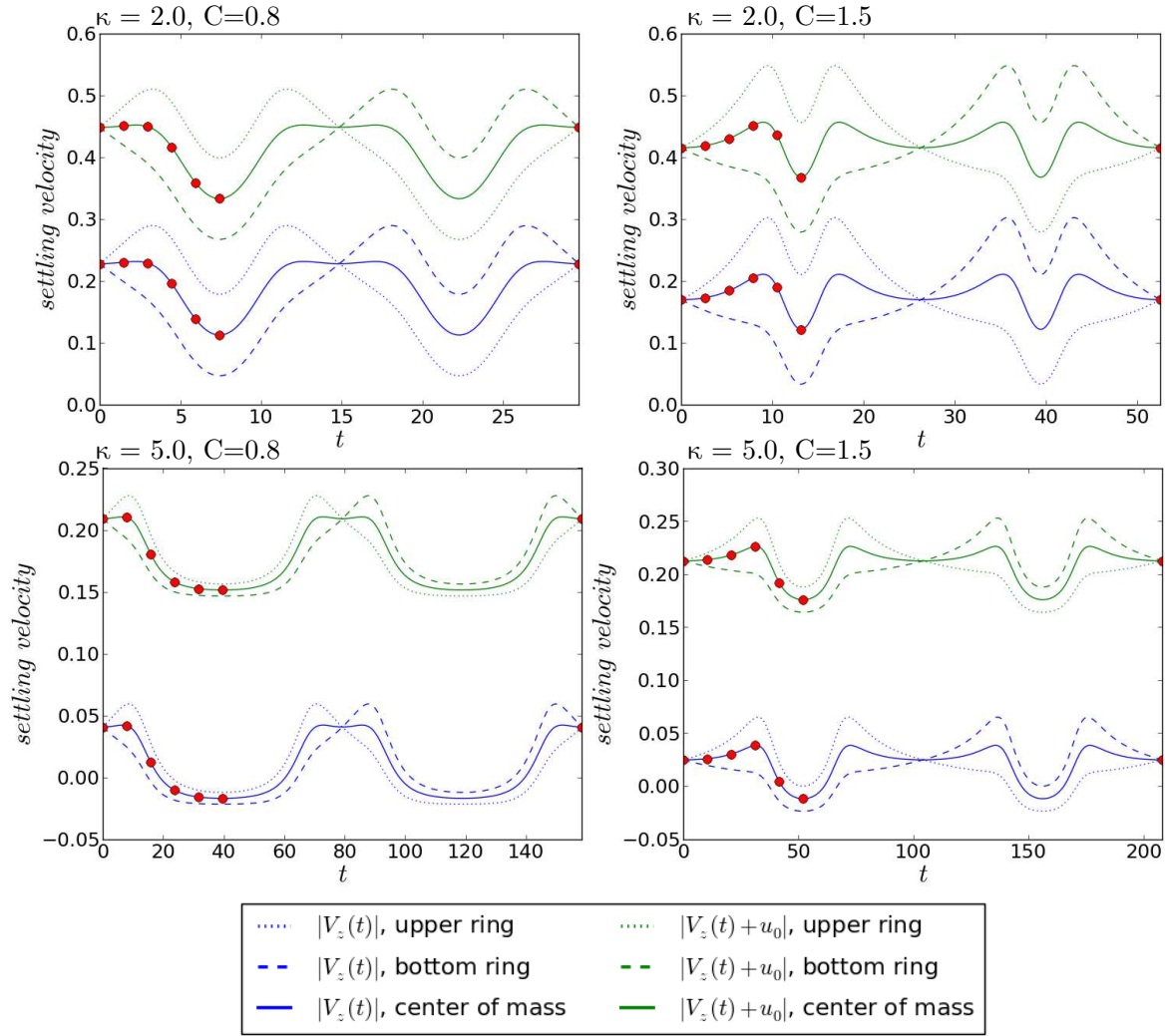
Figure 5.3: The settling velocity $|V_z(t)|$ (blue lines) and $|V_z(t) + u_0|$ (green lines) of each ring and the centre-of-mass of two rings, $M = 32$. Left: $C = 0.8$, right: $C = 1.5$. The time-points of $T/20, 2T/20, 3T/20, 4T/20, 5T/20$ are marked with red dots.

Another important factor is the number of particles in the system, M. Similarly as in the Stokes fluid (Section 3.2) trajectories of particles in the system with smaller M are more elongated (as shown in Fig. 5.5 for chosen M). Consistently with the elongation of the trajectories for smaller number of particles, the period of the motion increases, for a given value of κ (see Table 5.2).

Also the shape parameter of initial configuration, C, influences the trajectories as presented in Figure 5.6 for a chosen range. This dependence is very similar to the one for Stokes fluid. Note, however, that we do not examine here values of C close to the critical value of C_0. In Figure 5.3 the settling velocities during the period are shown, for the centre of mass of the cluster and for each ring separately. These velocities depend on the radius of particles a_p (Eq. 5.10). The results are shown for maximal value of the
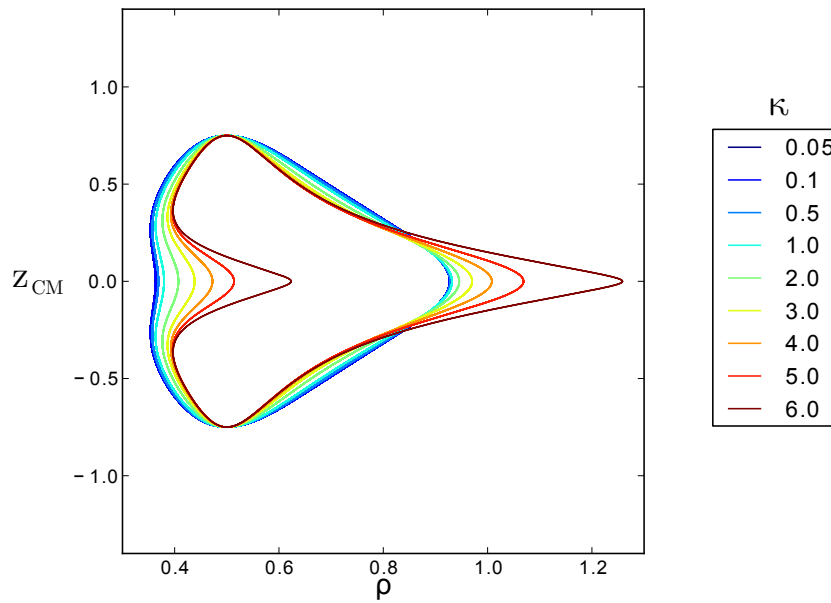
Figure 5.4: Trajectories of particles in the centre of mass reference frame for medium with different permeability coefficient $1/\kappa^2$. Results for $M = 32$ particles and $C = 1.5$.
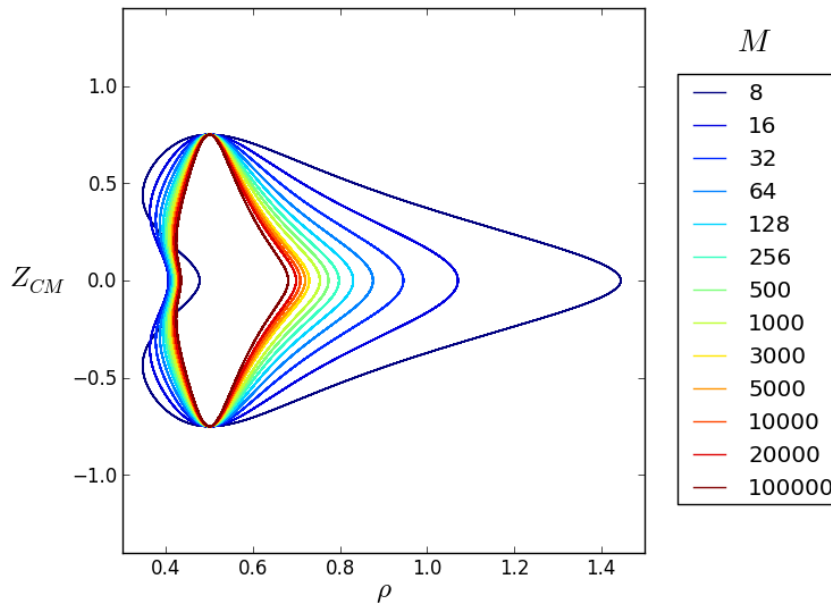
Figure 5.5: Trajectories of particles in the centre of mass reference frame for different number of particles M. Results for $\kappa = 2$ and $C = 1.5$.

radius (the particles touch each other when the ring radius is the smallest during the period) and without the contribution of self-term. For larger κ the difference between instantaneous settling velocities of the two rings is smaller. This tendency is kept for κ much larger than presented in the Fig. 5.3, providing that the motion is periodic (what requires larger number of particles).
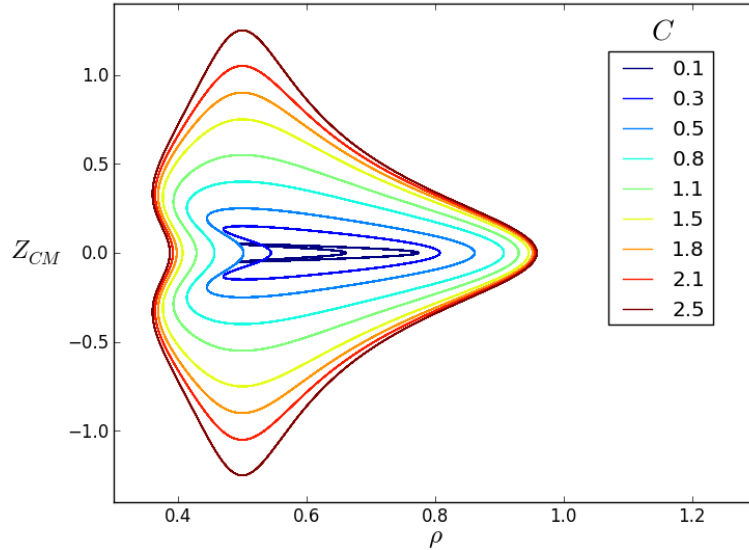
Figure 5.6: Trajectories of particles in the centre of mass reference frame for different values of C. Number of particles $M = 32$ and coefficient $\kappa = 2$.

5.4 Streamlines and fluid velocity field

The natural question is about the streamlines and fluid velocity value around point-particles placed in 2 rings in porous medium. The questions are similar to those which have been asked in Section 2.2.1: are the streamlines closed in the frame of reference comoving with the particles? How does the velocity field look like outside and inside the regular cluster of particles in permeable medium?

The expression for self-term of particle velocity u_0 is presented in Section 5 (Eq. 5.10). Similarly as in the Stokes fluid an important property of the fluid motion is whether the fluid moves faster than the particles or not. The vertical velocity of the fluid in the geometrical centre of mass of the particles is given by the equation:

$$
\begin{aligned}
v_c = \frac{1}{l_1} & \left(h_1(\kappa l_1) + \frac{(z_1 - z_{CM})^2 h_2(\kappa l_1)}{l_1^2} \right) + \frac{1}{l_2} \left(h_1(\kappa l_2) \right. \\
& + \frac{(z_2 - z_{CM})^2 h_2(\kappa l_2)}{l_2^2}
\end{aligned}
\tag{5.16}
$$

$$
l_1^2 = \rho_1^2 + (z_1 - z_{CM})^2 \tag{5.17}
$$

$$
l_2^2 = \rho_2^2 + (z_2 - z_{CM})^2 \tag{5.18}
$$

analogous to the Eq. (4.10).

Figure 5.8 is plotted in the reference frame moving with the centre-of-mass of the particles. It is shown that the fluid streams up through the group of particles. In the reference frame comoving with the settling centre-of-mass, streamlines of stationary

fluid would be vertical and pointing up. Streamlines around particles, presented in Fig. 5.8 show only slight deviation from this state. The alteration of fluid velocity is even smaller than in the Stokes fluid, where $\kappa = 0$ (Section 4). The fluid flow through the middle of the cluster is clearly visible in the figure presenting streamlines (Fig. 5.8) and also in the plot of vertical velocities of fluid and particles (Fig. 5.7) where the absolute value of the settling velocity of the fluid (blue line) is much lower than the one of the particles (black and grey lines). The only exception is the case of $M = 16$, $\kappa = 1$ where velocity of fluid is comparable to velocity of particles with maximal possible radii - this is not observed for the same number of particles but larger κ, $\kappa = 3$. The effect of slower motion of fluid in comparison to the velocity of particles, is stronger for bigger values of κ within the examined range , for which the periodic motions are observed. The direction of changes is consistent with the observed differences between permeable medium and Stokes fluid, equivalent to the limit $\kappa = 0$. More straight streamlines for bigger κ and M indicate also that smaller amount of fluid is dragged with particles.
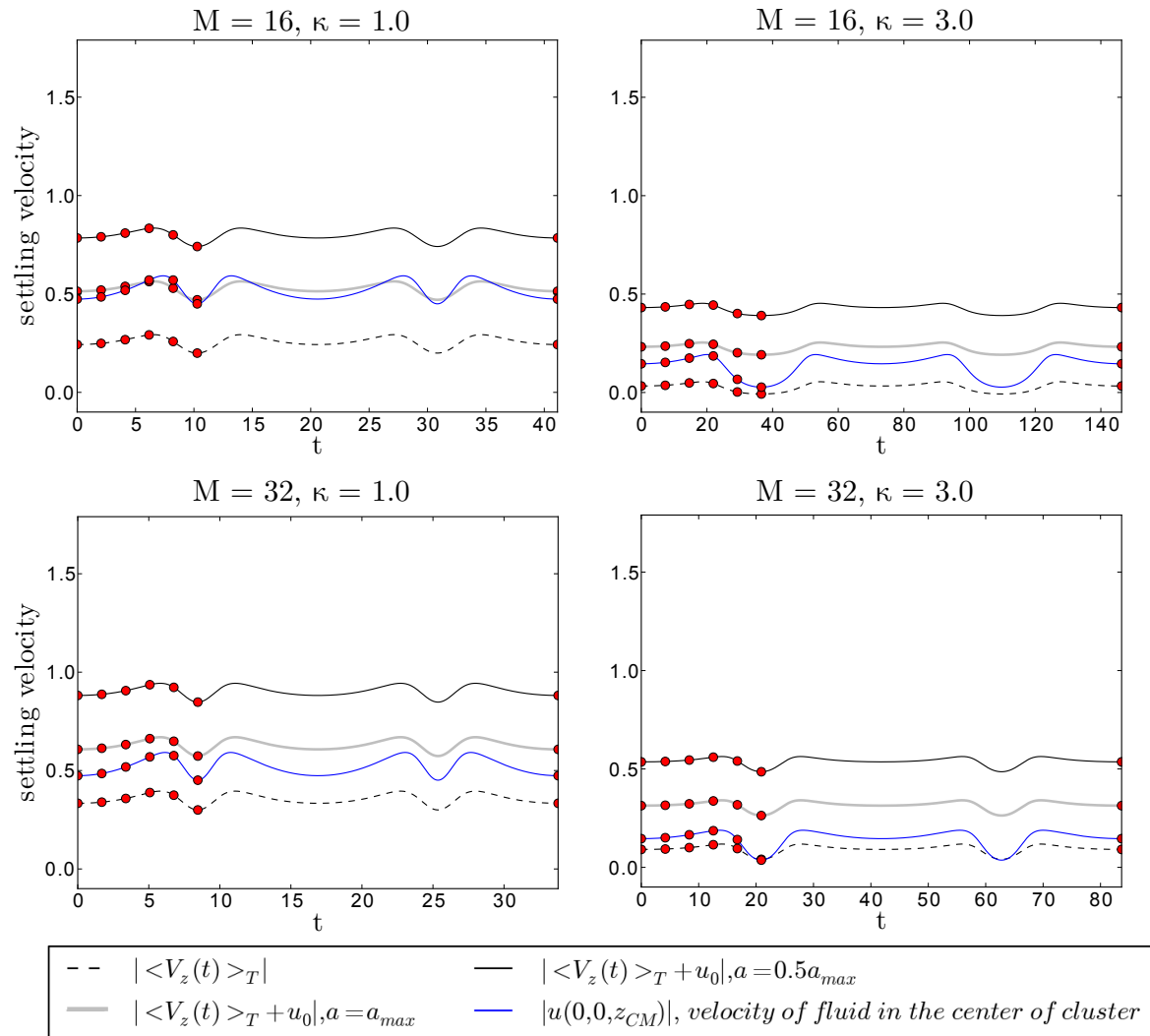
Figure 5.7: Dependence on time: velocity of the fluid (blue line), velocity of the particles without self-term u_0 (dashed line) and velocity of the particles for two different radii: $a_p = a_{p,max}$ (grey line) and $a_p = a_{p,max}/2$ (black solid line); plots for two different values of κ and M, $C = 1.5$. Chosen timepoints are marked with red dots: $t = 0$, $t = T/20$, $t = T/10$, $t = 3T/20$, $t = T/5$, $t = T/4$ and $t = T$.
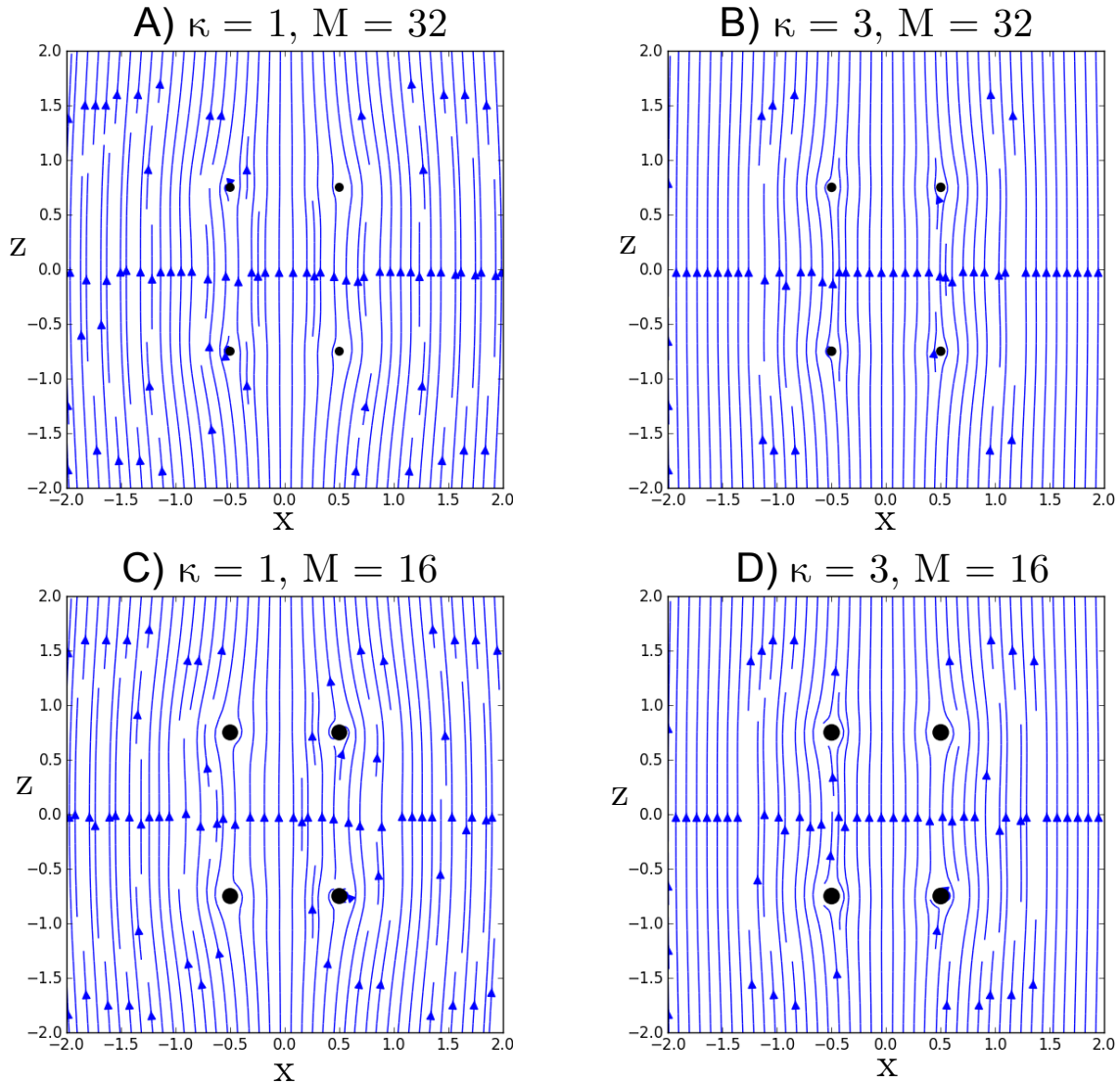
Figure 5.8: The streamlines (in the frame comoving with $\langle V_z \rangle_T + u_0$ presented in Fig.5.7 as black dashed line) around M point-forces for different values of κ and number of particles M: A) $M = 32$, $\kappa = 1$, B) $M = 32$, $\kappa = 3$, C) $M = 16$, $\kappa = 1$, D) $M = 16$, $\kappa = 3$. Positions of particles are marked with dots, drawn to scale. Parameter $C = 1.5$ and particles size a_p is equal to half of the maximal value, when they would touch each other. The streamlines are almost vertical and are getting even more vertical for larger κ (smaller screening length $\frac{1}{\kappa}$).

Chapter 6

Dynamics of 4 rings in a viscous fluid

6.1   Three-parameter family of initial configurations

In Section 3.1 we considered one-parameter family of initial configurations - the system consisting of 2 rings. In this Section we introduce the system with $K = 4$ (what refers to the number of rings as discussed in Section 2.1.2). The positions of particles in each ring are given by Eqs. (2.10) - (2.12).

The symmetrized dynamics of 4 rings is given by Eqs. (2.13) - (2.15) with $K = 4$ and $M = N \cdot K$. The initial configuration of system with 4 rings can be considered as a modification of the one investigated in case of 2 rings (Section 3.1). Rings 1 and 3 are analogous to the system presented before: initially they are placed one above the other, their diameter is equal to 1 and vertical distance between them is denoted as C. The other two rings, number 2 and 4, are initially placed in the plane $z = 0$ and their radii are denoted as R_2 and R_4, respectively. The angular coordinates of particles from rings 2 and 4 are shifted by $4\pi/M$ with respect to the particles from rings 1 and 3. This configuration with symmetrization implies that the particles will have no azimuthal component of velocity during the motion, what is also imposed by the model applied in this work.

Initial configuration of the system for a given number of particles is described by three parameters: C, R_2 and R_4, what can be seen in Figure 6.1. Initial positions
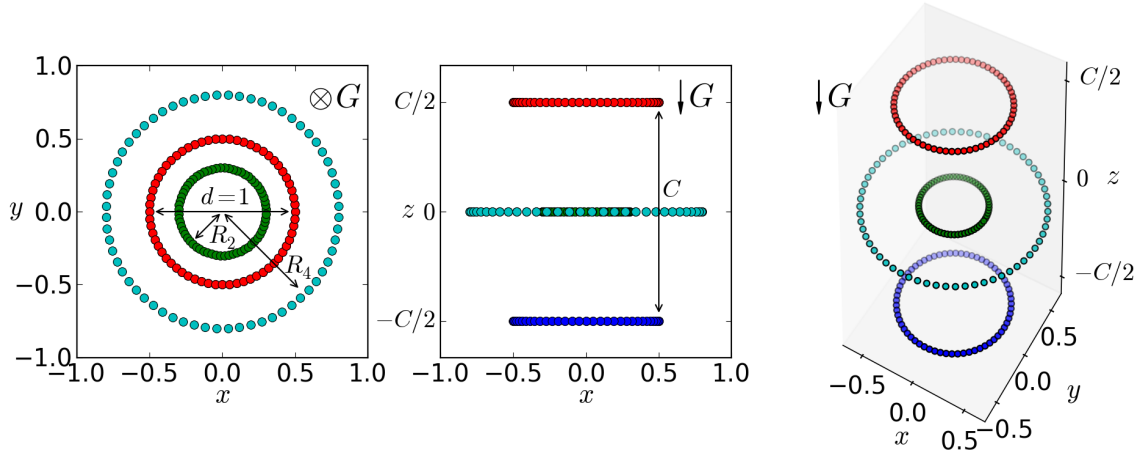
Figure 6.1: Initial configuration of the system of $M = 256$ particles. The coordinates are given by Eqs.(6.1) - (6.4). C, R_2 and R_4 are three parameters of initial configuration for a given number of particles. Top, side and 3D views are presented. Reprinted from [86].

$\boldsymbol{r}_i = (\rho_i, \phi_i, z_i)$ of the particles $i = 1, \ldots, M$ are given by [86]:

$$\boldsymbol{r}_{4n-3} = \left(\frac{1}{2}, \frac{2\pi(n-1)}{N}, \frac{C}{2} \right), \tag{6.1}$$

$$\boldsymbol{r}_{4n-2} = \left(R_2, \frac{2\pi(n-1)}{N} + \frac{\pi}{N}, 0 \right), \tag{6.2}$$

$$\boldsymbol{r}_{4n-1} = \left(\frac{1}{2}, \frac{2\pi(n-1)}{N}, -\frac{C}{2} \right), \tag{6.3}$$

$$\boldsymbol{r}_{4n} = \left(R_4, \frac{2\pi(n-1)}{N} + \frac{\pi}{N}, 0 \right). \tag{6.4}$$

with $n = 1, ..., N$ and $N = \frac{M}{4}$.

6.2   Analysis of decay of the group of particles

6.2.1   General description of dynamics of 4 rings of particles

In Section 3 we discussed the dynamics of 2 rings of particles. Here we will present the dynamics of system consisting of 4 rings of particles with initial configuration shown in Section 6.1. The equations of symmetrized dynamics of 4 rings are given by Eqs. (2.13) - (2.15) with $K = 4$. The main observation is that depending on the initial parameters the dynamics can be different: the system breaks up immediately,
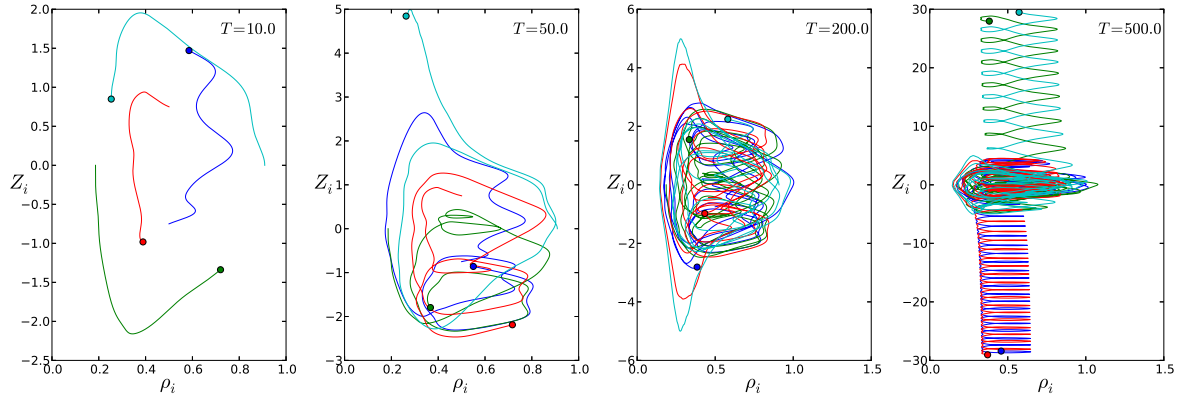
Figure 6.2: The trajectories of 4 particles (each from a different ring) in the centre-of-mass reference frame for different time intervals (from 0 to t as indicated) and $C = 1.5$, $R_2 = 0.186$ and $R_4 = 0.909$. The cluster breakage is visible at the last right plot. Different colours correspond to trajectories of different particles. Dots indicate particles positions at time t.
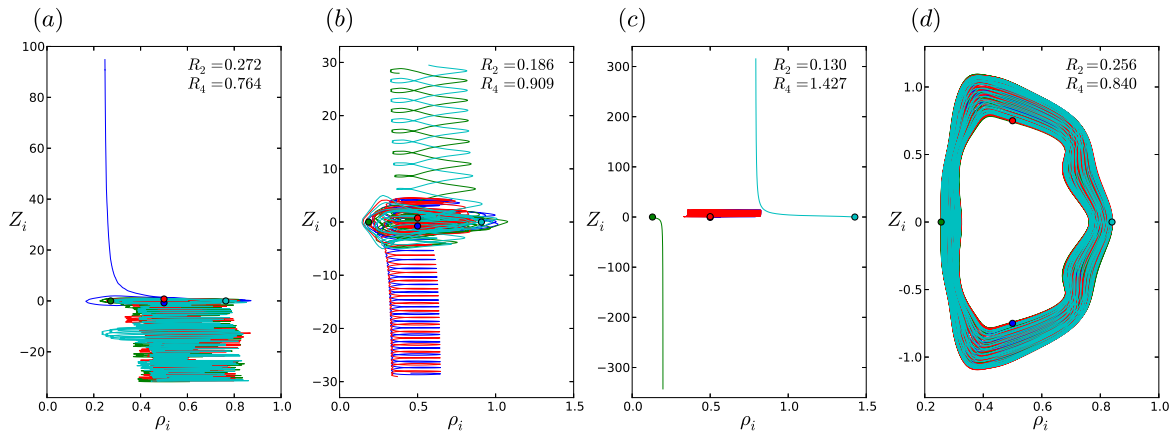
Figure 6.3: Trajectories of particles in the system of 4 rings. Trajectory of each ring is marked with a different colour. Unlike in Figure 6.2, dots represent initial positions of particles. Simulations were performed for $M = 256$ particles and $C = 1.5$. Four main scenarios of the dynamics are presented: (a) One of the rings separates from the cluster. (b) The group breaks up into two pairs of oscillating rings - one of them falls faster than the other. (c) The cluster breaks up into one pair of oscillating rings and two single rings. (d) lack of decay, quasiperiodic motion during the whole simulation time. In all cases the trajectories are plotted for the first 500 time units of the dynamics. Reprinted from [86]

after some time or stays together till the end of simulation time. The breakage of the system looks differently depending on initial parameters.

To effectively illustrate the dynamics at selected time intervals we plot the trajectories of particles (4 particles each from a different ring) in the centre-of-mass frame

increasing the time of observation. The results are shown in Figure 6.2. One can
see that at the beginning all particles move not far away from each other, until time
$t = 200$ rings stay together (Fig. 6.2C). For $t = 500$ we observe that two rings of
particles separate from the others: the system breaks up (see Fig. 6.2D).

When considering the symmetrized dynamics during the whole simulation time, a
few scenarios are observed, presented in Figure 6.3. Some rings may separate from the
rest: one ring separates from the other three (Fig. 6.3 a)), two pairs of rings separate
from each other (Fig. 6.3 b)), or two rings independently separate from one oscillating
pair of rings (Fig. 6.3 c)) . The next observed scenario of the dynamics is quasiperiodic
(or in limiting case periodic) motion during the whole simulation time (Fig. 6.3 d)) .

Analysing exemplary trajectories presented in Figure 6.3 it becomes clear that the
analysis of decay of the cluster is an essential characteristic of the dynamics. In the
following sections I will discuss what criterion should be use to accurately define this
event.

6.2.2   Discussion of existing criteria for break-up of a group of particles

An objective criterion of cluster decay is required to accurately characterise the dy-
namics presented in the previous paragraph. Usually in this kind of problems distance-
based criteria are applied. Janosi et al. [39] used a maximal vertical distance between
particles as the condition of decay, for a group consisting of 3 particles. The thresh-
old was set to 100 times the particle radius a_p. Although simple and convenient, this
approach was shown not be adequate in relatively innumerous, but important cases
of dynamics where the particles are temporally separated by longer distance but later
come back and form the group again [98]. Ekiel-Jeżewska and Wajnryb have proposed
an alternative criterion [98], which takes into account the relative distances between
particles of the group and uses the knowledge of the typical pattern of the decay: it is a
single particle that is left behind and the remaining pair settles faster. In consequence,
it is not allowed that the cluster break-up into a doublet (pair of particles with the
closest distance) at the top and a singleton at the bottom, because this configuration
can not be kept - pair of particles will always settle faster than a single one. The new
criterion was formulated as following: 1) both particles from the doublet, defined as in
previous sentence, must be below the singleton, 2) the vertical distance between lower
particle from the doublet and the singleton is 3 times longer than distance between

particles from the doublet. Apart from being adequate in cases were the distance-based criterion fails, this improved method allowed also to reduce systematic overestimation of interaction time between particles [98]. Criterion described here, applicable for system of 3 particles, cannot be simply generalised the case of many particles. Thus a new criterion is necessary.
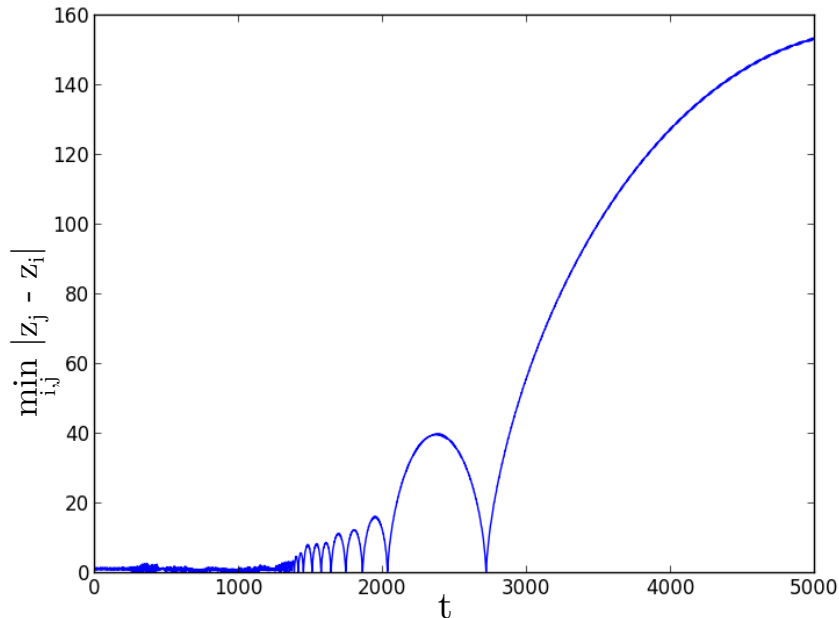

Figure 6.4: The time-dependent maximal vertical distance between the particles (distance between the top and the bottom rings), for a chosen initial configuration: $C = 1.5$, $R_2 = 0.3$, $R_4 = 0.712$. In this type of dynamics distance-based criteria of the decay are likely to fail, because although the vertical size of the group temporary reaches high values, hydrodynamic interactions between rings are still non-negligible and particles may come back again.

For the case of the system of four rings, presented in this dissertation, applicability of both described methods was analysed. Data presented in Figure 6.4 show that distance-based criterion would suffer from similar drawbacks as in the case of three particle system studied by Janosi et al. [39]. For quite a number of initial configurations the vertical distance between rings can be temporary very large, before decreasing again to the values typical for quasi-periodic motions.

As mentioned before, a method based on geometry of the cluster and some knowledge about the dynamics might be more successful in indicating the moment of break-up of the group. However, in the case of complex dynamics of four rings system formulating such a criterion would be a challenging task. Unlike in the system of three particles, a single ring that separates from the group can settle either slower or faster

than the rest of the cluster, depending on its radius. There is no evident relation be-
tween the geometry of the group and its decay. Taking into account these limitation a
new criterion of decay is needed to describe the dynamics.

6.2.3   Formulation of a new criterion for break-up

As described in section 6.2.1 the cluster decay is one of the observed scenarios of the
dynamics in the system consisting of 4 rings (e. g. Fig. 6.5). Therefore the question
appears how to define the event of the cluster decay? The examples of long-living
clusters show that the particles perform relative oscillations. This observation lead
us to investigation of oscillations within pairs of particles. To determine the cluster
lifetime τ we introduce a new criterion based on relative distances between oscillating
pairs of rings. The first step is to determine if the rings i and j oscillate within a pair.
To achieve this we investigate the difference in their z coordinates, $\Delta z_{ij} = z_i - z_j$. If
this value oscillates around zero and has repeating roots we denote that the rings i and
j belong to the same group. We assume that the time interval between consecutive
roots cannot be arbitrary large and a certain threshold is set.If these conditions are
full-filled we define that rings i and j stay together.

Thus we apply this idea of belonging to the same group to construct the definition
and determine the cluster decay. For each pair of rings $i, j \in \{1, 2, 3, 4\}$ and $i \neq j$ we
calculate the difference of their z coordinates Δz_{ij} as a function of time. The maximal
allowed time interval between consecutive roots is set to 1000. If this value is exceeded
we denote that specific pair of rings i and j is separated. The time referring to the last
root of Δz_{ij} before separation will be denoted as $t_\alpha(i, j)$. The time of cluster decay is
determined as:

$$\tau = \min_{i,j} t_\alpha(i, j), \tag{6.5}$$

what means that the moment of decay is defined as the time when one pair of rings
stops to oscillate. Such an event is always followed by lack of oscillations in some of
other pairs: e.g. when ring number 1 separates from the rest, there are no oscillations
between this ring and any of the others - in result there are no roots in functions Δz_{12},
Δz_{13} and Δz_{14}.

To better illustrate our criterion of the cluster decay we applied it to the example
shown in Fig. 6.4. In Figure 6.6 we present Δz_{ij} dependence on time for each pair
of rings. It is visible that in four pairs of rings (Fig.6.6 A, B, E, F) the function
Δz_{ij} has repeating roots only until specific time during the whole simulation, but in
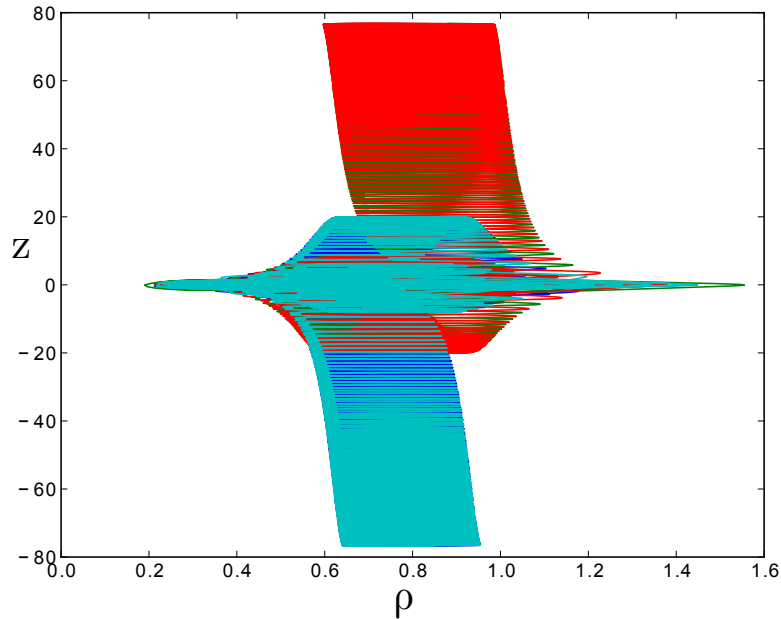
Figure 6.5: Trajectories of 4 particles (each from different ring) in the centre-of mass reference frame, for the same system as in Fig. 6.4 and Fig. 6.6. Decay of the cluster is clearly visible, with two pairs of rings oscillating together: rings number 1 and 4 (blue and cyan) in one pair and 2 together with 3 (green and red) in the other.

case of Fig. 6.6 C, D till the end of simulation time. The cluster lifetime $\tau = 2715$, determined according our criterion, is marked with green line. It accurately indicate the time up to when all rings form a group [1]. It works better than distance-based criteria because it is not mislead by temporary large distance between rings which still oscillate, so their interactions are relevant for description and cannot be neglected. Similarly as the method introduced by Ekiel-Jeżewska and Wajnryb [98] this criterion builds on fundamental features of the dynamics, what may result in better capturing of its important aspects. The criterion presented in this chapter not only allows to determine the decay of the cluster but also type of decay (as discussed in Section 6.2.1). It will be carefully discussed in the next section.

6.2.4   Criterion of types of decay of a cluster

Classifying type of decay allows to better characterise the dynamics. Different possible scenarios of decay were presented in Figure 6.3 A, B, C. The approach based

---

[1]The algorithm presented here is not perfect and there exist some cases which it can be misclassified as a decay. However, because this criterion is based on fundamental features of dynamics of the system, it works much better than distance-based criteria and, in contrast to them, is accurate in vast majority of the cases.
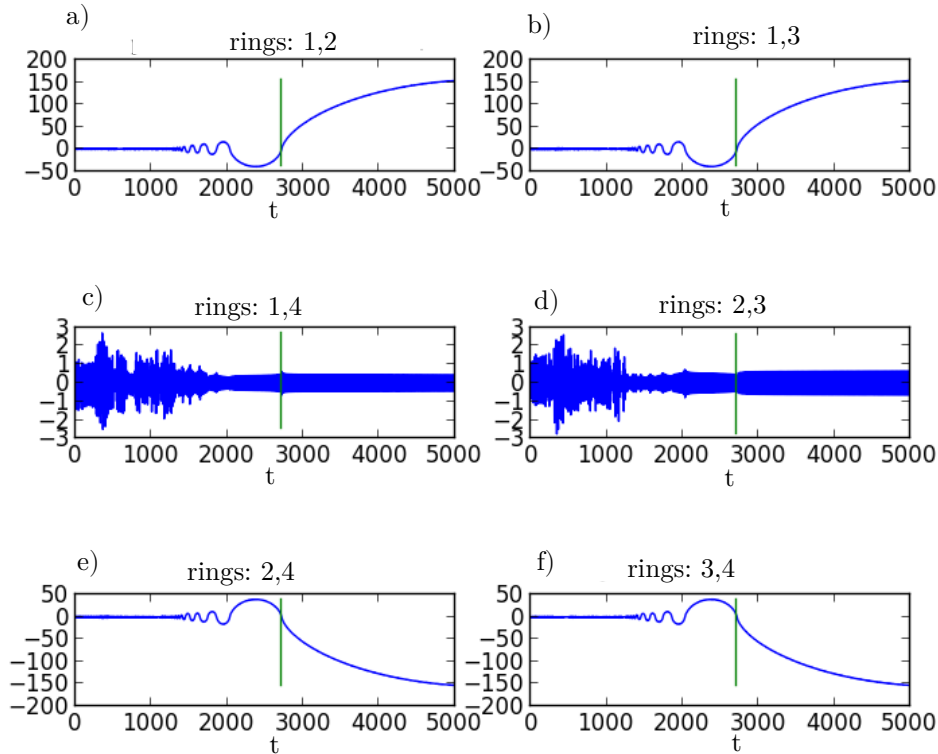
Figure 6.6: Difference of vertical positions between particles Δz_{ij} as a function of time. The subplots are drawn for each pair of the rings. The green vertical line denotes the cluster decay time $\tau = 2715$.

on relative oscillations between pairs of rings enables us to distinguish between them in unambiguous way. In the dynamics of presented system oscillations between rings may be identified with non-negligible hydrodynamic interaction, significant for the dynamics. Following this observation, if the cluster breaks up into subgroups, rings belonging to the same subgroup will perform oscillations (what implies that function Δz_{ij} has repeating roots). Different types of decay will result in different number of oscillating pairs: the decay '3+1' (one ring separates from the other three, Fig. 6.3 A), corresponds to 3 pairs of oscillating rings. The decay '2+2' (decay into two pairs of oscillating rings, Fig. 6.3 B) corresponds to two oscillating pairs and '2+1+1' type of decay (decay into one pair of oscillating rings and two single rings, Fig. 6.3 C) to a single oscillating pair.

The distinction between different types of decay cannot be defined in the exact moment marked as the decay time, since definition in Eq.(6.5) in general means that at time τ only one pair of rings does not oscillate anymore. We have chosen the interval of 1000 time units $[\tau, \tau + 1000]$ as the interval when the type of decay will be identified. This interval is shorter if $\tau + 1000$ exceeds the simulation time. During this interval we consider a pair of particles i and j as belonging to one group if the number of roots

is not smaller than 5. If the interval is shorter than the one given above, we demand the number of roots to be proportionally smaller.

As an example let's consider the case presented in Fig. 6.6. One can observe that all pairs of rings except of pairs $(1, 4)$ and $(2, 3)$ are separated, what manifests in lack of roots of function Δz_{ij} in the last part of simulation time. Our criterion is insensitive to temporal increase of the distance between rings (what can be missed using distance-based criterion presented in Section 6.2.2). Applying our criterion we classify the cluster decay as a '2+2' type of decay. Further analysis of type of decay and cluster lifetime for different initial configurations will be discussed in the next section.

6.3 Dependence of the cluster lifetime and types of decay on the initial configuration

6.3.1 Maps of type of decay for different initial configuration

After formulation criteria of cluster lifetime and type of decay let us investigate how these characteristics depend on the initial configuration parameters R_2 and R_4, with parameters C and M fixed to $C = 1.5$ and $M = 256$. The parameters R_2 and R_4 are examined within ranges $[0.002, 1.2]$ and $[R_2 + 0.002, 1.4]$, respectively, with the resolution 0.002. We investigate only the region for which $R_2 < R_4$ because the opposite situation would correspond to permutation of indices of the rings 2 and 4. The scheme of the system is recalled in Fig.6.7 with colours corresponding to the labels of the rings. The results of cluster lifetime are presented in Figure 6.8. The map is plotted in logarithmic scale and colours correspond to different values of the cluster lifetime: the shortest lifetime refers to the darkest blue colour and the longest one (till the end of simulation time $t = 5000$) to the dark red colour. On bottom right of the figure the zoom of a chosen fragment of parameter space is drawn. In Figure 6.9 the maps of types of decay are shown. Figure 6.9A presents the dependence of the type of decay (as defined in Section 6.2.4) on the initial conditions. Figures 6.9 B,C and D present details of the particular types of decay: '3+1', '2+1+1', '2+2' respectively. In Figure 6.9B the colour denotes the label of the ring which separates from the others. In Fig. 6.9C the labels of rings which oscillate within a pair are indicated. In Fig. 6.9D the labels of oscillating pairs of rings are denoted. The enlarged parts are drawn for the same parameter range in all subplots.
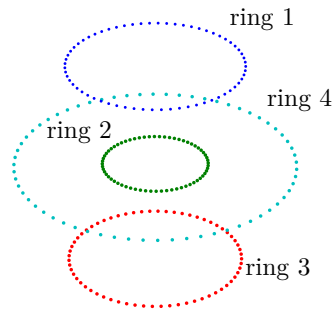
Figure 6.7: The scheme of the studied system with labels of ring numeration.
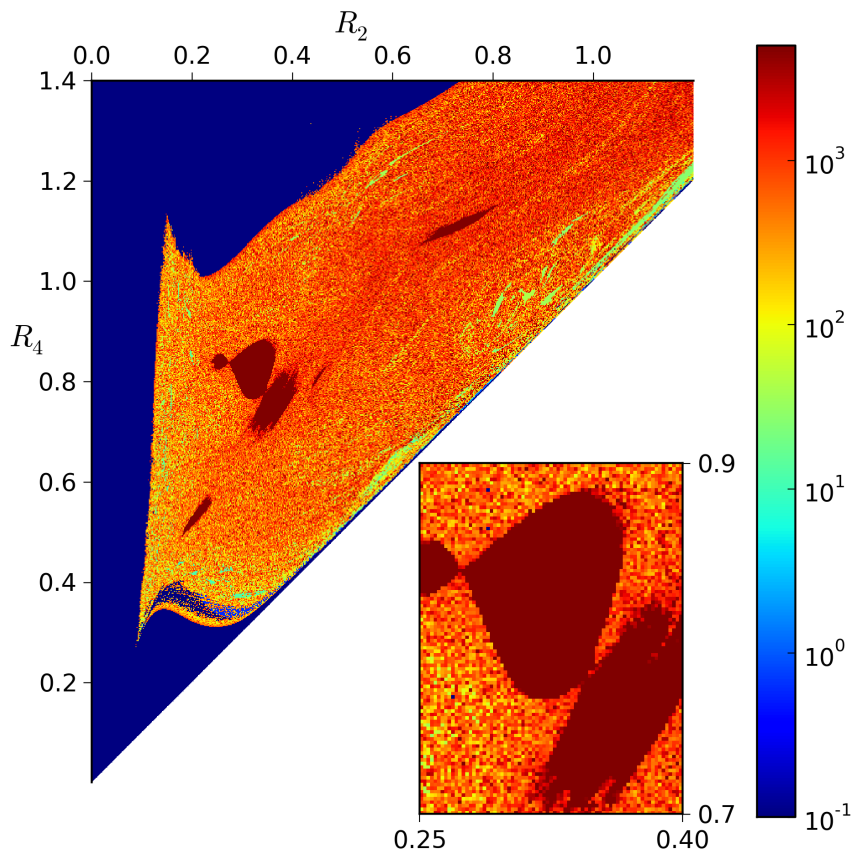
Figure 6.8: Cluster lifetime τ for around 240 000 different initial configurations with R_2 and R_4 parameters in range $[0.002, 1.2]$ and $[R_2 + 0.002, 1.4]$, respectively. Simulations were performed for $C = 1.5$, $M = 256$ and simulation time $t = 5000$. The darkest red colour indicates that the group does not break up during simulation. Resolution of the map is equal to 0.002×0.002. Reprinted from [86].

In Fig.6.8 the regions where cluster breaks up immediately or after a very short time are located in the left, top-left and bottom parts of the map [86]. The region on
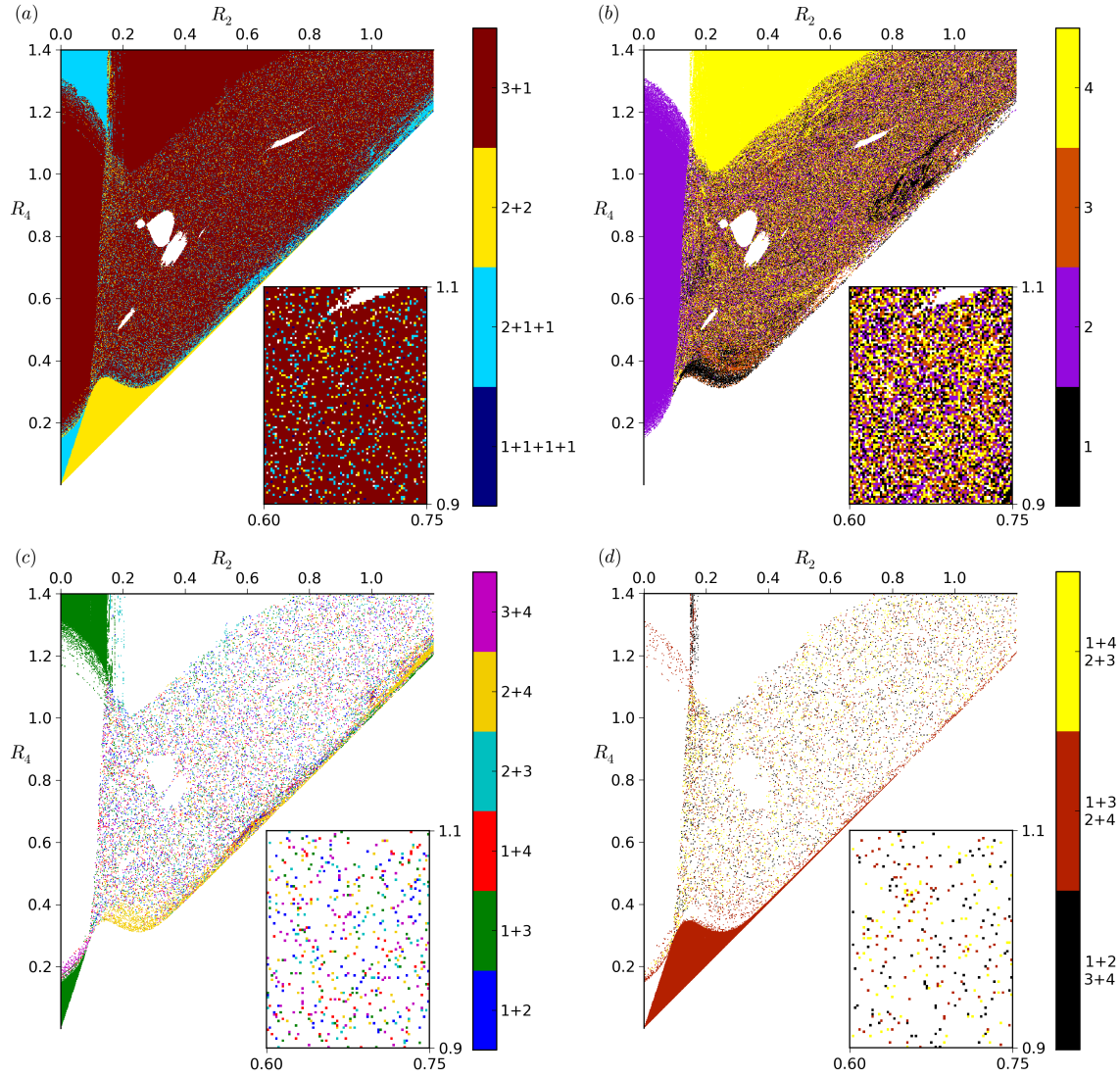
Figure 6.9: Dependence of patterns of the cluster decay on the initial configuration parameters R_2 and R_4 , for $C = 1.5$ and $M = 256$. (a) Different types of decay: '3+1', '2+2', '2+1+1', or '1+1+1+1', as described in Section 6.2.4. (b) '3+1' type of decay: the colour indicates the label of the ring that separates from the other three. (c) '2+1+1' type of decay: the colours indicate the labels of the interacting pair of rings after decay. (d) '2+2' type of decay: the colours indicate which rings form interacting pairs after decay. Reprinted from [86].

the left (small R_2) corresponds mainly to '3+1' decay where ring number 2 separates (Fig. 6.9A and B). Small radius of ring 2 results in its high settling velocity and in consequence separation of this ring below the others. Similar mechanism is responsible for a quick decay of the cluster for large R_4. Large radius of ring 4 causes its weak interactions with the others and much lower settling velocity. As a result ring number

4 separates and stays above the group (Fig. 6.9A and B). Situation for the top-left corner of the map in Fig. 6.8, where '2+1+1' type of decay takes place (see Fig. 6.3C), corresponds to a mixture of described scenarios: ring number 2 with small radius settles faster than the rest of the group, while ring number 4 separates due to its lower settling velocity. For relatively small values R_2 and R_4, and R_4 only a little larger than R_2, the decay '2+2' is observed (see Fig. 6.3B). In this case rings 2 and 4 are close to each other and oscillate together. Due to small radii and short distance between each other, this pair of rings settles down much faster than rings 1 and 3, and the decay of the group takes place. Apart from compact regions described above for the main area of the parameter space both lifetime and type of decay are very sensitive to a small change of the initial parameters. Sensitivity to initial conditions will be further discussed in Section 6.3.2. Although in the central part of the map, in general colours change significantly from point to point, there exist also distinct, uniform bands. In Figure 6.8 they are visible most clearly for values of R_2 similar to R_4. In case of types of decay the bands are most pronounced in bottom-left and top-right parts of Fig.6.9B (black ones) and at the bottom edge of Fig.6.9C (yellow colour). The discussion of regions where the cluster does not break up (white ones) will be presented in the next section.

To quantitatively describe the possible types of decay one can summarise the total number of decays of each type. The most common one is '3+1' type (78.4%), the second is '2+1+1' (10.8%) and the third one is '2+2' (7.6%). Configurations that do not lead to decay during simulation time are relatively infrequent: 3.2%. There are also a tiny number of decays ($< 0.01\%$) classified as '1+1+1+1' type of decay, where none pair of the rings oscillates after decay. In most cases for such trajectories at least two rings stays closely together, although they do not oscillate.

We investigated whether quasiperiodic trajectories converge to an limiting one, either contrary: become wider with time. It turned out that quasiperiodic trajectories do not converge to any specific one. Trajectory width in majority of cases is reached relatively quick and rings oscillate many times without clear sign of expansion. Before decay trajectory usually gets thicker and less regular. This findings suggest that there is no attractor (except for not excluded possibility of strange attractor) nor repeller in this system.

For chosen parameters for which the group stays together till the end of simulation, additional much longer simulations were perform, up to $t = 100000$. This times correspond to more than 5000 quasiperiods. Even for such a long time in majority of cases

no decay is observed. Parameters (R_2, R_4) for which decay time $5000 \leq \tau < 100000$ in map presented in Fig. 6.8 are represented by isolated non-decaying configurations or lay close to the borders of long-lifetime regions. Parameters corresponding to interior of these long-lifetime regions lead to quasiperiodic motions which do not decay up $t = 100000$.

6.3.2 Sensitivity to the initial conditions

The map of cluster lifetimes can be considered in analogy with the one obtained by Janosi et al. [39] for the system of three particles. Similarly as in the system presented in this dissertation, also in work by Janosi et al. there were two variable parameters of initial configurations, namely vertical and horizontal coordinates of one particles, with fixed positions of the other two. The pattern observed by the authors was fractal structure of regions with similar lifetime. Inside fractal bands there exist homogeneous deterministic regions with almost uniform lifetime. In other places a fine-scale fractal structure can be find with very high sensitivity on initial configuration. Having in mind this picture as an analogy, let us discuss results obtained in the system of four rings.

As illustrated in Figure 6.8 the cluster lifetime changes significantly from point to point with a slight change of R_2 and R_4, apart from a few deterministic regions discussed in the previous section. This variability is also visible in Fig.6.9 which presents different types of decay. To investigate this sensitivity, in this section we will present a cross-section through the map of cluster lifetime as well as zoom of a chosen region of the map of cluster lifetime.

In Fig.6.10 lifetimes with the same value of R_2 and different R_4 (and vice versa) are presented (cross-section through the map of cluster lifetime presented in Fig.6.8). The high sensitivity to initial conditions is observed for most of the points from parameter range. The deterministic region of long lifetime $\tau = 5000$ for $R_4 \in [0.71, 0.9]$ is visible in Fig.6.10a) (compare to the darkest red colour in Fig. 6.8). For large values of R_4 the cluster breaks up immediately what corresponds to τ approximately equal to 0. In Fig.6.10b) for small values of R_2 the lifetime is extremely short. In the other part of the range of R_2, τ is highly variable. Significantly longer lifetimes for $R_2 \sim 0.35$ correspond to the area close to the main long-lifetime island. Increasing the resolution of R_4 a self-similar structure is found (highly variable, with both short and long times of decay), what is shown in the inset of Fig.6.10a). Unlike in the map obtained by

Janosi et al. [39] , there are no deterministic bands what is a significant difference. Fractal structure is not visible and high sensitivity to initial configuration is present for almost entire range of parameters values.
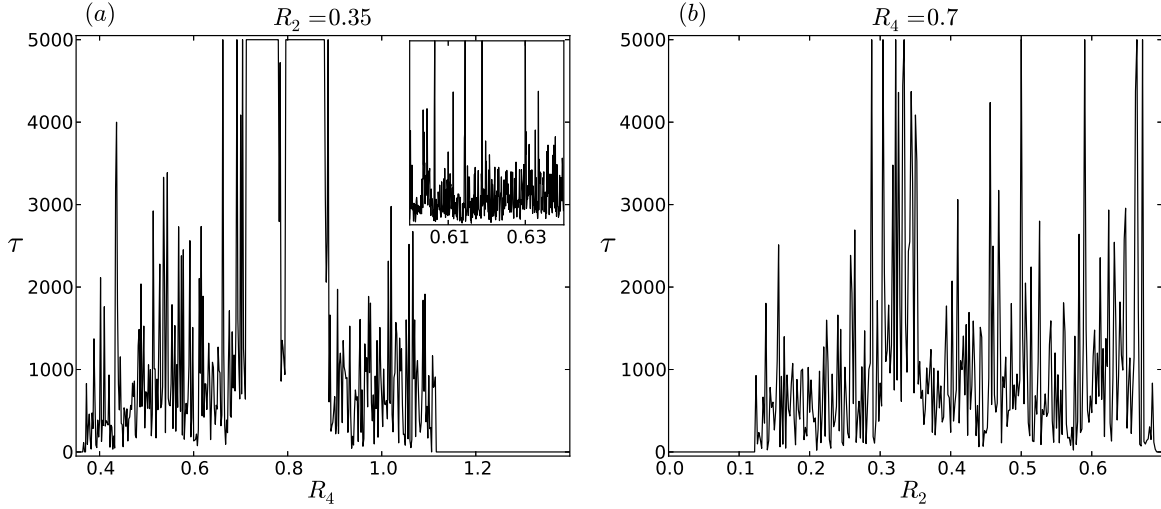

Figure 6.10: Cross-section through the map of the cluster lifetime presented in Fig. 6.8 (resolution: 0.002): a) $R_2 = 0.35$, b) $R_4 = 0.7$. Inset with the higher resolution 10^{-4}. Analogous figure for different values of the parameters R_2 and R_4 can be found in [86].

To further explore sensitivity of the dynamics to initial conditions, additional simulations were conducted for a chosen range of R_2 and R_4. Values of R_2 and R_4 were sampled with higher resolution than before: for the region $R_2 \in [0.45, 0.55]$, $R_4 \in [0.8, 0.9]$ the resolution was 0.001×0.001 , and $10^{-4} \times 10^{-4}$ for the sub-region $R_2 \in [0.495, 0.505]$, $R_4 \in [0.845, 0.855]$. The region was chosen next to the borders of long-lifetime island to have a closer look on the dynamics near irregular borders of the island.

In Figure 6.11 decay times are presented for systems with R_2 and R_4 parameters from described ranges. The region of long-lifetimes is visible in bottom-left corner of the Fig.6.11A. Outside from the island area (where $\tau > 5000$) we can observe that decay times are highly variable, and it is not unusual that long-living configuration are neighbours of configurations with very short lifetime, e.g. below 500. However, apart from this variability one can see that there exist regions, were concentration of configurations with short- or long decay times is larger: in the bottom-right corner there are more blue pixels (short-living clusters) whereas along the line approximately between points $(0.48, 0.84)$ and $(0.52, 0.9)$ there are more configurations with long lifetime (red and brown colours), but there is also a smaller number of configurations with short lifetime. It illustrates, that the variability of decay time in parameters space is a multiscale phenomena, with both very short (ΔR_2, $\Delta R_4 < 0.001$) and moderate
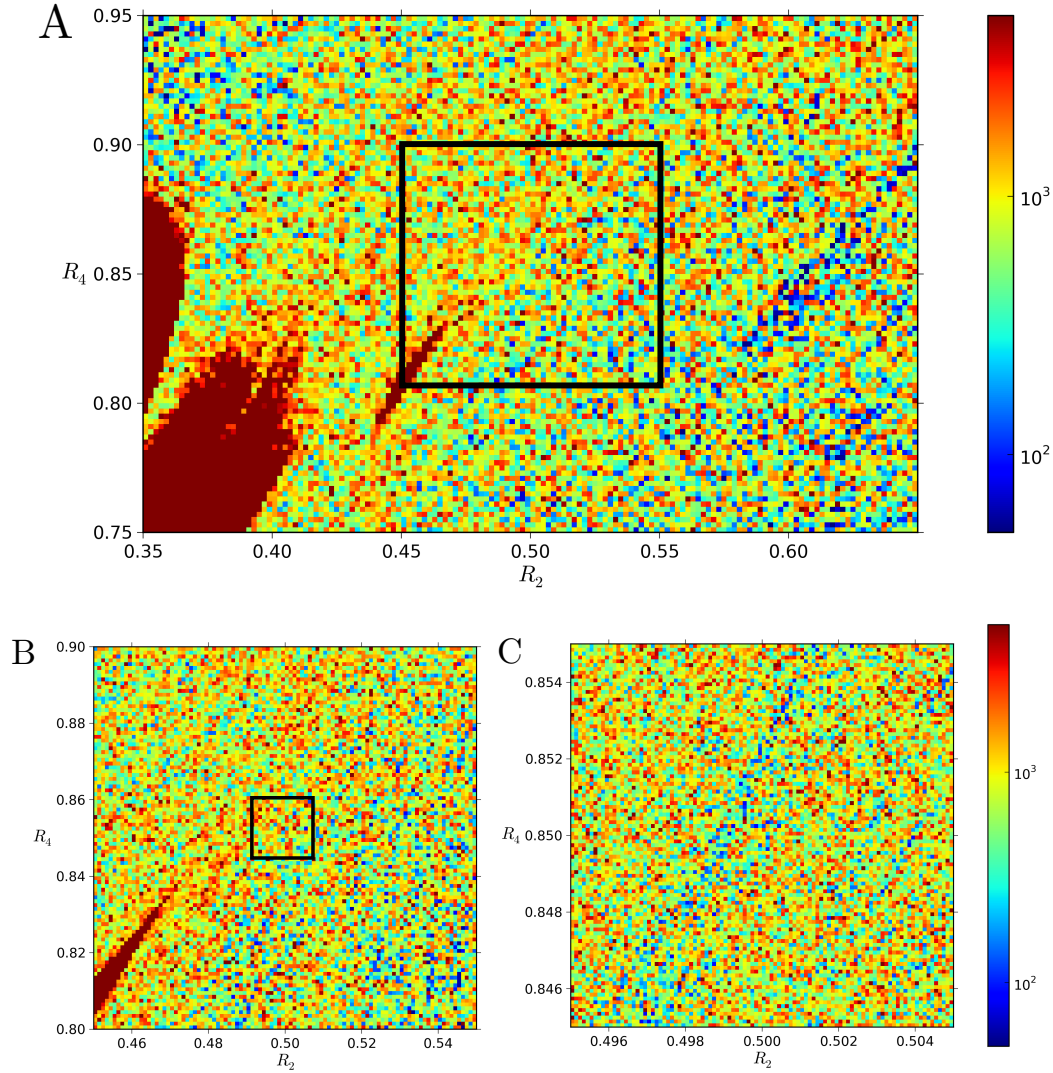
Figure 6.11: Cluster lifetime τ for different initial configurations, $M = 256$, $C = 1.5$. The resolution of initial configuration parameters R_2 and R_4 is equal to 0.002×0.002 for the plot A), 0.001×0.001 for the plot B) which is the zoom of A) and $10^{-4} \times 10^{-4}$ for plot C) (the zoom of plot B). Black rectangles indicate enlarged regions.

length scales. The self-similar structure can be found in each length scale.

Features of the dynamics discussed above are also visible in a finer scale, with resolution $10^{-4} \times 10^{-4}$ (Fig.6.11B). As an example, on the line between points $(0.498, 0.848)$ and $(0.501, 0.854)$ we find a band with significantly shorter decay time. Also neighbouring configurations with very short and very long decay time can be observed.

6.4 Method of quantitative comparison of trajectories of non-decaying clusters

As it was shown in Section 6.3 there exist a few compact regions, in the parameter space, where we observe long-living quasi-periodic oscillations. When examined in the centre of mass reference frame, the trajectories of particles look similar over the time, but are not exactly repeated. In order to find parameters that lead to periodic dynamics (or very close to periodic one) we would need to quantify the changes of trajectory over time, and identify for which R_2 and R_4 they are the smallest (inside long-lifetime regions discussed in Sec 6.3). This would allow to extract the best values of parameters from huge number of performed simulations for which the trajectory is the thinnest. We have approached this task by quantifying similarity of the trajectory in subsequent quasi-periods, which begins and ends at moments when z coordinate (in centre of mass reference frame) of the first ring changes the sign to positive.

A method commonly used to achieve this is Dynamic Time Warping (DTW) which was developed to work with time series data [99]. Depending on the application, different variants of this method are used. In our case we will use One-Way-Distance (OWD), a method which is simplified version of DTW, and was developed to measure similarity of trajectories [100].

First I will briefly discuss DTW method, later OWD, and finally I will present one-way-distance implementation for our specific problem. Dynamic Time Warping allows to determine the closest distance between two time series, with trajectories as a special case [99]. Time series are defined as sequences of observations, e. g. sequence of positions of particles during the motion. Time transformations are allowed for both time series to fit them to each other in the best way. Let's consider two time series we want to compare: $X = (\boldsymbol{x}_1, ..., \boldsymbol{x}_\alpha)$ and $Y = (\boldsymbol{y}_1, ..., \boldsymbol{y}_\beta)$. Let us define the distance function between points $\boldsymbol{x}_i, \boldsymbol{y}_j$:

$$d(i, j) = f(\boldsymbol{x}_i, \boldsymbol{y}_j) \geq 0, \tag{6.6}$$

e. g. $d(i, j) = ||\boldsymbol{x}_i - \boldsymbol{y}_j||$.

Let T denote the number of matches between corresponding points in series X and Y. The main aim is to specify the function $\phi(k)$, $k = 1, ..., T$ (warping curve):

$$\phi(k) = (\phi_x(k), \phi_y(k)), \tag{6.7}$$

$$\phi_x(k) \in \{1, ..., \alpha\}, \tag{6.8}$$

$$\phi_y(k) \in \{1, ..., \beta\}, \tag{6.9}$$

where ϕ_x, ϕ_y denote corresponding indexes of X and Y. The function ϕ defines matches between corresponding points from X and Y series.

Usually it is required for the functions ϕ_x and ϕ_y to meet the following conditions:

1. monotonicity condition: both functions ϕ_x and ϕ_y are non-decreasing,

2. no point from series X and Y is skipped: $\phi_x(\{1, .., T\}) = \{1, ..., \alpha\}$, $\phi_y(\{1, .., T\}) = \{1, ..., \beta\}$,

3. boundary condition: $\phi_x(1) = \phi_y(1) = 1, \phi_x(T) = \alpha, \phi_y(T) = \beta$,

4. points in the warping curve are not repeated: $\phi(k) \neq \phi(k+1)$.

As one can see these conditions allow for multiple match of a single point and imply that $\max(\alpha, \beta) \leq T \leq \alpha + \beta - 2$.

The next step is the calculation of total distance:

$$d_\phi(X, Y) = \sum_{k=1}^{T} d(\phi_x(k), \phi_y(k)). \tag{6.10}$$

Our aim is to minimise the total distance by choosing optimal function ϕ, which meets criteria listed before. The DTW distance given by the expression:

$$D(X, Y) = \min_{\phi} d_\phi(X, Y). \tag{6.11}$$

In order to minimise the cost of computational complexity different some additional constrains are commonly imposed. This will be discussed later in our specific implementation.

One way distance allows to calculate similarity between template trajectory (time series X) and query trajectory (Y). This method can be considered as a case of DTW where:

1. function ϕ_x is defined as $\phi_x(k) = k$, and

2. some points from the query trajectory Y may be skipped.

Property (1) states that distances from all points in template trajectory are used exactly once. The second one means that requirements (2) and (3) for DTW are not valid in OWD calculation.

Let's define the distance between point $\boldsymbol{x}_i$ from template trajectory X and query trajectory Y:

$$D_{point}(\boldsymbol{x}_i, Y) = \min_{\boldsymbol{y}_j \in Y} ||\boldsymbol{x}_i - \boldsymbol{y}_j||. \qquad (6.12)$$

The OWD distance between template trajectory X and query trajectory Y is defined as:

$$D_{owd}(X, Y) = \frac{1}{\alpha} \sum_{i=1}^{\alpha} D_{point}(\boldsymbol{x}_i, Y) \qquad (6.13)$$

In our problem we will need to measure how similar are trajectories in the centre of mass reference frame during subsequent quasi periods. The time series X, which is the sequence of positions of particles during first quasi-periods, is used as the template. Y is the time series representing query trajectory. Vector $\boldsymbol{x}_i$ (or $\boldsymbol{y}_i$) is a vector of positions of particles in $i - th$ measurement time, defined as $\boldsymbol{x} = (\rho_1, z_1, \rho_2, z_2, \rho_3, z_3, \rho_4, z_4)$, where ρ_l and z_l are ρ and z coordinates of particles from $l - th$ ring in the centre of mass reference frame. Trajectory X will be compared, using OWD measure, with each of the trajectories from subsequent completed quasi-periods. The final score is the average of OWD over scores obtained in this manner for all quasi-periods. We will introduce two additional constrains to our algorithm, both commonly used in this type of problem. First is the monotonicity condition, equivalent to the (1) condition for DTW: $\phi_y(k) = n \Rightarrow \phi_y(k + 1) \geq n$. This means that once we match a point from template trajectory to the closest point in the query, the next point from the template can be matched or with the same point in query, or with subsequent ones. Matching with the previous points is forbidden. The second constraint is step size condition: we look for the closest point not within whole trajectory, but only in some neighbourhood $\phi_y(k) = n \Rightarrow n \leq \phi_y(k + 1) \leq n + \frac{1}{50}\beta$. It is imposed to speed up the computation. With these modifications, the point-to-trajectory distance is calculated as follow:

$$i = 1 : \quad D_{point}(\boldsymbol{x}_i, Y) = \min_{j \in \{1, \dots, 1 + \frac{\beta}{50}\}} ||\boldsymbol{x}_i - \boldsymbol{y}_j|| \qquad (6.14)$$

$$i > 1 : \quad D_{point}(\boldsymbol{x}_i, Y) = \min_{j \in \{n, \dots, n + \frac{\beta}{50}\}} ||\boldsymbol{x}_i - \boldsymbol{y}_j||; \quad n = \phi_y(i - 1). \qquad (6.15)$$

Using point-to-trajectory distance as defined above, one way distance between trajectories is calculated with the formula (6.13).

The algorithm described above was applied to the trajectories obtained for a range of R_2 and R_4 parameters around long-living regions. Cases for which decay was observed were omitted. Simulation time was set to 5000, what corresponds to roughly 500 quasi-periods. Since the trajectory is represented as discreet set of points the OWD may not be exactly 0 even for strictly periodic motion. However in our case the

minimal calculated value of OWD is greater than the one expected for periodic orbit.
All maps of OWD are plotted in log scale because the OWD value changes in range
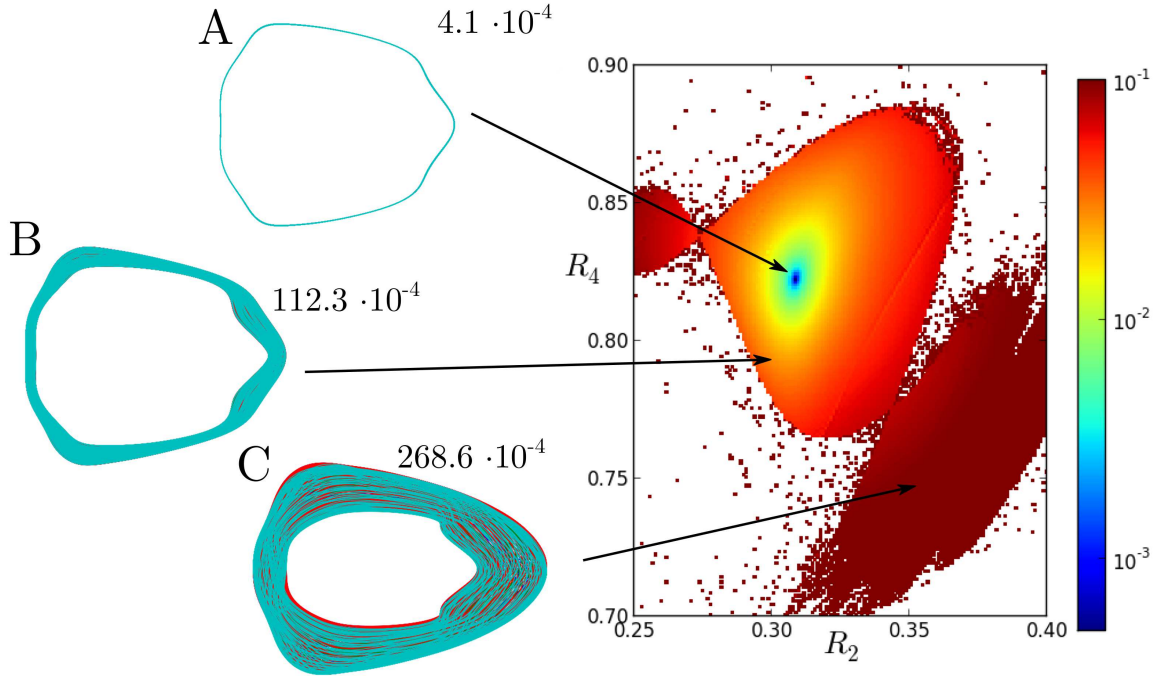$(10^{-1}, 10^{-3})$. The colour in each plot corresponds to the value of OWD.

Figure 6.12: The map of One-Way-Distance (thickness of trajectories) for the first
region of initial parameters which lead to extremely long lifetimes. The values of D_{owd}
are drawn in log scale (the colour corresponds to different values). Three exemplary
trajectories of four particles (each from different ring) in the centre-of-mass frame
are plotted for the following values of the parameters: A) $R_2 = 0.308$, $R_4 = 0.821$
, B) $R_2 = 0.3$, $R_4 = 0.792$, C) $R_2 = 0.35$, $R_4 = 0.75$; D_{owd} was calculated for the
total simulation time 5000, while trajectories are plotted for the first 1000 time units.
Resolution of the map is 0.001.Right part of the plot reprinted from [86].

The first region where cluster lifetime is extremely long (till the end of simulation
time 5000) is located between $R_2 \in (0.25, 0.4)$ and $R_4 \in (0.7, 0.9)$. The OWD measured
for the trajectories from this region (only these which do not break up) is shown in
Figure 6.12. One can see that an 'island' of long-living clusters forms a compact region
in space of R_2 and R_4 parameters. The colour corresponds to the value of OWD - the
smaller the value is, the thinner the trajectory is. There are quasi-periodic trajectories
which surround the main island and their OWD value is much greater that these placed
in the centre of the map. An example of such a trajectory from outside the main island
is also shown in Figure 6.12C. Similar values of OWD refer to similar thickness of the
trajectories. One may compare the trajectories A and B to the one presented in C. It is

visible that the OWD value clearly reflects the thickness of trajectories. In the island there are relatively thick trajectories for which the red colour dominates (the OWD value is large). However in the central part of the island there is a small region where OWD value is much smaller, of the order 10^{-3} (blue colour). This indicates that there are trajectories which are thinner that the others. We found a minimum of OWD for this part of the map which is smaller than $4,1 \cdot 10^{-4}$ The corresponding trajectory is presented in Figure 6.12A. This is the solution where all particles move along the same trajectory but in different planes (particles from rings 1 and 3 move in $\phi = 0$ plane, from 2 and 4 ring in plane $\phi = \pi/N$).
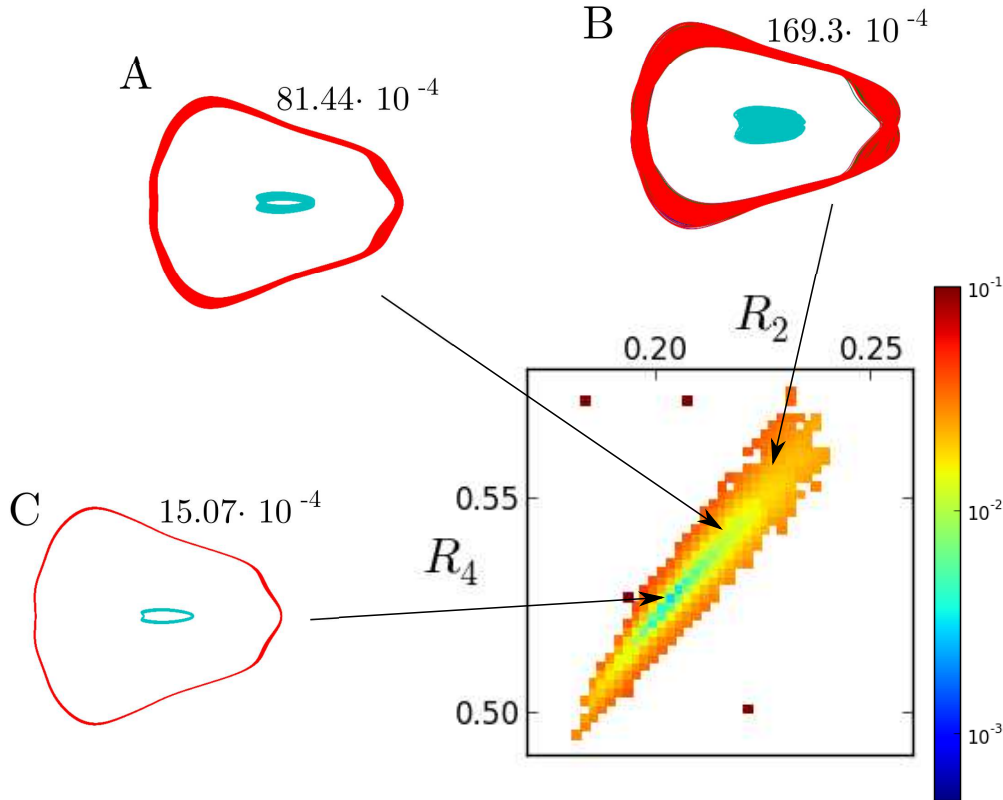

Figure 6.13: The map of One-Way-Distance (thickness of trajectories) for the second region of initial parameters which lead to extremely long lifetimes. The values of D_{owd} are drawn in log scale (the colour corresponds to different values). Three exemplary trajectories of four particles (each from different ring) in the centre-of-mass frame are plotted for the following values of parameters: A) $R_2 = 0.22$, $R_4 = 0.54$, B) $R_2 = 0.224$, $R_4 = 0.56$, C) $R_2 = 0.202$, $R_4 = 0.526$; D_{owd} was calculated for the total simulation time 5000, while trajectories are plotted for the first 1000 time units. Resolution of the map is 0.002.The map reprinted from [86].

We analysed also the other region of long lifetime of the cluster which is placed between $R_2 \in (0.2, 0.25)$ and $R_4 \in (0.5, 0.6)$. The map of OWD for this specified region (resolution 0.002) is presented in Figure 6.13. This region has more elongated shape
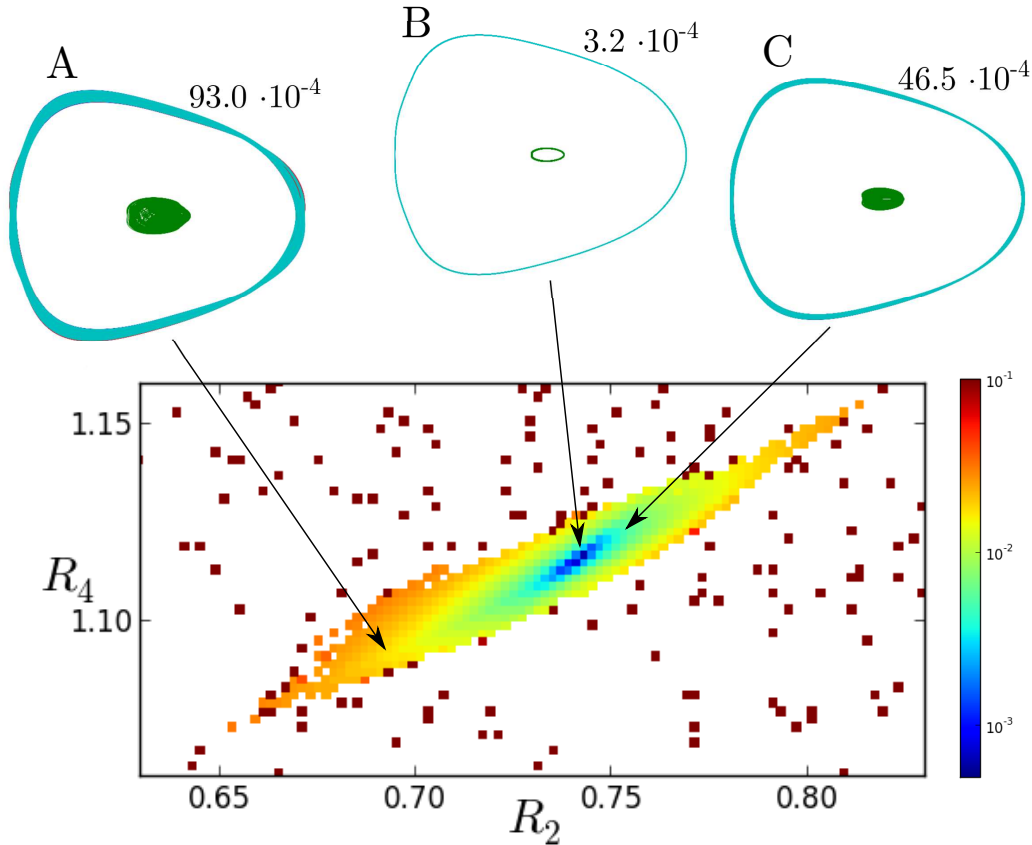
Figure 6.14: The map of One-Way-Distance (thickness of trajectories) for the third region of the initial parameters which lead to extremely long lifetimes. The values of D_{owd} are drawn in log scale (the colour corresponds to different values). Three exemplary trajectories of four particles (each from different ring) in the centre-of-mass frame are plotted for the following values of the parameters: A) $R_2 = 0.69$, $R_4 = 1.086$, B) $R_2 = 0.742$, $R_4 = 1.116$, C) $R_2 = 0.76$, $R_4 = 1.122$; D_{owd} was calculated for the total simulation time 5000, while trajectories are plotted for the first 1000 time units. Resolution of the map is 0.002. The bottom part reprinted from [86].

and does not contain as much trajectories which do no break up as the first region, discussed in the previous paragraph. One can observe that majority of trajectories have OWD value in range $(10^{-2}, 10^{-1})$ which corresponds to the orange and yellow colour. This indicates that the trajectories are thinner in comparison to most of the trajectories from island in Figure 6.12. The examples of trajectories for different values of OWD are shown in Figure 6.13A, B and C. The local minimum of OWD from this region has been also found and is smaller than $15,07 \cdot 10^{-4}$. The trajectory for this value is presented in Figure 6.13C. This is the second periodic solution: particles from ring number 2 move in the central part, and the particles from the other three rings move along the same trajectory but in different planes.

The third region of long-living clusters is between $R_2 \in (0.65, 0.8)$ and $R_4 \in$

(1.05, 1.15). The shape of this island is more elongated than the other two. There are some trajectories surrounding this island, which do not break up and have OWD value of the order 10^{-1}. The example of a wider trajectory from the island is presented in Figure 6.14A. In the central part of the map the OWD values are in a range of $(10^{-2}, 10^{-3})$. An example of trajectory from the middle of the island is shown in Figure 6.14C. One can compare both trajectories and observe that OWD value is sufficiently sensitive to changes of thickness of trajectories. This island of long-living clusters contains one local minimum of OWD value which is smaller than $3, 2 \cdot 10^{-4}$ and the corresponding trajectory is shown in Figure 6.14B. Here the particles from ring 4 move in the central part and the other three rings move along the same trajectory.

In all three cases discussed above the OWD method was successful to find periodic solutions. The algorithm presented in this section was precise enough to effectively analyse huge range of initial conditions in reasonable computational time. The periodic solutions which have been found will be discussed in Sec. 6.5.

6.5   Families of periodic solutions

In the previous chapter there were presented 3 regions of long-lasting quasiperiodic dynamics and we have found minima of One-Way-Distance (OWD) between rings trajectories in subsequent quasi-periods. These 3 found minima correspond to periodic solutions, with the precision of R_2, R_4 parameters limitted by accuracy of computation - namely resolution of examined values of R_2 and R_4. Trajectories of these periodic solutions are shown in Figure 6.15 in the centre of mass reference frame.

In the first solution (Fig. 6.15A) trajectories of all rings are identical. The period is equal to $T = 11.7$ time units. The system repeat initial configuration after every $\frac{T}{4}$ with the particles interchange.

In solution number 2 (Fig. 6.15B) the second ring is circulated by the other three. The period of the motion is equal to $T = 10.7$. During a single period, ring number 2 follows its trajectory three times, while the other three rings perform one run. The system repeats the initial configuration every $\frac{T}{3}$ with the particles interchange. For the second solution period is the shortest among all three, what can be explained in such a way that radii of rings are the smallest and the hydrodynamic interactions between the particles are very strong. In consequence motion of the rings is, on average, the fastest.
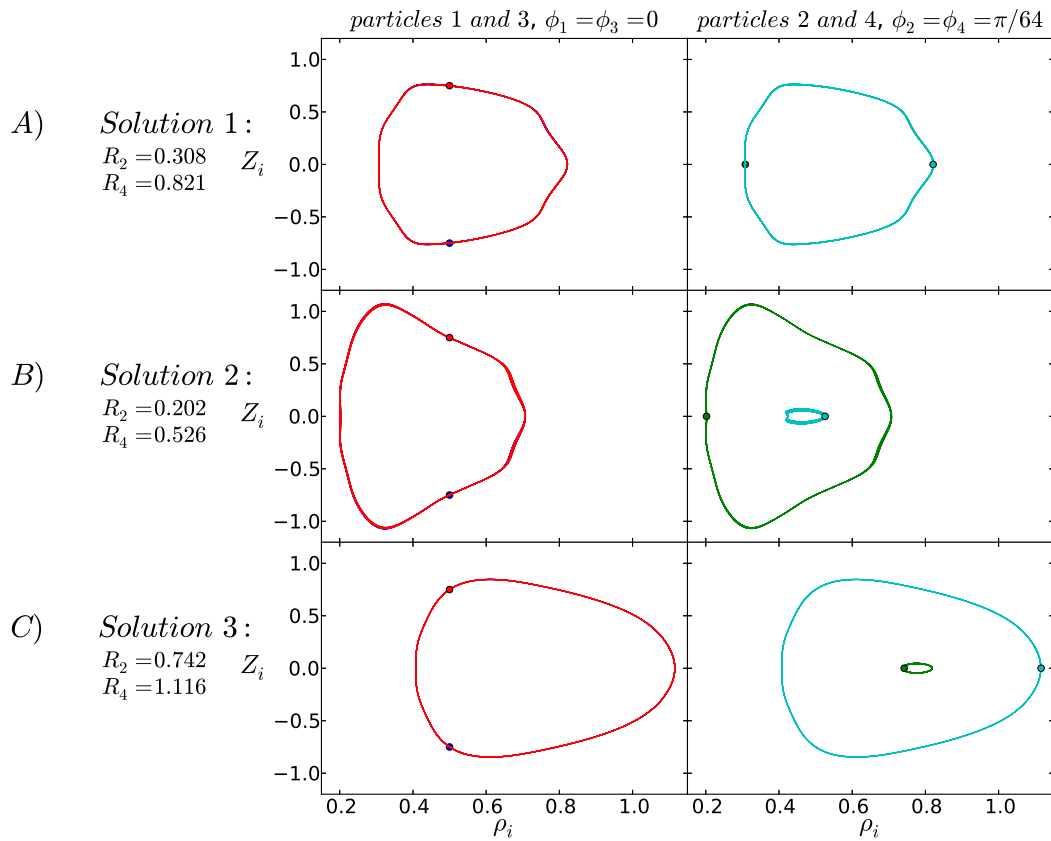
Figure 6.15: Periodic trajectories of four particles (each from a different ring) in the centre of mass frame for $M = 256$ and $C = 1.5$. Initial positions of particles are marked with dots. Colours are the same as in Fig. 6.7. Reprinted from [86].

The solution number 3 (Fig. 6.15C) is similar to the second one. The difference is that this time it is the ring 4 which is circulated by the other ones. The period for the third solution is the longest, $T = 15.6$, due to the largest radii of the rings. It can be noticed, that solutions 2 and 3 have a lot in common. Indeed, after closer look we can classify them to the same family. As it is shown in Figure 6.16, configuration of particles in solution 3, after time $\frac{T}{6}$ is analogous to the initial configuration of solution 2, but with different R_2, R_4, C and also size of the system (defined as diameter of upper and lower ring in initial configuration, d). Also in solution number 3 after $\frac{T}{6}$ configuration of particles is analogous to initial configuration of solution 2, but with different parameters. With this reasoning, our solution 2 ($C = 1.5, d = 1, R_2 = 0.202, R_4 = 0.526$) corresponds also to solution 3 but with parameters: $C = 0.916, d = 1.6012, R_2/d = 0.253, R_4/d = 0.509$, and solution 3 ($C = 1.5, d = 1, R_2 = 0.746, R_4 = 1.116$) corresponds to solution 2 with parameters: $C = 3.539, d = 0.5852, R_2/d = 0.727, R_4/d = 1.207$.
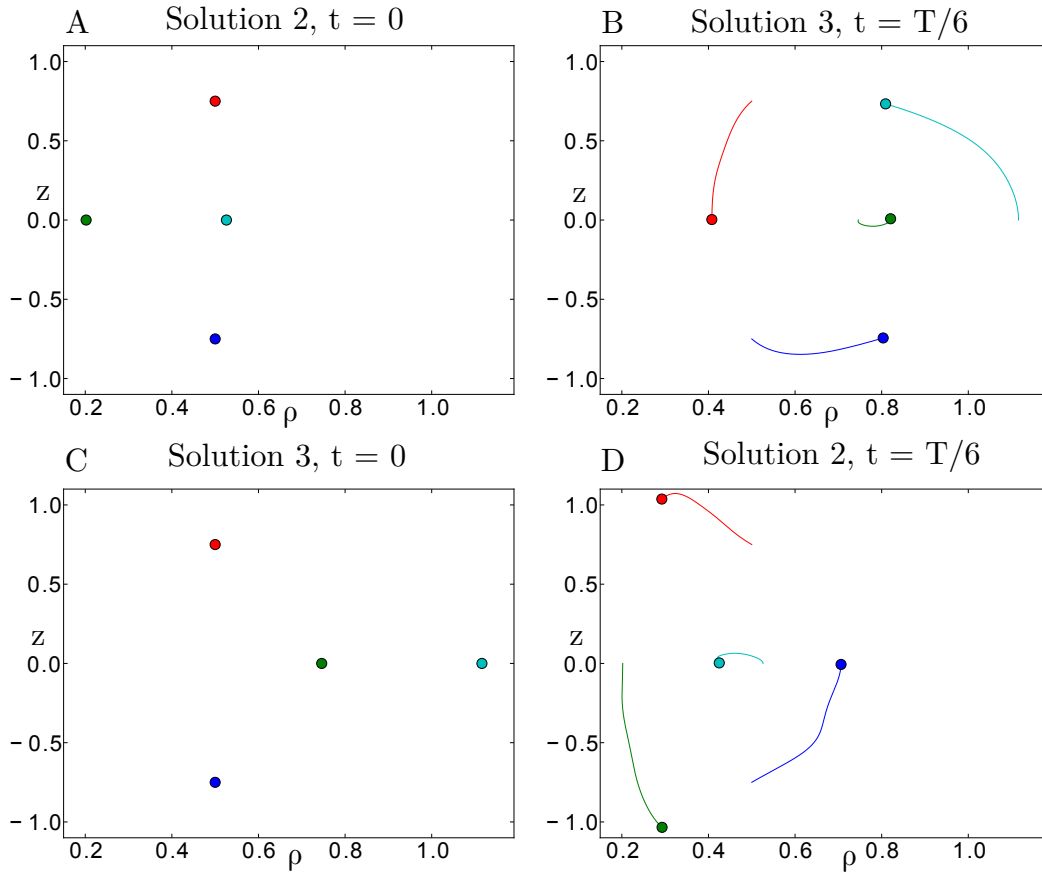
Figure 6.16: Periodic solutions 2 and 3 belong to the same family: initial configuration of solution 2 (A) is analogous to configuration of solution 3 after $T/6$ (B); cyan (A) and green (B) rings are circulated by the other ones. Current positions of rings are marked with dot, and their travelled trajectories with lines of corresponding colours. Analogous situation may be observed in (C) and (D): initial configuration of solution 3 (C) corresponds to configuration of particles after $T/6$ for solution 2 (D)

6.6   Periodic solutions for different values of C and M

In Section 6, number of particles $M = 256$ and $C = 1.5$ are the parameters chosen to study in details many aspects of the dynamics of a 4 - rings system. In this section I will present the dynamics of 4-rings system with other values of C and M and show that the results obtained in Section 6 are generic.

In order to find periodic solutions for other values of C and M, the corresponding parameters R_2 and R_4 were searched for in vicinity of the values corresponding to periodic solutions already known (for $C = 1.5$, $M = 256$). After finding periodic solutions for new values of C or M the procedure was repeated iteratively with a new set of parameters as the new starting point. This method works well and allows, using small steps, to find solutions for parameters C and M even much different from the initial ones.

The detailed procedure of searching for periodic solutions was as follows. Let us assume that there is a known periodic solution for C^A with parameters $R_2 = R_2^A$ and $R_4 = R_4^A$. Our aim is to find parameters $R_2 = R_2^B$, $R_4 = R_4^B$ of initial configuration corresponding to periodic solution of different C, $C = C^B$. If $|C^B - C^A|$ is small, we expect that R_2^B is close to R_2^A and R_4^B is close to R_4^A. In analysis performed in this study, $|C^B - C^A|$ was equal to 0.01. In the first step, 49 (7×7 grid) different initial configurations were examined. One of them, in the centre of the grid, was $\left(R_2^A, R_4^A\right)$. Initial configurations tested in the first step can be written as: $R_2 \in \left\{R_2^A + i\, d_{res}\right\}$, $R_4 \in \left\{R_4^A + j\, d_{res}\right\}$ where $i, j \in \{-3, ..., 3\}$ and d_{res} is a certain small number, resolution of the grid. In this study d_{res} was equal to 0.001. For all 49 initial configurations a short simulation was performed, with total time equal to $1.5T_A$, where T_A is the period for C^A. Positions of particles were recorded with very high resolution. Subsequently among these trajectories the one that is the closest to the periodic is chosen. More precisely we measure the difference between initial position of particles and the most similar configuration during the dynamics, excluding from this comparison time just after beginning, $t < \frac{T_A}{10}$. In this way we find the best pair of $\left(R_2^B, R_4^B\right)$ parameters out of 49 examined. Having them identified, new 7×7 grid of initial configurations in built, with the $\left(R_2^B, R_4^B, C^B\right)$ found in previous step in the middle and resolution d_{res} equal to half of the value used before. In order to find the periodic solution for C^B, 5 such iterations are performed with final resolution $6.25 \cdot 10^{-5}$. $\left(R_2^B, R_4^B\right)$ parameters found in this way for C_B were used to start the whole procedure (for the next value of C, close one to C^B).

In order to find periodic solutions for $C = 1.5$ but different number of particles the same algorithm was applied (starting from $M = 256$, $M = 4N$). For decreasing number of particles we searched for periodic solutions starting from 63 particles in one ring ($M = 252$) down to $M = 8$. When looking for solutions for larger M, the change of M in one step was larger than 4 but always equal or smaller than $\frac{1}{8}$ of the previous M.

The results show that three presented periodic solutions may be found for a broad range of parameters C and M. However, it may be not possible for values that are too small. First let us discuss the dynamics with different values of parameter C.

Periodic solutions of type 1 were found for $C \in [0.32, 2.48]$. This range of C is an approximate one, since when we are coming closer to its borders, quasi-periodic and close to periodic trajectories can be found in more and more narrow range of R_2 and R_4. Thus, the existence of periodic solutions outside this range is not excluded, but

their finding becomes very challenging. Examples of trajectories for other values of C are presented in Figure 6.17A. Trajectories for smaller C have more oblate shape, while their shape for grater C become more complex, with more sharp bends.

Figure 6.17: Periodic trajectories of rings in type 1 solution in the centre of mass reference frame A) for different values of C and $M = 256$, B) for different numbers of particles M and $C = 1.5$.
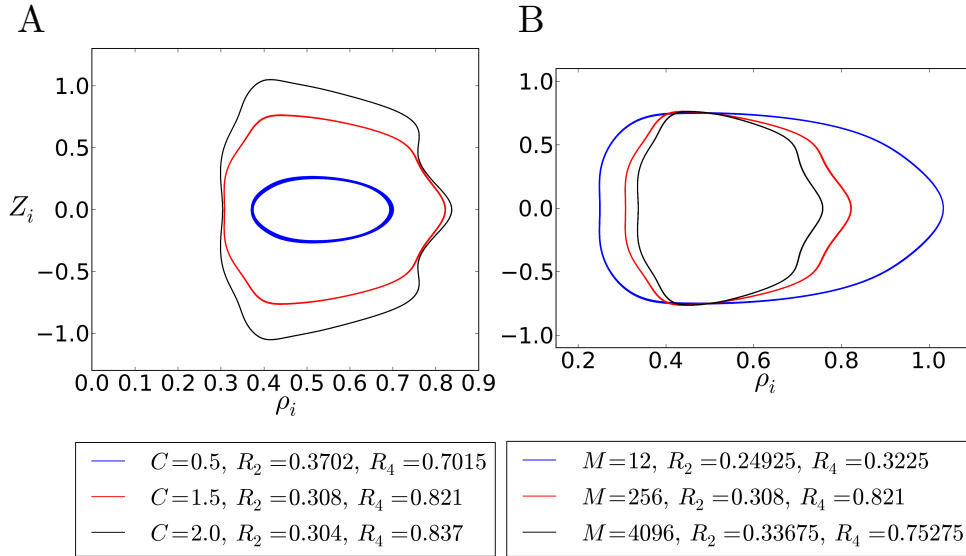

Figure 6.18: Periodic trajectories of rings in type 2 solution in the centre of mass reference frame A) for different values of C and $M = 256$, B) for different numbers of particles M and $C = 1.5$.

For solutions type 2 and 3 periodic orbits were found in ranges $C \in [0.73, 1.99]$ and $C \in [0.94, 2.7]$, respectively (higher values of C have not been investigated). In case of smaller values of C the motion is unstable - quasi-periodic orbits destabilise after
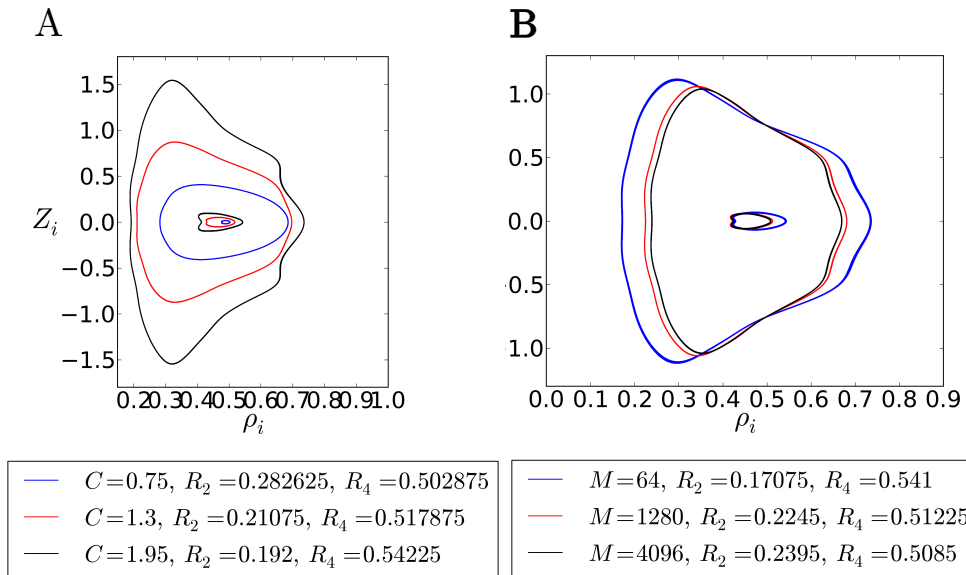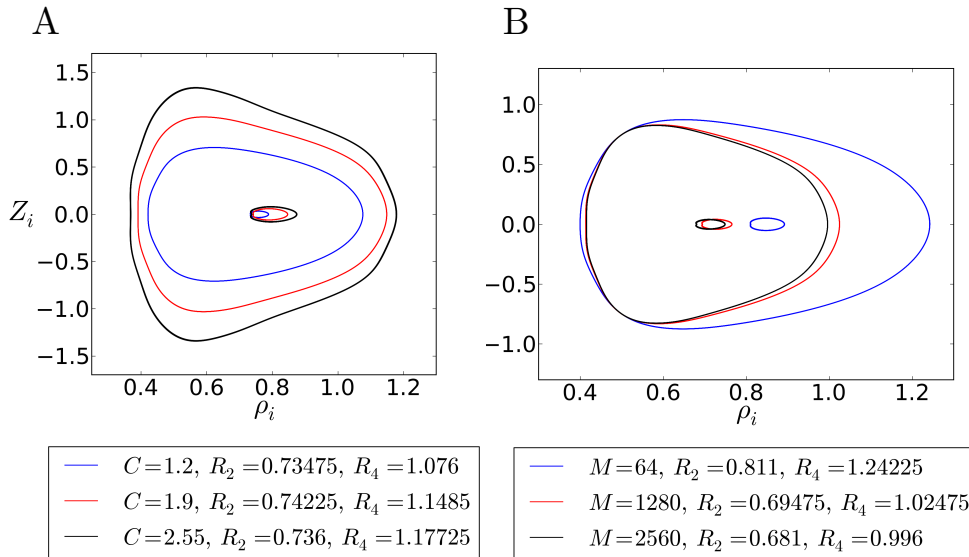
Figure 6.19: Periodic trajectories of rings in type 3 solution in the centre of mass reference frame A) for different values of C and $M = 256$, B) for different numbers of particles M and $C = 1.5$.

short time or immediately and there exist for very narrow ranges of R_2 and R_4. The smaller parameter C is, the faster the destabilisation. Similar problem is encountered for $C > 2$ for 2nd type of periodic solution. A few examples of 3 periodic solutions are presented in Figure 6.17A, 6.18A and 6.19A. Orbits for smaller C are more oblate and the width of trajectory is smaller. Periodic (or at least very close to periodic) motions of different type exist also for values outside mentioned ranges, and their trajectories are more complex and can be seen in Appendix B.

Now let us discuss the dependence of periodic solutions on M. The number of particles in the system M also influences the shape of trajectories. The upper boundary up to which periodic solutions were investigated, was $M = 14336$. For $M \in [60, 14336]$ there exist periodic solutions analogous to those presented in Section 6.5. The bottom border of number of particles, for which exist periodic motions is not lower than $M = 12$ for type 1 solution, and $M = 60$ and $M = 40$ for solutions type 2 and 3, respectively. Since solutions 2 and 3 belong to the same family (and we can treat them as the same type of solution, but for different C, see Section 6.5), we can observe that this critical number of particles is likely to be dependent on the value of C parameters. The influence of different number of particles on the shape of trajectory is shown in Figure 6.17B, 6.18B and 6.19B. The main difference are more oblate shape and bigger difference between R_4 and R_2 for small M. Periodic solutions are not observed for smaller values of M (value depends on C parameter and type of periodic solution), however their existence for larger values of M (larger than 14336) has not been investigated in this work.
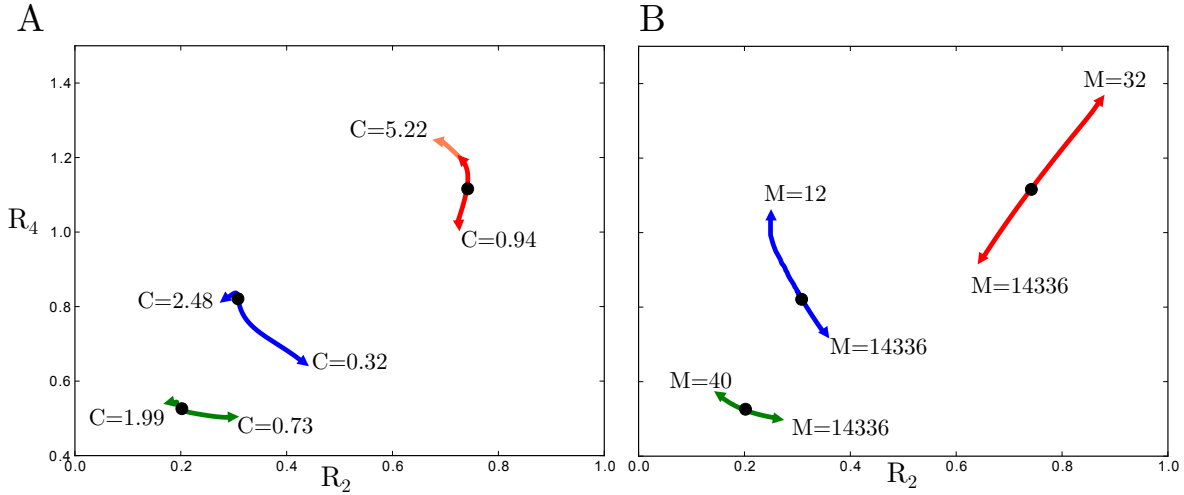
A

B

Figure 6.20: R_2 and R_4 parameters of three periodic solutions (1st solution - blue lines, 2nd solution - green lines, 3rd solution - red lines) for (A) different C, B) different number of particles M. Periodic solutions for $M = 256$ and $C = 1.5$ are marked with black dots.

Values of R_2 i R_4 that correspond to three periodic solutions for different parameters C and M are presented in Figure 6.20A and B, respectively. We can observe, that the increase of parameter C has much smaller effect on R_2 and R_4 than its decrease. For the solution 1, both changes in C and M seem to shift its position along similar direction. In both Fig. 6.20A and B we can observe that R_2 and R_4 parameters of periodic solution can change noticeably.

In Section 6.5 it was argued that periodic solutions number 2 and 3 belong to the same family: during the period initial configuration of 2nd periodic solution is repeatedly transformed to the initial configuration of 3rd one and vice verse. This means that to a given periodic trajectory from this family two different sets of $(C, \frac{R_2}{d}, \frac{R_4}{d}, d)$ can be assigned, where d is the diameter of top and bottom rings, in the initial configuration by identity equal to 1 (normalisation unit). In Figure 6.21 sets of parameters $(C, R_2/d, R_4/d)$ are shown for all three periodic solutions. Parameters from 2nd (green) and 3rd (red) periodic solutions which correspond to the same trajectory are linked with arrows. It can be observed that small differences in C for 2nd solution correspond to much larger differences in 3rd solution. It is consistent with much broader C range of sufficiently stable periodic solutions in case of 3rd solution with respect to the 2nd one. For all three periodic solutions parameters R_2 and R_4 parameters are plotted in the whole ranges where periodic orbits were found. It is the widest for 3rd solution, much more narrow for 1st one and the narrowest for the 2nd. Analogous plot of R_2 and R_4 for different number of particles is shown in Figure 6.22.
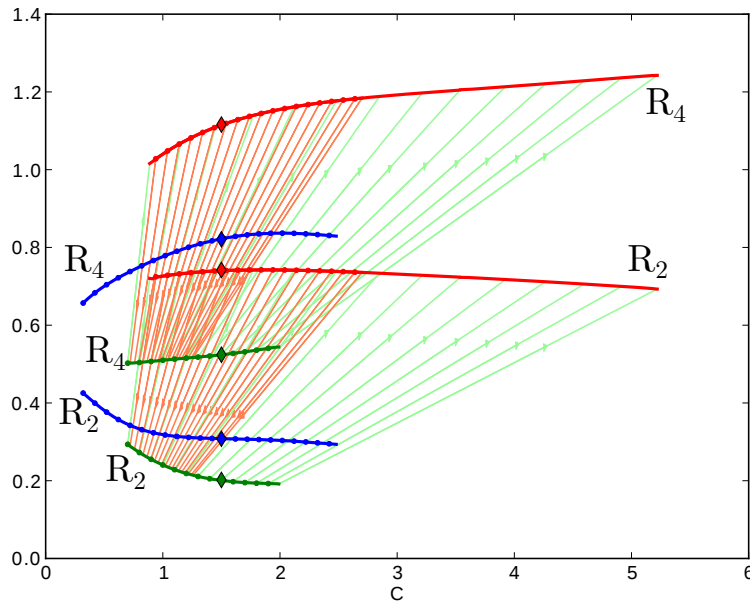
Figure 6.21: R_2 and R_4 values for different values of parameter C. Colours correspond to different types of periodic solutions: blue: 1st, green: 2nd and red: 3rd. By definition $(R_2 < R_4)$ lower line of the same colour indicates R_2 and upper R_4. Arrows join alternative values of (C, R_2, R_4) between solutions type 2 and 3.

Analysis performed in this section has shown that results obtained for $M = 256$ and $C = 1.5$ are not specific for chosen values of parameters. Basing on iterative method described at the beginning of this section, it was possible to find all three periodic solutions for different values of C and M. It turned out that periodic orbits exist for broad range of these parameters, which depend on type of the solution. Approaching boarders of the ranges periodic motions become more and more difficult to find: R_2 and R_4 must be determined very accurately to get a trajectory close enough to the periodic one. For this reason ranges of C and M indicated in this work are conservative. For C and M values out of these ranges there are observed quasiperiodic motions and periodic ones, but with more complex trajectories (Appendix B).
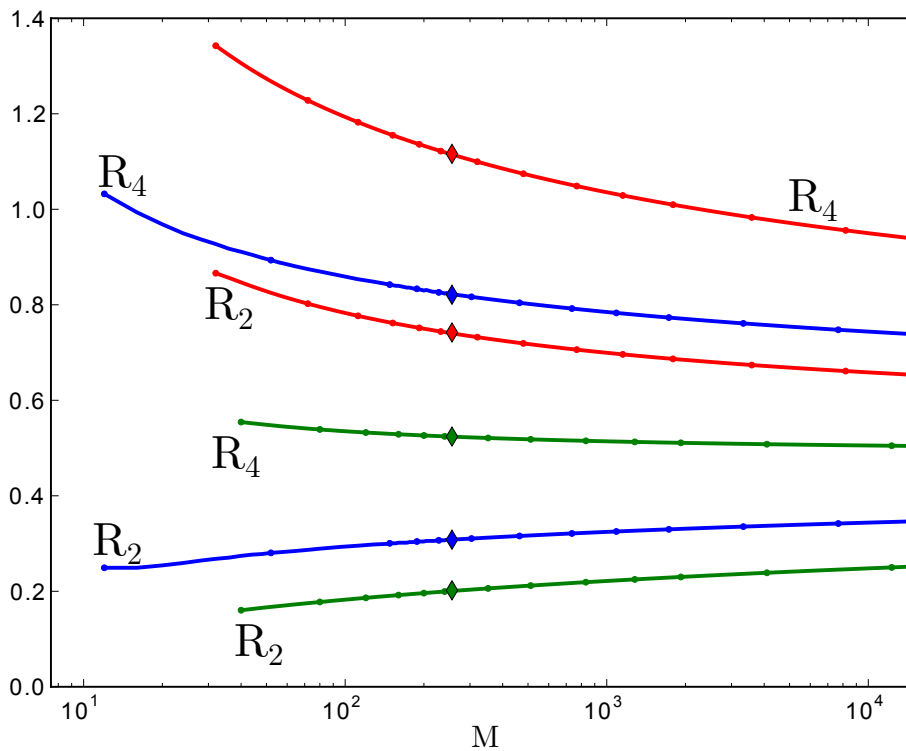
Figure 6.22: R_2 and R_4 values for different values of parameter M. Colour code is the same as in Figure 6.21, colours correspond to 3 different types of periodic solutions: blue, green and red to 1st, 2nd and 3rd, respectively. Lower line of the same colour indicates R_2 and upper R_4. Note logarithmic scale on x axis.

Chapter 7

Fluid motion around the periodic solutions in the system of 4 rings in a viscous fluid

In this section we would like to compare the fluid motion in two different systems: consisting of 2 rings of particles settling under gravity (dynamics of particles discussed in Section 3) and consisting of 4 rings (dynamics of particles presented in Section 6). There exist some significant differences in the fluid motion in the system of 2- and 4 rings, which are related to the dynamics of particles. In case of 2 rings every configuration (except of very 'flat' system with $C < C_0$) leads to periodic motions. However this is not the case for 4 rings, where only 3 periodic solutions were identified (see Section 6.5). The rest of initial configurations leads to fast of slow decay of the group, or quasiperiodic motion. These basic differences are reflected in motion of fluid around the particles. The fluid motion around initial configurations which lead to decay will not be discussed here.

The analysis of fluid behaviour around the particles presented in this section will be conducted for 3 periodic solutions in the system of 4 rings. Long-lasting quasiperiodic motions have trajectories close to periodic ones what implies that dynamics of fluid around them is not expected to be significantly different. Fluid dynamics in the system of 2 rings, presented in Section 4, will serve here as a useful reference, since many aspects remain similar in both systems. We will compare the systems with 2 and 4 rings for the same value of C parameter and the same total force G exerted on M particles. Therefore the total mass remain the same, but particles have different configurations. In the system of 2 rings it has been observed that for larger number of

particles ($M \geq 32$) the particles move faster than the fluid in the centre of the cluster. Here we will investigate if the same effect is observed in the system of 4 rings.

As discussed in Section 4 settling velocity of the particles is dependent on their radii a_p and can be split into two terms: the first one u_0 - velocity of an isolated, settling particle, so called 'self term', inversely proportional to a_p; and the second term V_z - settling velocity related with an influence of hydrodynamic interactions with other particles (called 'interaction term'), which does not depend on particles radii in case of point-particle approximation. Maximal radius of particles possible in system of 4 rings, $a_{p,max}$ can be calculated as follows, in a way analogous to Equation (4.7):

$$a_{p,max} = \min_{t,l} \left(\rho_l \left(t \right) \right) \sin \left(\frac{4\pi}{M} \right). \tag{7.1}$$

where $l = 1, \ldots K$ is the number of ring (see Section 2.1.2).
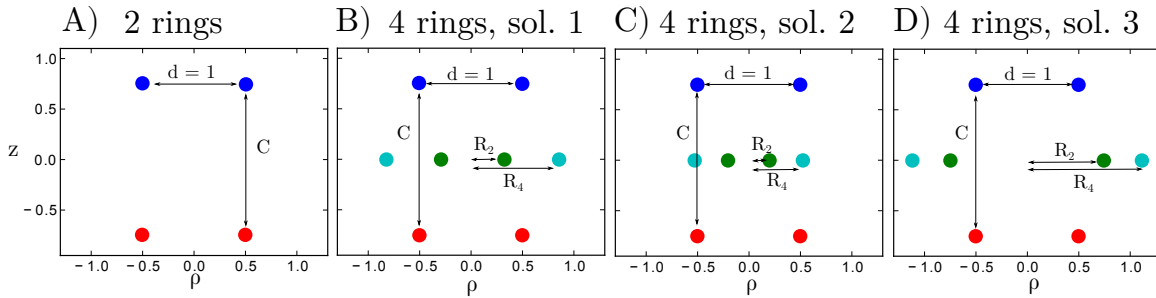
Figure 7.1: Scheme of the initial configurations in the periodic systems: A) 2 rings, B) 4 rings, solution 1, C) 4 rings, solution 2, D) 4 rings, solution 3; $C = 1.5$.
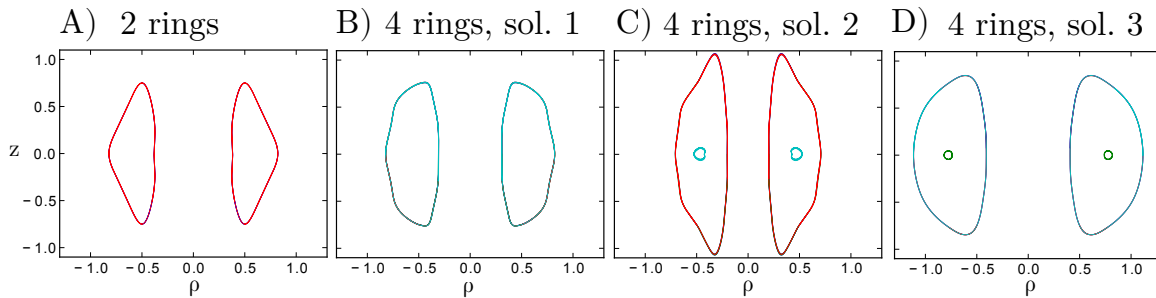
Figure 7.2: Periodic solutions for the systems with the same number of particles $M = 256$ and $C = 1.5$: A) 2 rings, B) 4 rings, periodic solution 1, C) 4 rings, periodic solution 2, D) 4 rings, periodic solution 3.

The initial configurations of $M = 256$ particles which lead to periodic orbits are recalled in Figure 7.1: the system of 2 rings, and three different initial configurations of the system of 4 rings. Corresponding trajectories of particles are shown in Figure 7.2.

Let us begin with analysis of two quantities which do not depend on particles radius: period-averaged velocity of the fluid in the centre of the cluster, $|\langle u\left(\boldsymbol{r}=\left(0,0,z_{CM}\right)\right)\rangle_T|$, (Table 7.1) and the average value $|\langle|V_z\left(t\right)\rangle_T|$ of particles mean velocity (Table 7.2). Both will be measured in the laboratory reference frame.

M	2 rings	4 rings, solution 1	4 rings, solution 2	4 rings, solution 3
32	2.010	2.063	2.148	1.485
64	2.011	2.050	2.173	1.518
256	2.013	2.038	2.185	1.570

Table 7.1: Absolute value of the fluid settling velocity $|\langle u\left(\boldsymbol{r}=\left(0,0,z_{CM}\right)\right)\rangle_T|$ in the centre of the group. Values are given for different numbers of particles and different periodic solutions. In all cases $C=1.5$.

M	2 rings	4 rings, solution 1	4 rings, solution 2	4 rings, solution 3
32	1.545	1.364	1.627	1.054
64	1.748	1.503	1.789	1.184
256	2.236	1.764	2.074	1.570

Table 7.2: Absolute value of particles settling velocity (without self-term) $|\langle V_z(t)\rangle_T|$ for three different numbers of particles and different periodic solutions. In all cases $C=1.5$.

In section 4 it was proved that vertical velocity of the fluid is independent of the number of particles in rings but depends only on (ρ, z) coordinates of each ring and the total force G (see Eq. (4.9)). As it was discussed this argumentation is valid for any number of horizontal rings centred around the same axis, what is a consequence of superposition rule in point-forces model. For different numbers of particles the periodic trajectories are different (see Figs. 6.17B, 6.18B, 6.19B) what effects in different fluid motion. Therefore the period-averaged fluid velocity in general may depend on the number of particles in the system, because different M leads to different shapes of periodic orbits, what in turn cause changes in the fluid motion. Indeed, in Table 7.2 we can observe that fluid velocity varies slightly due to different numbers of particles M. Apart form solution 1, $|\langle u\left(\boldsymbol{r}=\left(0,0,z_{CM}\right)\right)\rangle_T|$ is larger for larger M. These changes however are much smaller than differences observed between different periodic solutions.

Interaction term $|\langle V_z(t) \rangle_T|$ of particles velocity depends strongly on the number of particles (Table 7.2). For all considered systems the differences between values obtained for $M = 32$ and $M = 256$ exceed 25%. Correlation of $|\langle V_z(t) \rangle_T|$ and radii of rings during the motion is visible (Tab. 7.2): for systems with 4 rings solutions where particles are closer to the centre (rings are smaller) have higher settling velocity. This rule does not apply to system of 2 rings, where distances between particles are smaller than for 4 rings and in consequence hydrodynamic interactions are stronger in the same ring.
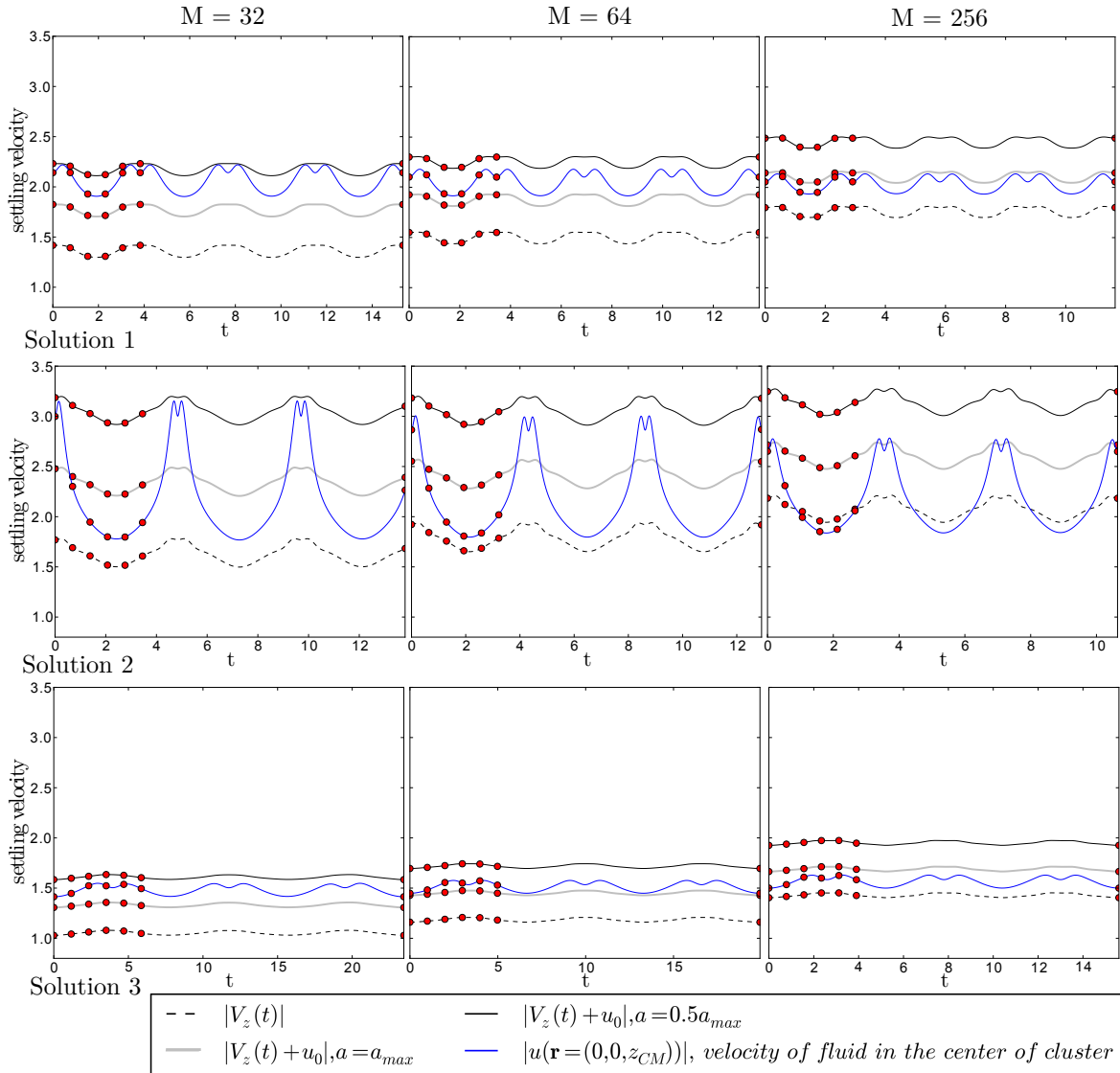
Figure 7.3: Velocity of the fluid (blue line), velocity of the particles without self-term u_0 (dashed line) and velocity of the particles for two different radii: $a = a_{max}$ (grey line) and $a = a_{max}/2$ (black solid line); plots for two different values of M, for three different periodic solutions. Chosen time-points are marked with red dots: $t = 0$, $t = T/20$, $t = T/10$, $t = 3T/20$, $t = T/5$, $t = T/4$ and $t = T$. $C = 1.5$.

After analysing mean values, let's check how the velocities $V_z(t)$ change during the period, what is shown in Figure 7.3. Blue line refers to $u\left(\boldsymbol{r} = (0, 0, z_{CM})\right)$, dashed line refers to $|V_z(t)|$ and solid grey and black lines show total particles settling velocity for maximal possible particles radius, $a_{p,max}$, and for half of $a_{p,max}$, respectively. For 1st and 3rd solutions with $M = 32$ and $M = 64$ we can observe that for some values of particle radii, $a_p < a_{p,max}$, fluid in the centre of the cluster moves down faster than particles during the whole period. In case of 2nd solution the fluid velocity changes during the period from greater to smaller than particles velocity, for all values of M. As mentioned at the beginning of this section, fluid moving down in some regions (in the centre of the cluster) faster than the particles is a prerequisite for circulation of the fluid within cluster. For system with two rings it does not take place even for the smallest analysed M, $M = 32$. The situation is different in the system of 4 rings, where $|\langle u\left(\boldsymbol{r} = (0, 0, z_{CM})\right)\rangle_T| - |\langle V_z(t)\rangle_T|$ is greater for 1st and 2nd periodic solutions in comparison to system of 2 rings (see Tables 7.1 and 7.2). When including self-term into consideration it is worth to notice that in the system of 4 rings also $a_{p,max}$ is larger (particles are far from each other in comparison to the system of 2 rings), what contributes to smaller self-term. In consequence value of $|\langle u\left(\boldsymbol{r} = (0, 0, z_{CM})\right)\rangle_T| - |\langle V_z(t)\rangle_T + u_0|$ is greater for 4-rings system than for the system of 2 rings.

In order to understand better the differences between behaviour of systems with 2 and 4 rings let us analyse fluid streamlines around initial configuration leading to periodic orbits in the system of 4 rings. In Figure 7.4 the streamlines are presented for different numbers of particles ($M = 32, 64, 256$) and 3 different periodic solutions. The colourful regions show where the fluid moves faster than the particles (light blue) and slower (light red). The circles (drawn in scale) denote initial particles positions as follows: blue ones refer to particles placed in plane $\phi = 0$, red ones to those in plane $\phi = 4\pi/M$. Having this remark made, let us analyse fluid streamlines for different types of periodic solutions and different M.

Streamlines of fluid in the centre of mass reference frame around 1st periodic solutions passing the central part of the cluster are closed for all cases shown in Figure 7.4. From now on a region of closed streamlines in the central part of the cluster will be called 'drop' (independently whether it is a sphere-like shape or it has torus-like shape). In cases of $M = 32$ and $M = 64$ the shape of the drop is close to spherical, and its size is nearly of the size of the cluster. In the system of 256 particles some of the fluid streams up through the cluster, although this flux is weak, as can be seen in Figures 7.3 and 7.5. The detailed picture of the streamlines can be found in Appendix A.2.
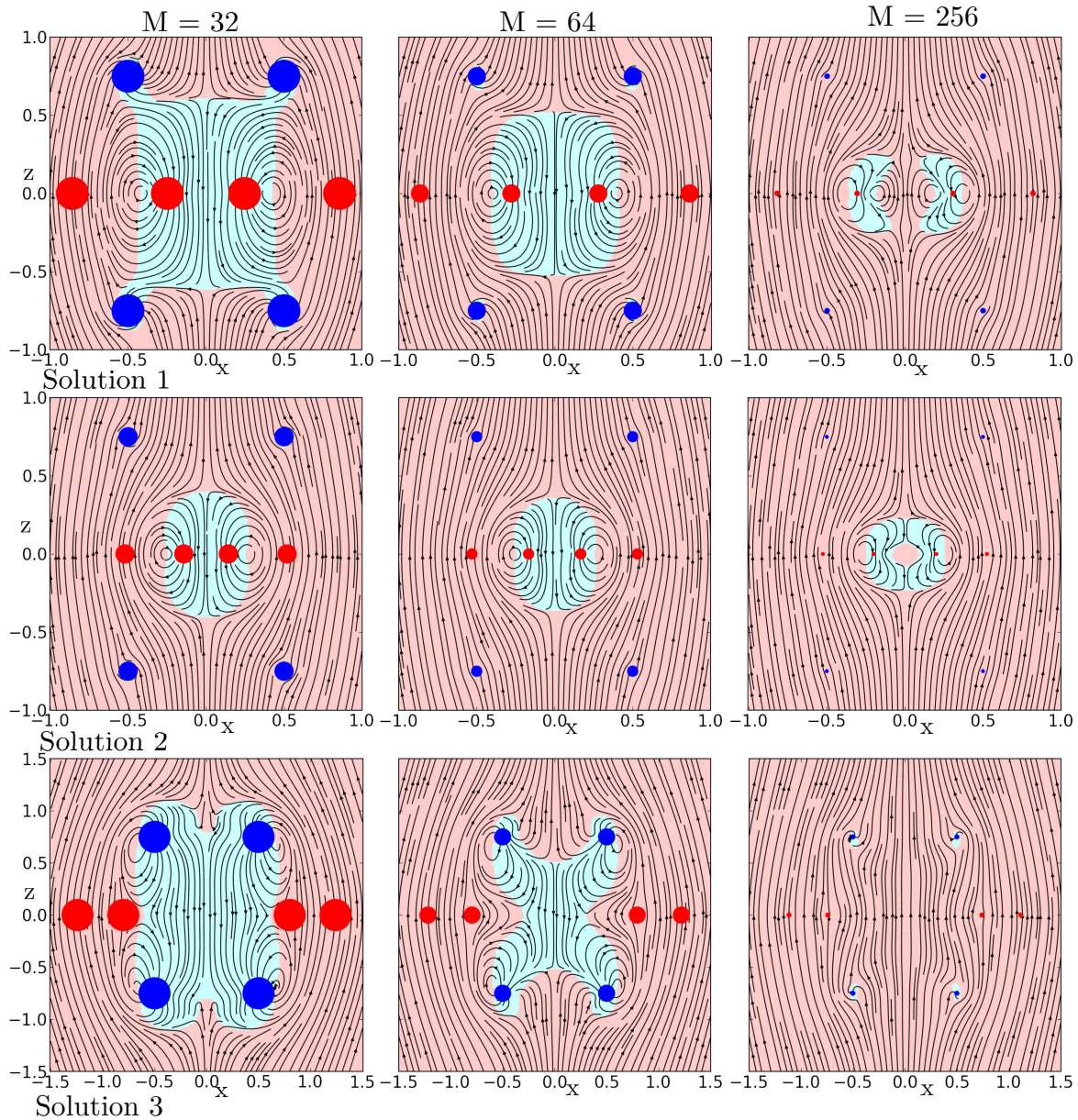
Figure 7.4: Streamlines around initial configurations of particles, plotted for three different values of M and for three different periodic solutions. Regions where fluid moves down faster than particles are coloured in light blue, and where situation is the opposite-in light red. Streamlines shown in plane $y = 0$. Positions of particles in this plane are denoted with blue dots (drawn to scale). In red positions of particles from plane shifted by $\frac{4\pi}{M}$. The particles for $M = 256$ are not visible because of too small radii.

The fact that the fluid streams up through the centre of the drop made of $M = 256$ particles is the main difference in comparison to the solution for smaller numbers of particles ($M = 32, 64$).

For the 2nd solution we observe closed streamlines in the central part of the cluster
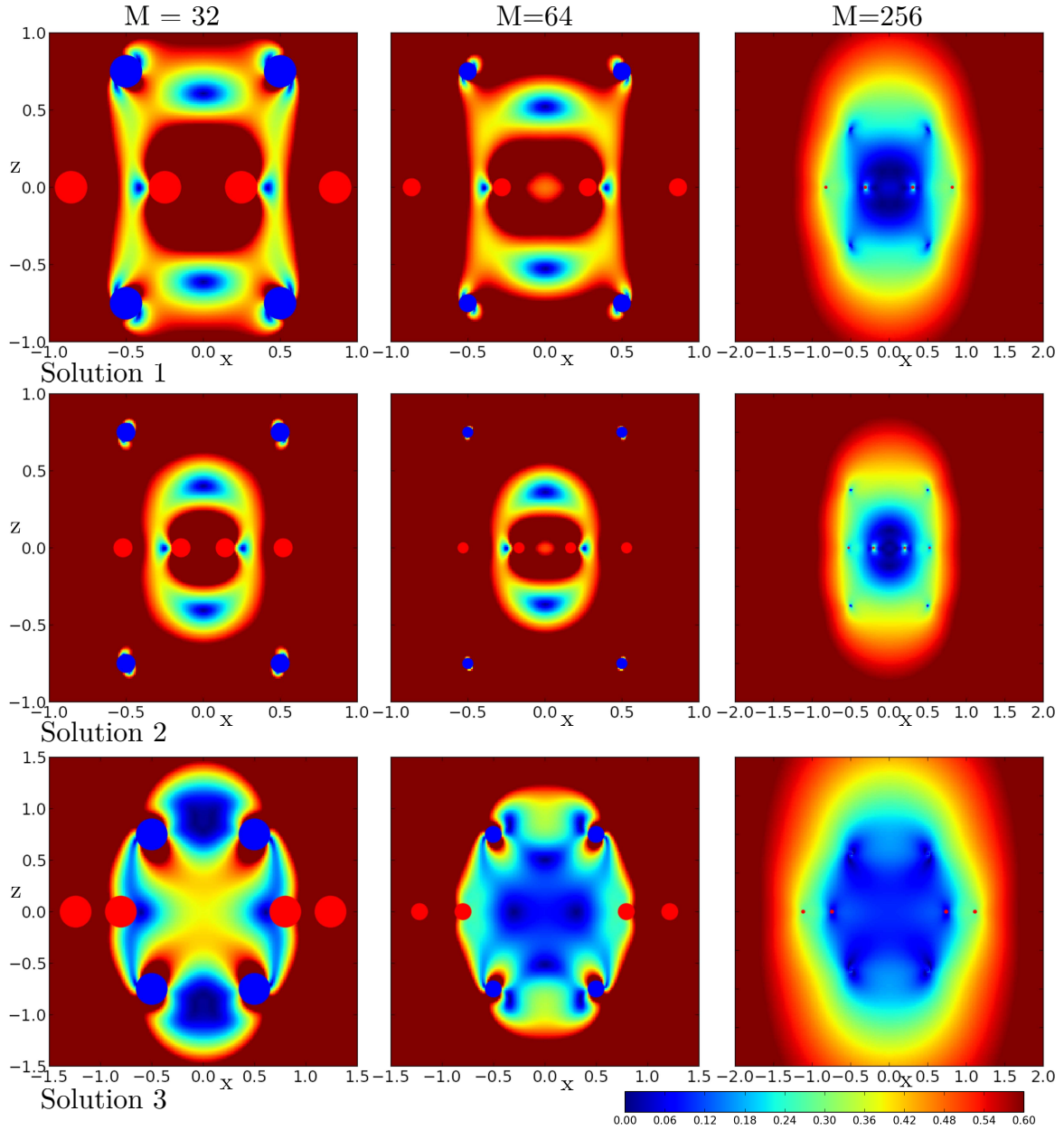
Figure 7.5: Normalised absolute value of fluid velocity field in the centre of mass reference frame, $W(\boldsymbol{r}, t)/|\langle V_z(t)\rangle_T + u_0|$. Results for different values of M for three different periodic solutions. Velocity value is given in plane $y = 0$. Positions of particles in this plane are denoted with blue dots (drawn to scale). In red positions of particles from plane shifted by $\frac{4\pi}{M}$, $a = a_{max}$.

for all presented M (it is not the case for even larger number of particles). The shape of the drop is close to spherical for $M = 32$ and $M = 64$. Size of the drop is decreasing with growing number of particles in the system. In the centre of drop for $M = 256$ we can observe an empty space, what is due to fine-scaled flow structure (see Appendix A.2). Fluid flow in this region is very weak. As can be seen with background colour in

Figure 7.4 direction of fluid motion is reversed in this region with respect to the fluid in surrounding structure. Similarly as in the case of 1st solution, size of the drop in the 2nd solution is smaller than the cluster size.

Streamlines around 3rd periodic solution are closed for $M = 32$ and $M = 64$, so the drops are observed. For $M = 64$ shape of the drop is irregular. In the system with large number of particles, $M = 256$, there are no closed streamlines in the central part of the cluster. Streamlines are close to vertical in almost the whole region. The only closed streamlines can be observed around the particles from rings 1 and 3, which settle down faster than the centre of mass of the cluster.

Information obtained with analysis of streamlines can be enriched with velocity values in centre of mass reference frame, $W(\boldsymbol{r}, t)$. Values of $W(\boldsymbol{r}, t)$, normalised by cluster settling velocity $W(\boldsymbol{r}, t)/|\langle V_z(t)\rangle_T + u_0|$ are presented in Figure 7.5 with $a_p = a_{p,max}$. Range of x and z axis is larger here in order to capture whole interesting part and absence of fine-scale details as it was in case of streamlines plots (Fig. 7.4). Now we can compare corresponding regions of streamlines and fluid velocity value. For $M = 32$ and $M = 64$ regions of closed streamlines of various shapes were observed. Regions with the highest speed of fluid in the central parts of the cluster in Fig. 7.5 correspond to places where fluid moves down faster than the particles. We can observe that fluid moves much slower in solution 3 in the central part of the cluster. For $M = 256$ particles a drop can be found only for 1st and 2nd periodic solution. As mentioned before, fluid velocity is close to 0 in the centre of drop, what corresponds to dark blue colour. For other two periodic solution we also observe low fluid velocity in the centre of cluster, but the movement of fluid is partially (solution 1) or entirely upward.

M	4 rings, solution 1	4 rings, solution 2	4 rings, solution 3
32	0.877	0.831	0.746
64	0.646	0.627	0.589
256	1.224	1.121	0.961

Table 7.3: Effective values of radius a_{eff} calculated from Eq. (4.3) for three periodic solutions for different numbers of particles.

In discussion of streamlines pattern, a useful reference is solution for a settling drop of heavier fluid, introduced in Section 4. Shape of such a droplet is exactly spherical. Its size can be chosen in a way to get the same drop settling velocity as the velocity

of the particle cluster for dragging force G (Eq. (4.3)) and the obtained value is called 'effective radius' of the cluster, a_{eff}. Effective radii for configurations showed before in Figure 7.4 are presented in Table 7.3. It can be noticed that for $M = 32$ and $M = 64$ values of effective radii are similar to the radii of 'drop' of the fluid around clusters (for cases where they occur), but always slightly larger. For $M = 256$ only in solution 1 and 2 we observe non-spherical drop, in case of 3rd solution there is no drop.

Results for $M > 256$ are not shown because streamlines are almost vertical and much more undisturbed than for $M = 256$ (Fig. 7.4). Fluid streams up through the middle of rings for all three periodic solutions. For large M particles are close to each other so their radii are much smaller. One can imagine that for a very thin ring fluid streams up through it.

The main difference between fluid motion in the systems of 2 and 4 rings is the possibility of fluid circulation in the latter one (in the centre of mass reference frame), for some particles radius $a_p < a_{p,max}$. This was shown for relatively small numbers of particles (e.g. $M = 32$ and $M = 64$) for the 1st solution and $M = 32$ for the 3rd solution during whole period, and for chosen time-points it is true also for the 2nd solution. Fluid circulation may occur only if in some regions fluid moves down faster than the particles. In Tables 7.1 and 7.2 it was shown, that settling velocity of particles depends on the number of particles (keeping total mass fixed, larger M implies larger $|\langle V_z(t) \rangle_T|$) while the fluid velocity in the centre of the cluster, $|\langle u(\boldsymbol{r} = (0, 0, z_{CM})) \rangle_T|$, changes only slightly with varying M. In consequence $|\langle u(\boldsymbol{r} = (0, 0, z_{CM})) \rangle_T| - |\langle V_z(t) \rangle_T + u_0|$ decreases with number of particles in the system and for large M it is always smaller than 0, what means that the fluid cannot circulate in the central part of the cluster. In the limiting case of $M \to \infty$ results should converge to dynamics of continuous rings (see Section 2.4), which may be imagined as very thin fibres. It this approximation fluid would stream up through the middle of rings, what is actually the case for large M.

In streamlines analysis performed in this section, the upper limitation of particles radius, $a_p = a_{p,max}$ was used. Applicability of point-force approximation in this type of analysis was discussed in Section 2.3, where it was shown that in similar systems this model accurately describes particles dynamics [94, 97]. In order to extend the conclusions presented above (circulation of the fluid inside cluster for some a_p), more detailed analysis can be performed with applying methods incorporating higher terms of multipole expansion and lubrication correction, responsible for very short-range hydrodynamic interactions. Software packages implementing this approach that can

be used are HYDROMULTIPOLE [89, 91] and implementations developed by Ladd [101] or by Durlofsky, Brady and Bossis [102].

In comparison to system of 2 rings the fluid flow observed around 4 rings resembles much more solution for Hadamard - Rybczyński drop. For some a_p fluid circulations may be observed, what is not the case for 2 rings. Apart from describing drop of heavier fluid, Hadamard - Rybczyński solution can also serve as an approximation of fluid motion around spherical swarm of particles (discussed in Section 4), if the number of particles is large enough and the particles are small. Since larger number of rings leads to more uniform mass distribution in space, fluid dynamics is more similar to drop consisting of particles.

Chapter 8

Dynamics of 4 rings and fluid motion in permeable medium

8.1 Introduction

The dynamics of 2-rings system in permeable medium was discussed in Section 3. Here we would like to state a question what is the dynamics of 4 rings in this medium. The case with 4 rings in the Stokes fluid [86] was shown to be more complex than with 2 ones: periodic solutions were found only for specific initial configurations while majority of them lead to decay of the cluster. The opposite situation was observed in case of 2 rings, when for all initial parameters rings performed periodic oscillations. Dynamics of particles in Stokes fluid studied in previous section can be identified with dynamics in limiting case of permeable medium where $\kappa = 0$. The $\frac{1}{\kappa^2}$ is the permeability coefficient. Therefore it is expected that at least for very small κ (very large permeability), dynamics should be similar. The basic question is how the value of κ influences the existence of periodic solutions?

The dynamics is described by Brinkman-Debye-Büeche equations (5.1 - 5.2), which have been presented in Section 5. Solutions for velocity field $\tilde{\boldsymbol{v}}(\boldsymbol{r})$, pressure $\tilde{p}(\boldsymbol{r})$ and the form of Green tensors are given by Eqs. (5.3 - 5.8). Normalisation for dynamics in permeable medium, given in Section 5, is identical as in the Stokes fluid (Section 3) apart from time unit, which here is 2 times shorter and equal to $(4\pi\eta d^2)/G$ and velocity unit $G/(4\pi\eta d)$ The value $1/\tilde{\kappa}$ is normalised by length unit d and dimensionless $\tilde{\kappa}$ will be denoted as κ.

Periodic solutions for different values of κ were found using the same iterative method which was applied for different C and M for the Stokes fluid (Sec. 6.6). Here,

C and M parameters were fixed ($C = 1.5$ and $M = 256$). The value of κ in each step was changed by 0.02. This procedure of search of the initial values of R_2 and R_4 giving periodic trajectories was not repeated for other C and M since prior analysis of 2-rings system in permeable medium, as well as of 4-rings in Stokes fluid have shown that results obtained for $C = 1.5$ and $M = 256$ are representative for wider ranges of these parameters.

8.2   Analysis of periodic motion in 4-rings system

In the system of 4 rings in permeable medium there exist analogous periodic solutions to those three types found in the Stokes fluid. The results for selected values of κ, with all other parameters kept constant, are shown in Figs. 8.1. For all three types of periodic solutions the trajectory width defined as:

$$\max_{i\in\{1,...,4\},t\in T} \rho_i\left(t\right) - \min_{i\in\{1,...,4\},t\in T} \rho_i\left(t\right)$$

is consistently smaller for larger values of κ. The largest changes in trajectory shape are observed for 1st periodic solution, where range of κ is the widest. With decreasing permeability of the medium, mild bends of trajectory became sharper. In case of 2nd type of solution the shape and the width of trajectory does not change significantly for different values o f κ. For 3rd solution the trajectory width decreases with larger κ, while the length of trajectory of ring number 2 (in the middle) increases. The trajectories presented in Fig. 8.1 are similar to those for the Stokes fluid (Fig. 6.17, 6.18,6.19).

In the system of 2 rings in permeable medium it has been observed that periodic motion occur for some limited range of κ (Fig. 5.2). For larger values of κ the system breaks up. Similar situation is observed in the 4-rings system in permeable medium, with limiting value of κ specific for each type of periodic solution. For this reason periodic trajectories in Fig. 8.1 are drawn up to different values of κ.

In Figure 8.2A, parameters R_2 and R_4 for three periodic solutions for different κ are shown. The range of κ for which periodic trajectories were found is the widest in case of 1st type periodic solution, up to $\kappa = 4.18$. This value is still significantly lower than for 2-rings system ($\kappa \approx 8$, Section 5). Periodic motions of 2nd type can be found only for small values of $\kappa \leq 0.60$. Periodic solution of 3rd type exists for $\kappa \leq 1.98$. Approaching borders of these ranges, quasiperiodic motions exist for more and more
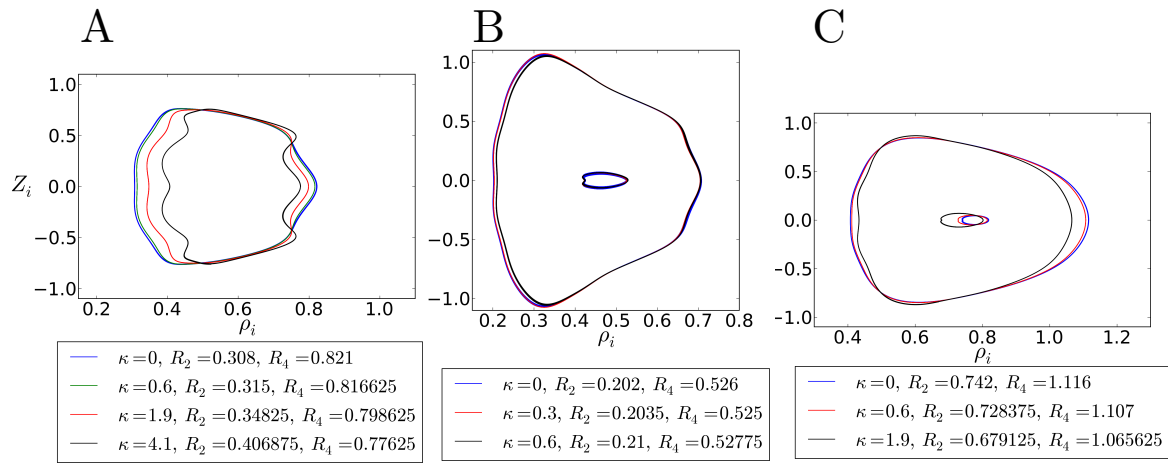
Figure 8.1: The trajectories of particles in centre of mass reference frame in permeable medium with different values of parameter κ. Three types of periodic solutions are shown in subplots (A)-(C), analogous to those in the Stokes fluid (Figs.6.17, 6.18,6.19).
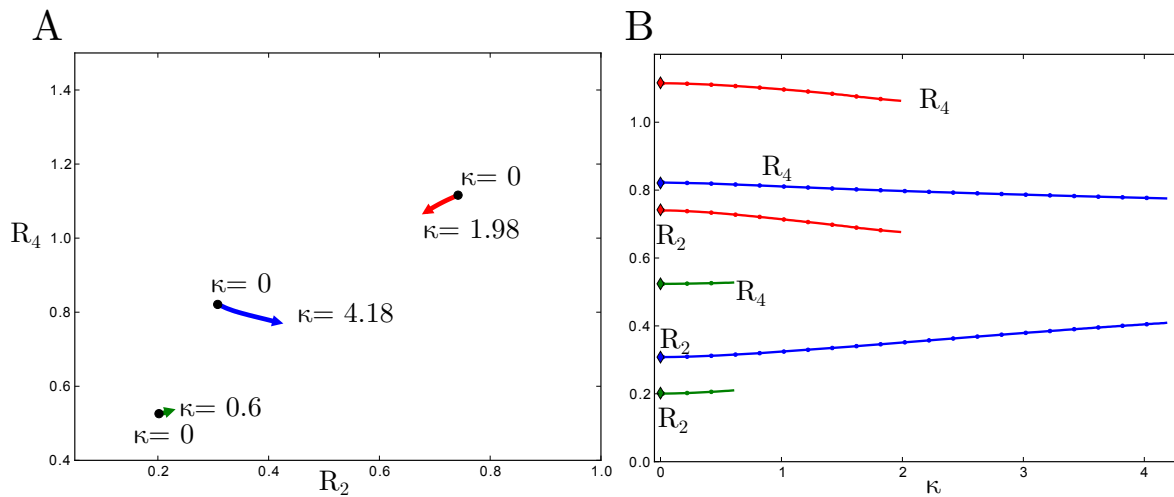

Figure 8.2: R_2 and R_4 parameters corresponding to three periodic solutions for different values of κ: (A) shown in $R_2 \times R_4$ parameters space (B) R_2 and R_4 plotted against κ. Colours correspond to different types of periodic solutions: blue: 1st, green: 2nd and red: 3rd.

narrow ranges of R_2 and R_4. Analogous situation has been observed in the Stokes fluid for varying C and M. The changes of parameters R_2 and R_4 for different κ in Fig. 8.2B are reflected in trajectories shown in Fig. 8.1. It is visible that the trajectories of periodic solutions does not change significantly with changing permeability.

Settling velocity of the cluster in permeable medium is shown in Figure 8.3. Settling is slower for greater κ (compare Fig.8.3A to decreasing permeability in Fig.8.3B,C,D). For all values of κ it can be observed that 2nd periodic solution leads to the fastest settling, 1st to an intermediate, and 3rd to the smallest. This order is not changed in media of different permeability. For greater values of κ (Fig. 8.3C,D) not all types of
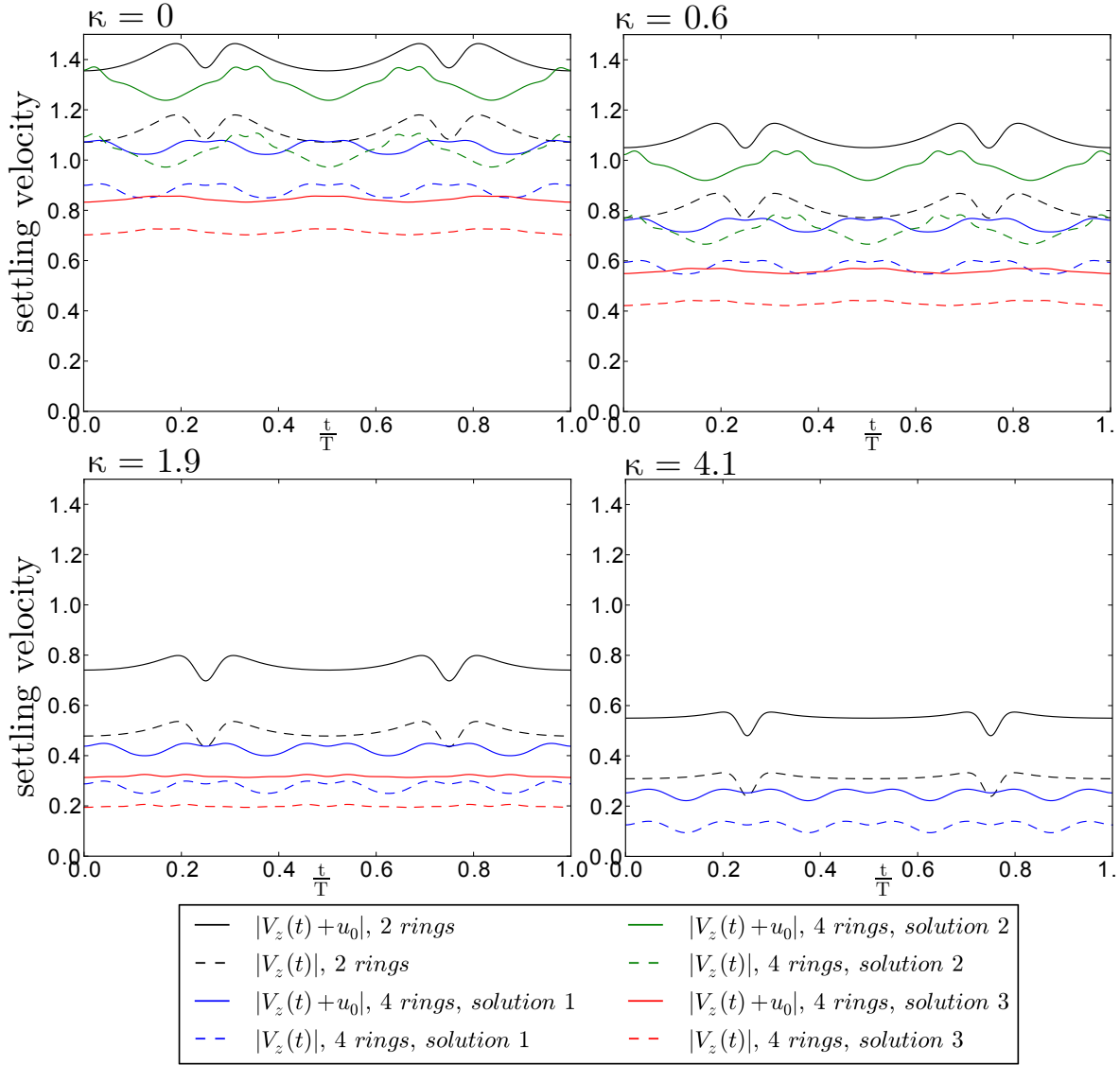
Figure 8.3: Settling velocities of clusters for different values of κ. Velocity values are shown both without self-term (dashed lines) and with self-term calculated for $a_p = a_{p,max}$ (solid lines). Colours blue, green and red correspond to 3 different types of periodic solution for 4-rings system, while black lines denote values for system of two rings with the same $M = 256$ and $C = 1.5$.

periodic solutions were found. Settling velocity of two rings is comparable to the one of 2nd solution of 4-rings system.

Results obtained in this section with different permeability and specified number of particles $M = 256$ and initial configuration parameter $C = 1.5$ are representative for others values of C and M. Such results can be obtained in a similar way as the ones for Stokes fluid (the procedure of generating families of periodic solutions for different values of C and M was discussed in Section 6.6). For gradually increasing value of κ from zero all three types of periodic solutions were found. For larger values of κ

periodic motions are harder and harder to find, since even small deviations in R_2 or
R_4 lead to fast decay of the group. These observations suggest that above these limits
with growing κ periodic motions become unstable or do not exist at all. Therefore we
found periodic solutions only for κ not exceeding a certain limiting value, specific for
the type of periodic solution. It was the greatest in case of type 1 and the smallest for
type 2. Let us remind here that in case of 2-rings system periodicity was lost for large
κ due to qualitatively different behaviour of rings of particles than in the Stokes fluid
(for large κ smaller ring moves slower than the larger one, see Section 5.2). Limiting
value of κ for periodic solutions in case of 2 rings was significantly larger than the
values found for 4 rings (Sec. 5).

The results presented in this section show that lower permeability of medium leads
to some changes in the dynamics in cases for which periodic orbits were found. The
periodic motions are not observed for small permeability (large value of κ). For smaller
values of κ trajectories of particles change slightly, only for larger κ ($\kappa > 2$) the
trajectory shape changes significantly. Settling velocity of the cluster is lower in less
permeable medium.

8.3   Streamlines and fluid velocity field in the system of 4 rings in permeable medium

After analysing dynamics of particles in permeable medium, let us now look closer
at fluid motion around the cluster for $\kappa > 0$. In case of 2 rings, discussed in Section
5.4, in less permeable medium lower amount of fluid was dragged with particles. In
general, both for $\kappa = 0$ and $\kappa > 0$, fluid streamed up (in the centre of mass frame)
through the middle of the group even for very small numbers of particles. The drops
were not observed for any number of particles (Figs. 4.3A, 5.8). In the system of 4
rings in Stokes fluid the situation was different: even for as large as $M = 256$ in case
of 2nd periodic solution streamlines in the central part of the cluster were closed and
the drop had a spherical shape. The torus-shaped drops were also observed for other
periodic solutions and different numbers of particles ($M \leq 256$). For smaller number
of particles the spherical drop is observed for all periodic solutions. The questions we
would like to answer here for 4-rings system is how κ coefficient influences existence
and shape of drop and amount of fluid dragged with settling particles?

Figure 8.4 illustrates how period-averaged fluid velocity (given by equation analo-
gously to Eq.(5.16)) and particles settling velocities depend on medium permeability.

Both of them are smaller for larger values of κ, but settling velocity of fluid in centre of the cluster (dashed lines) decreases faster than the velocity of particles (solid lines). In less permeable medium (larger κ) the difference between velocity of particles and velocity of fluid is larger. From Fig. 8.5 one can observe that for the same number of particles not only time-averaged particles velocity but also velocity in arbitrary time instance is larger than fluid velocity. Consequences of this fact will be clearly visible in streamlines analysis, what will be discussed later. Described properties apply to all three periodic solutions.

It is worth to add that lower settling velocity of the cluster of particles for larger κ is mainly caused by weaker hydrodynamic interactions rather than by smaller settling velocity of a single particle, u_0. Indeed, settling velocity of the cluster without u_0 term (dotted lines in Fig. 8.4) decreases with κ almost as rapidly as the total settling velocity, with u_0 included (solid lines in Fig. 8.4).
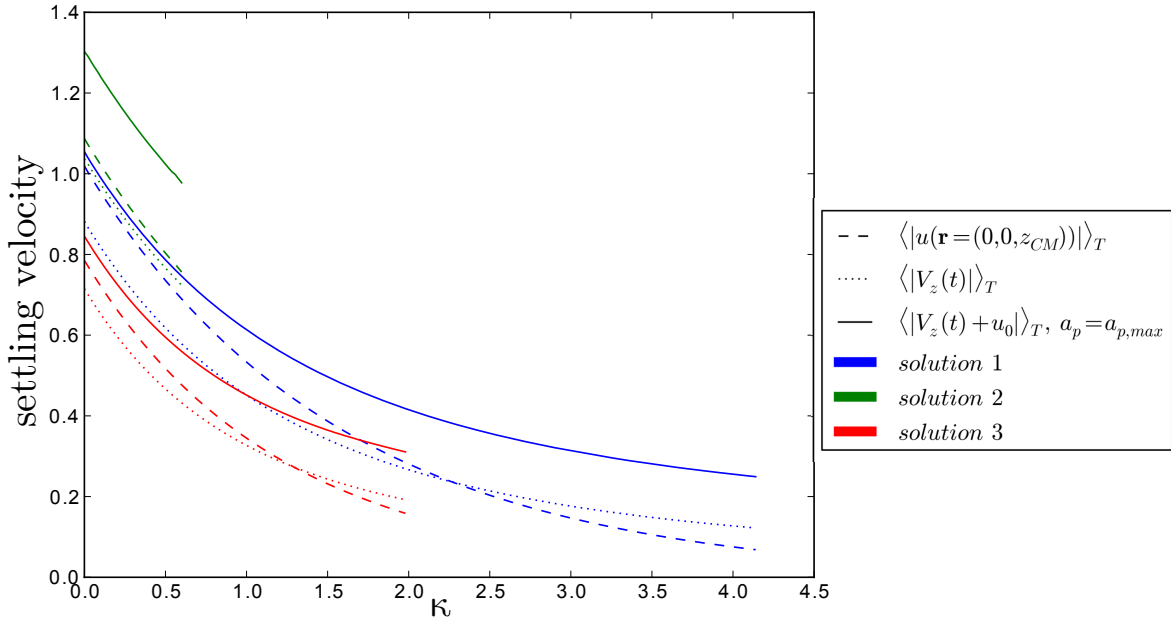

Figure 8.4: Settling velocities (normalised by velocity unit defined in Sec. 2.1.1) of particles and fluid, averaged over period, for different values of κ. Velocities of particles are given: without self-term (dotted lines) and with self-term calculated for $a_p = a_{p,max}$ (solid lines). Fluid velocity (dashed lines) is calculated in the centre of the cluster. Colours of the lines correspond to different periodic solutions. $C = 1.5$, $M = 256$.

In the Stokes fluid for the system of 2 and 4 rings we found drops for smaller numbers of particles ($M \leq 256$). Therefore fluid motion will be analysed for $M = 256$ as well as for smaller number of particles, $M = 32$ and $M = 64$ (figures for the last two numbers of particles can be found in Appendix A.3). Ranges of κ for which periodic solutions exist depend on number of particles and type of solution. When looking on

particles and fluid velocities during one period (Fig. 8.5 for $M = 256$) one can observe
that in all plots fluid velocity is in general smaller in relation to particles velocity.
Analogous plots for $M = 32$ and $M = 64$ can be found in Appendix A.3. While in
Stokes fluid for 2nd solution and $M = 256$ fluid in the centre of the cluster settles faster
than particles in some moments (Fig. 7.3) for less permeable media it may happen
only for small values of κ: for $\kappa = 0.3$ this situation can be observed in very short
instances and for $\kappa = 0.6$ it does not happen at all. The second aspect clearly visible
in the figure is the reduction of settling velocities of particles for growing κ, discussed
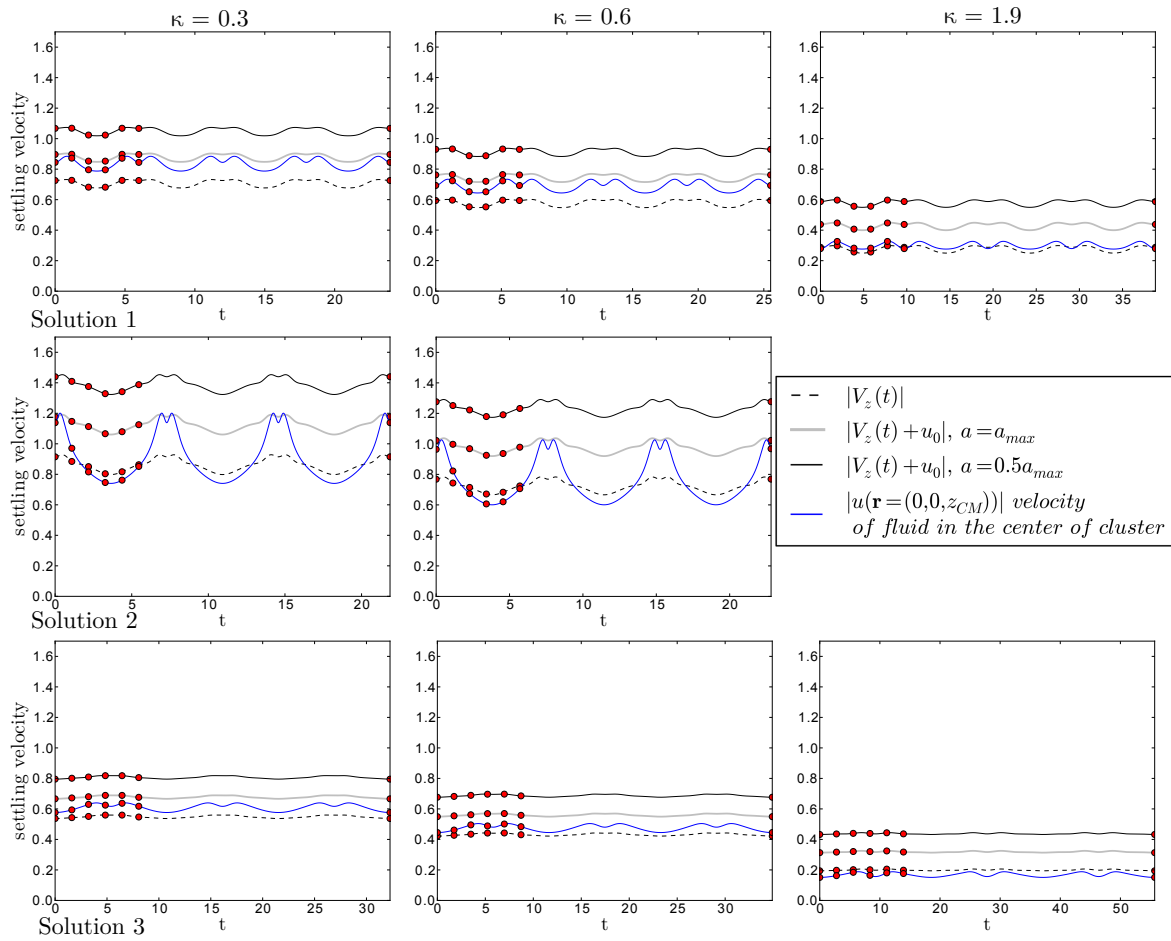in previous paragraph.

Figure 8.5: Velocity of the fluid $|u(\boldsymbol{r} = (0, 0, z_{CM}))|$ (blue line), velocity of the particles
$|V_z(t)|$ without self-term u_0 (dashed line) and velocity of the particles $|V_z(t) + u_0|$ for
two different radii: $a = a_{max}$ (grey line) and $a = a_{max}/2$ (black solid line); plots for
different values of κ, for three different periodic solutions. Red dots denote time points:
$t = 0$, $t = T/20$, $t = T/10$, $t = 3T/20$, $t = T/5$, $t = T/4$ and $t = T$. $C = 1.5$, $M = 256$.

For smaller numbers of particles ($M = 32$, Appendix A.3) and relatively small
permeability ($\kappa \leq 1.4$) drops are visible during whole period. This behaviour (in case
of $M = 64$, Appendix A.3) is responsible for temporal or permanent lack of spherical

drop in case of 1nd and 3rd solution, respectively. For larger number of particles
($M \geq 256$) the particles move much faster than the fluid what implies that spherical
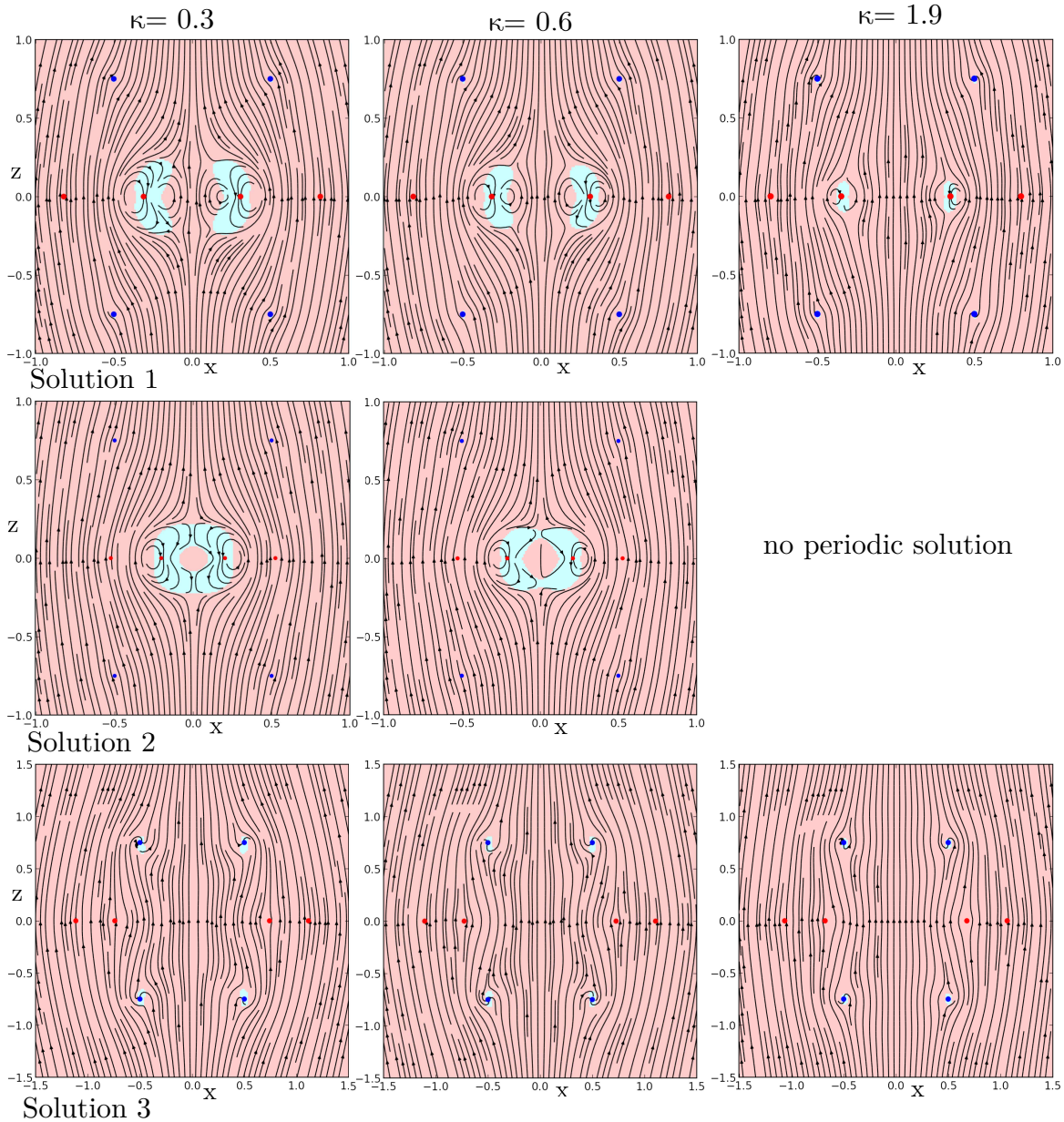drops are not observed.

Figure 8.6: Streamlines around initial configurations of particles, plotted for different
values of κ and for three different periodic solutions. Regions where fluid moves down
faster than particles are coloured in light blue, and where situation is the opposite - in
light red. The streamlines shown in plane $y = 0$. Positions of particles in this plane
are denoted with blue dots (drawn to scale). In red positions of particles from plane
shifted by $\frac{4\pi}{M}$. Particles are hardly visible due to small radii. $C = 1.5$, $M = 256$.

Now let us analyse streamlines of fluid in the reference frame comoving with the
centre of mass of the particles. The results for $M = 256$ are shown in Figure 8.6 and for

$M = 32$ and $M = 64$ in Appendix A.3. Settling velocity of the cluster is chosen as the minimal possible value, corresponding to maximal radii of particles, $a_p = a_{p,max}$ ($a_{p,max}$ was defined in Section 7). We can observe that larger values of κ lead to smaller size of region of closed streamlines ('drop'). As mentioned before, for $M = 256$, particles move down faster than the fluid in the centre of the cluster for most of the period and in consequence, the drop is torus-shaped rather than spherical and therefore has much lower volume: less fluid is dragged with settling particles.

The main observation is that in permeable medium drops are not observed for larger numbers of particles. The amount of fluid dragged with particles is reduced in comparison to the Stokes fluid. With increasing κ, (decreasing permeability) shape of the drop is becoming more toroidal rather than spherical. This behaviour is related to the fact that although larger value of κ effects in lower velocities of both particles and fluid, this decrease is stronger in case of the fluid velocity.

Chapter 9

Dynamics of system of 2 and 4 rings without symmetrization in the Stokes fluid

In section 2.1.2 we presented system consisting of K rings. After symmetrization we reduced the system of $3M$ equations to the system of $2K$ equations, where M denotes the total number of particles. We argued that the symmetrization is done to avoid non-symmetric numerical perturbations. In this section we discuss what is the dynamics of non-symmetrized system: we investigate the same initial conditions and compare the dynamics imposing symmetrization and without it. The main question is how does the symmetrization affects the dynamics of the 2- and 4-rings system?

The non-symmetrized dynamics of M particles is given by the Eq.(2.7). Similarly as before, the dynamics will be studied in reference frame moving with velocity $\boldsymbol{u}_0$, so that the self-term may be excluded from equations of motion. We solve $3M$ equations. In normalised variables (normalisation the same as in section 2.1.1) equations of motion for i-th particles ($\boldsymbol{r_i} = (x, y_i, z_i)$ with $i = 1, 2, \dots M$) are as follows:

$$\frac{dx_i}{dt} = -\frac{1}{M} \sum_{\substack{j=1 \\ j \neq i}}^{M} \frac{(x_j - x_i)(z_j - z_i)}{R_{ij}^3}, \tag{9.1}$$

$$\frac{dy_i}{dt} = -\frac{1}{M} \sum_{\substack{j=1 \\ j \neq i}}^{M} \frac{(y_j - y_i)(z_j - z_i)}{R_{ij}^3}, \tag{9.2}$$

$$\frac{dz_i}{dt} = -\frac{1}{M} \sum_{\substack{j=1 \\ j \neq i}}^{M} \frac{1}{R_{ij}} \left(1 + \frac{(z_j - z_i)^2}{R_{ij}^2} \right), \tag{9.3}$$

$$R_{ij}^2 = \sqrt{(x_j - x_i)^2 + (y_j - y_i)^2 + (z_j - z_i)^2}, \tag{9.4}$$

Initial positions are given by:

$$\boldsymbol{r}_i(0) = \left(\frac{1}{2}\rho_i^{(0)} \cos \phi_i^{(0)}, \frac{1}{2}\rho_i^{(0)} \sin \phi_i^{(0)}, z_i^{(0)} \right), \tag{9.5}$$

where $\rho_i^{(0)}$, $\phi_i^{(0)}$, $z_i^{(0)}$ are the initial particle coordinates. Denoting label of the ring with k and label of particle in the ring with n for the system of 2 rings, we have:

$$\rho_{2(n-1)+k}^{(0)} = \frac{1}{2} \tag{9.6}$$

$$\phi_{2(n-1)+k}^{(0)} = \frac{2\pi(n-1)}{N} \tag{9.7}$$

$$z_{2(n-1)+k}^{(0)} = \begin{cases} \frac{C}{2}, & \text{if } k = 1 \\ -\frac{C}{2}, & \text{if } k = 2. \end{cases} \tag{9.8}$$

In the system of 4 rings, ρ_i, ϕ_i, z_i are given by:

$$\rho_{4(n-1)+k}^{(0)} = \begin{cases} \frac{1}{2}, & \text{if } k = 1,3, \\ R_2, & \text{if } k = 2, \\ R_4, & \text{if } k = 4, \end{cases} \tag{9.9}$$

$$\phi_{4(n-1)+k}^{(0)} = \begin{cases} \frac{2\pi(n-1)}{N}, & \text{if } k = 1,3, \\ \frac{2\pi(n-1)}{N} + \frac{\pi}{N}, & \text{if } k = 2,4, \end{cases} \tag{9.10}$$

$$z_{4(n-1)+k}^{(0)} = \begin{cases} \frac{C}{2}, & \text{if } k = 1, \\ 0, & \text{if } k = 2,4, \\ -\frac{C}{2}, & \text{if } k = 3. \end{cases} \tag{9.11}$$

To demonstrate how symmetrization affects the dynamics of particles we compare numerical solutions of Eqs.(2.13) - (2.15) with solutions of Eqs.(9.1) - (9.4). We present their trajectories in reference frame moving down with velocity u_0 (settling velocity of an isolated particle, Figures 9.1 and 9.2) and in centre of mass reference frame (Figures 9.3 and 9.4). Initially lack of symmetrization does not affect the dynamics: periodic motions can be observed. However, after some time, non-symmetric numerical perturbations are growing and lead to destabilisation and decay of the cluster. This process occurs both in system of 2 rings (Fig. 9.1,9.3) and 4 rings (Fig. 9.2, 9.4). Time of destabilisation depends on number of particles and is shorter for larger M. It also depends on the numerical accuracy, however not strongly: changing integration accuracy

from 10^{-16} to 10^{-6} the number of observed periods does not change significantly (less than 15%) . For system of 2 rings the dependence on M is illustrated in Fig. 9.1: for 32 particles approximately one and a half of the period are observed, while for $M = 256$ only around half of the period. The same rule applies to the system of 4 rings (Fig. C in Appendix for $M = 256$).

For the systems with the same number of particles, but arranged in configuration of 2 or 4 rings, 4-rings system in general destabilises after longer time (also in terms of number of periods). This effect can be observed for 1st and 3rd periodic solution in 4-rings system.

Destabilisation occurs rapidly, what can be clearly seen in plots presenting particle motion in centre of mass reference frame (Figures 9.3 and 9.4). Periodic trajectories are marked with black line while trajectories of particles in non-symmetrized system are drawn with colour lines, with a different colour for each ring. It can be observed that once the deviation from periodic trajectory becomes large enough to be visible, it grows rapidly and for all particles form the ring at the same time. This stage corresponds to sudden lost of symmetry in particles motion, visible also in Figures 9.1 and 9.2.

Results presented in this section show that symmetrization of the dynamics is necessary to be able to effectively search for and analyse periodic motion of particles in presented system. This approach is especially useful when system consists of larger number of particles. If the system breaks up at time $t \sim T/2$, is it not possible to find the unstable periodic orbit precisely. In such cases symmetrization is necessary to analyse periodic motions. In consequence this approach allows to observe periodic motions in systems consisting of large number of particles and periodic motions with long period time and complex trajectories. Symmetrization also speeds up the computation by reduction of number of equations of motion.

Shorter destabilisation time for systems with larger M is consistent with the observations made by Ekiel-Jeżewska [38] for system with 2 rings. The general tendency is that the destabilisation time is longer in system of 4 rings (for all three periodic solutions) than in 2-rings system. These results seem to confirm hypothesis formulated in [38] and studied as a part of this dissertation: 4-rings system resembles better long-lasing quasiperiodic motions of particles in a random swarm, in comparison to the system of two rings. The stability of such systems will be the subject of future studies.
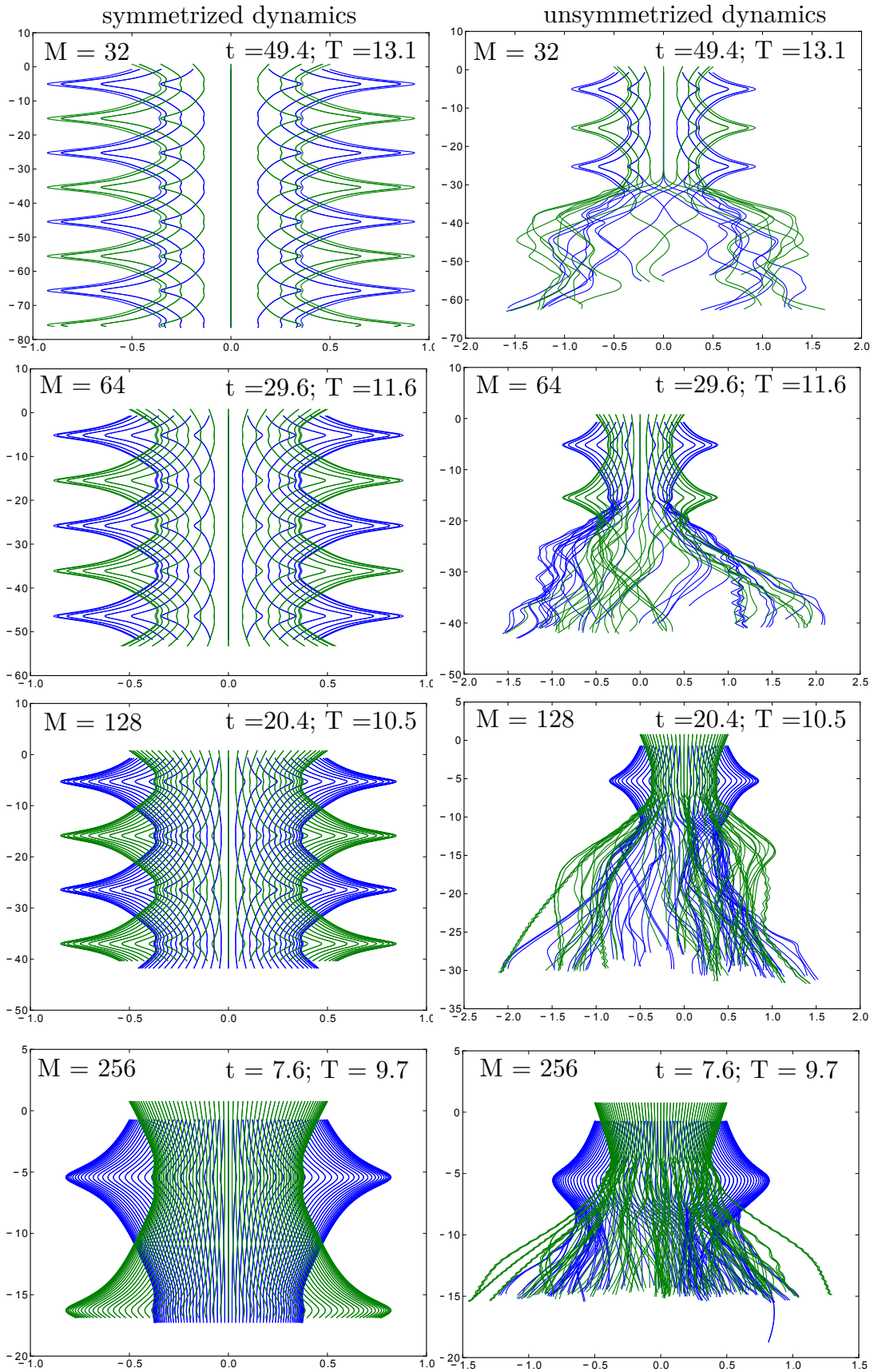
Figure 9.1: Comparison between trajectories in symmetrized (left column) and non-symmetrized (right) dynamics in the system of two rings. Plot for different numbers of particles in reference frame moving down with settling velocity of an isolated particle, u_0. Trajectories are shown up to a certain time t, different for each M, in order to show the process of destabilisation. $C = 1.5$.
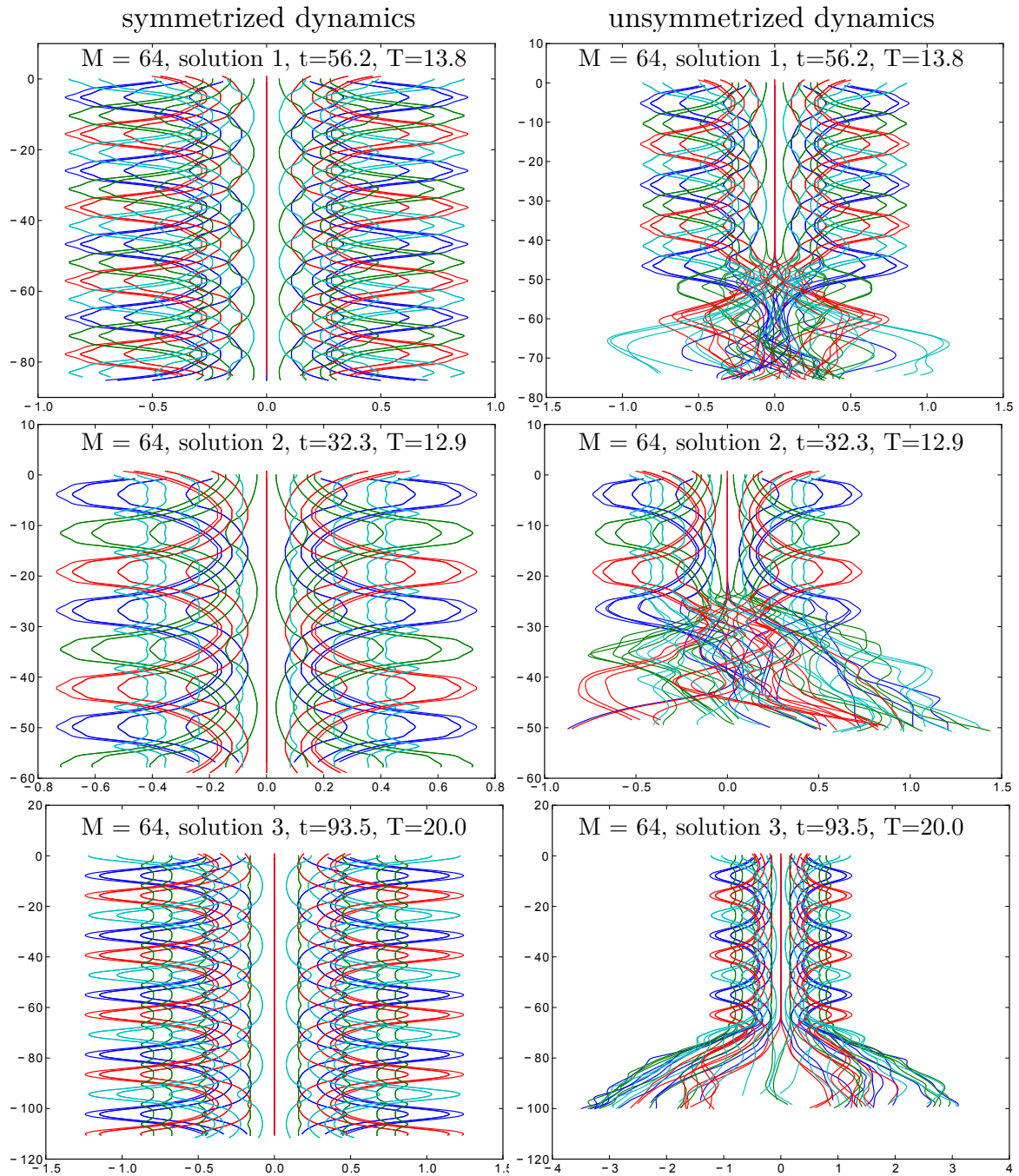
Figure 9.2: Comparison between trajectories in symmetrized (left) and non-symmetrized (right) dynamics in the system of four rings for three periodic solutions with parameters $M = 64$ and $C = 1.5$, in laboratory reference frame moving down with settling velocity of an isolated particle, u_0.
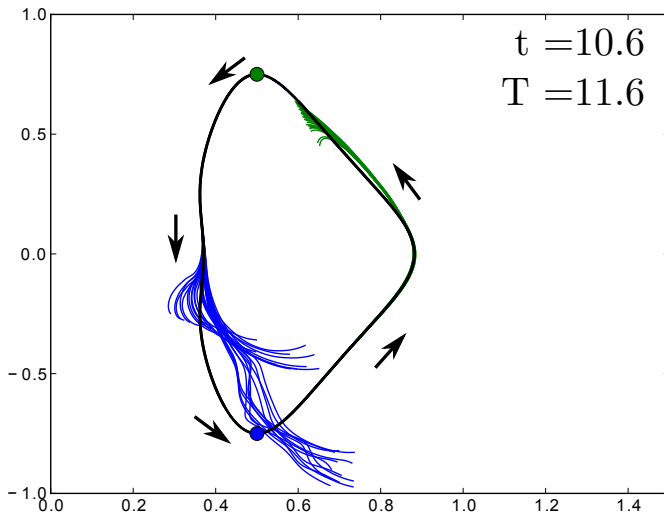
Figure 9.3: Trajectories of particles in the system of two rings in centre of mass reference frame. Periodic trajectory is drawn with black line. Colour lines represent destabilising trajectories of particles; different colours correspond to different rings. Initial positions of particles are denoted with dots of proper colour. At the beginning trajectories of particles are superimposed with black line, only after destabilisation they are visible. System of $M = 64$ particles, $C = 1.5$
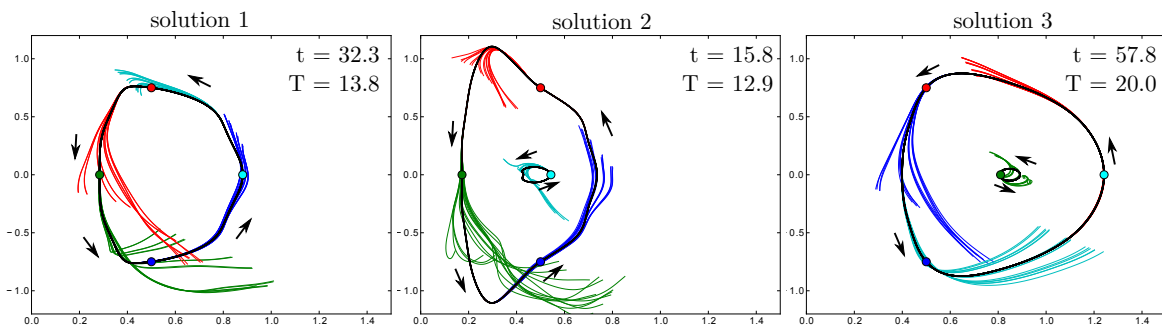

Figure 9.4: Trajectories of particles in the system of four rings in centre of mass reference frame for three different periodic solutions. Similarly as in Figure 9.3 periodic trajectories are drawn with black line and colour lines represent trajectories of particles. Initial positions of particles are denoted with dots of proper colour. Before destabilisation, trajectories of particles are superimposed by black periodic trajectory. System of $M = 64$ particles, $C = 1.5$

Chapter 10

Concluding remarks

10.1 Summary

In this thesis has been presented the numerical and theoretical analysis of dynamics of regular systems of many point particles falling under gravity. The fluid motion was described by the Stokes equations. The only interactions between non-Brownian and uncharged particles were hydrodynamic interactions. Summary of the main results and achievements of the thesis is presented as follows:

- It was shown that in the system of two rings periodic motions exist even for large numbers of particles (Chapter 3, [86]). Simulations were performed by taking into account symmetry of the system and using it to reduce number of equations of motion: without this modification group destabilises after very short time and periodic motions cannot be observed (Chapter 9). It was shown that for large number of particles M, trajectory width is smaller than for a small one.

- In the system of 4 rings three main types of periodic motions were discovered (Section 6.5, [86]). Solution number 1 is analogous to solution for 2 rings (all rings follow the same trajectory in the centre of mass reference frame). In solutions of 2nd and 3rd type one ring has its own, separate trajectory while the other three rings circulate around the 1st one and follow another trajectory, common for 3 rings. Solutions 2 and 3 belong to the same family and can be interpreted as two manifestations of the same type of motion, but for different values of the parameter C (defined in Section 6.1).

- Apart from 3 main periodic solutions, in the system of 4 rings, other periodic solutions with more complex trajectories have been found (Appendix B), where

during one period trajectory of particle multiple times crosses horizontal plane containing centre of mass of the cluster. These results show very rich dynamics of the system and suggest potentially huge number of periodic solutions. Existence of large number of complex trajectories may be significant for stability of sedimenting groups of particles [39, 70].

- Dynamics of 4-rings system for chosen M and C but varying R_2 and R_4 (defined in Section 6.1) was investigated. The decay and type of decay were determined (Section 6.3, [86]). In colour maps presenting these results there are large uniform areas, where the dynamics is deterministic, compact areas where periodic motions occur and chaotic regions where dynamics is sensitive to initial conditions. This picture is analogous to results obtained by Janosi et al. [39] for three sedimenting particles. Unlike in the system of three particles, in system of four rings, deterministic bands inside chaotic region have not been observed, at least in the resolution of R_2 and R_4 up to 10^{-4}.

- It was shown that in non-deterministic regions the system of 4 rings is very sensitive to initial conditions (Section 6.3.2, [86]). Simulations for a wide range of initial parameters were performed. Both in coarser scale (R_2, R_4 resolution 0.002) and in fine scale (resolution 10^{-4}) we observe huge differences of decay time for very close initial conditions. Type of decay of the cluster is equally sensitive to initial configuration.

- It was shown that in 4-rings system for initial parameters close to those leading to periodic motions, long-lasting quasiperiodic motions are observed. Lifetime of oscillations can easily exceed 10000 quasiperiods times (Section 6.3). Trajectories do not converge to any particular one. Comparing three periodic solutions we observe that quasiperiodic motions occur for the widest range of parameters around the 1st periodic solution.

- One-Way-Distance algorithm [100] was used in 4-rings system to measure similarity of parts of trajectory in subsequent quasiperiods. By looking for the thinnest trajectory (what refers to the minimal value of OWD) this method allows to find periodic trajectory even from huge set of quasiperiodic ones. It was shown that in each region of quasiperiodic motions a single OWD minimum exists (Section 6.4, [86]). The applied algorithm is universal and can be used to analyse any system performing periodic motion.

- Dynamics of two presented systems (2 and 4 rings) was investigated in permeable medium by using Brinkman-Debye–Büche (BDB) equations (Chapters 5 and 8). It was shown that for large permeability periodic motions exist, but have different shape of trajectory than in the Stokes fluid. For smaller permeability coefficient periodic motions have not been observed. This behaviour in system of 2 rings is caused by qualitative change in dynamics: smaller ring of particles settles down slower than a larger ring, a behaviour opposite to that in the Stokes fluid. In system of 4 rings periodic motions vanish for smaller κ what is accompanied by shrinkage of parameter range where quasiperiodic motions are observed (Section 8.2).

- It was shown that in permeable medium in the system of 4 rings quasiperiodic motions exist for smaller range of parameters than in the Stokes fluid.

- It was shown that for many parameters and initial conditions in systems of 2 and 4 rings fluid circulates inside settling group of particles and drop of fluid dragged with particles has spherical shape (Chapters 4 and 7). This effect is present when number of particles is not extremely large and depends strongly on particles sizes. Fluid motion inside 4-rings system is more similar to results for settling drop of suspension than it is in case of 2-rings system. Therefore it is justifiable to conclude that system of 4 rings better reflects the dynamic of suspension group than does the system of 2 rings.

- In permeable medium amount of fluid dragged with particles is smaller than in Stokes fluid. In consequence region of fluid circulation inside the cluster is smaller and drop of fluid dragged with particles is toroidal.

10.2   Original elements of the thesis

Original elements of this dissertation include:

- Adaptation and implementation of One-Way-Distance (OWD) method in order to measure similarity of parts of trajectory in the centre-of-mass reference frame in subsequent quasiperiods [86]. This algorithm allows to identify corresponding points between parts of trajectory and measure distance between these parts of trajectory. This method was applied to find periodic motions among trajectories for different R_2 and R_4 with given C and M: three main types of periodic motions

have been discovered. Application of recent OWD algorithm [100] is a unique approach to the problem of periodic motions and can be effectively implemented to any problem which is related to finding periodic orbits.

- Introduction of a new criterion of decay of group of particles [86]. The criterion is based on relative oscillations between pairs of rings. Observations of dynamics of particles in the centre-of-mass frame showed that the particles which stay together for a long time perform relative oscillations. Therefore a new idea based of physical behaviour of interacting particles was introduced: if the particles oscillate within a pair, they stay together. This new criterion turned out to be more adequate than distance-based criteria. The newly introduced criterion allows to determine both type of decay and cluster lifetime, and may be applied to many different systems, which perform any type of periodic and quasiperiodic motion.

- Development of an algorithm to find periodic solutions for different C or M based on a known periodic solution for close values of these parameters. The method is based on the fact that when C or M is slightly changed, the values of the other parameters should be changed a bit to obtain a new periodic solution. Having an initial periodic solution found (e. g. using OWD method), we build a grid with high resolution of R_2 and R_4, changing slightly C or M parameter and keeping the other one constant. Applying the newly introduced algorithm allowed to find periodic solutions for many values of C and M in computational time orders of magnitude smaller than it would have been needed to find them by systematic examination of $R_2 \times R_4$ parameter space. This algorithm may be used in various systems to find many periodic solutions belonging to the same family.

- Analysis of periodic motions in permeable medium described by Brinkman-Debye-Bùeche equations. First, we determined the range of values of the parameters leading to periodic orbits. To our knowledge it is the first work approaching this problem. Results included in this dissertation suggest that the problem is important since permeability coefficient has huge impact on the dynamics.

- Analysis of fluid motion around particles was performed. The question was whether the regions of closed streamlines are large enough to be significant in long-range transport of fluid inside the settling cluster, without mixing with the surrounding fluid. Apart from that a special attention was paid on spherical or toroidal shape of region of closed streamlines inside the cluster. It seems to be

significant since for drop of suspension it was shown that transition from spherical to toroidal shape of streamlines coincide with destabilisation of the drop [33].

All programs involved in the analyses conducted in this dissertation were created by the author.

10.3   Perspectives for future studies

Based on current knowledge in field of dynamics of regular systems of many particles settling in a viscous fluid [38, 39, 68–70, 72–74, 77, 103–106] and results obtained in this thesis, there exist some problems and open questions which can deepen understanding of periodic motions, chaotic scattering and dynamics of a suspension drop. All of these open questions are based on correspondence between periodic motions and dynamics of particles in concentrations closed to regular ones. The proposed further research would include the analysis of the following issues:

- Analysis of chaotic scattering in the system of 4 rings, including transition to chaos by varying initial parameters. The regions of long-lifetime cluster configurations (in space of initial parameters) are surrounded by bands with lifetime changing significantly from point to point. The open question is how the transition to chaos takes place? Sensitivity of dynamics on initial conditions (Section 6.3.2) suggests that linear equations of fluid motion leads to non-linear particles dynamics. The existence of complex periodic trajectories (presented in Appendix B) is likely to be a sign of transition to chaos. In addition it is worthy to investigate if the borders of long-lifetime regions have fractal structure. Work on this topic is in progress.

- Numerical study of stability in the system of 2 and 4 rings, especially in case of complex trajectories. Analysis based on Floquet theory. Preliminary studies have been already done and further research will be conducted in the future,

- Taking into account more perturbations in the system of 4 rings, e. g. by adding more rings, placed in different planes or rotated with respect to the others. The aim is to observe how much it is possible to perturb initially regular system to obtain periodic orbits. This is an important question because systems consisting of more rings are expected to exhibit behaviour more similar to a settling suspension drop. This will be a subject of future studies.

- Further study of fluid motion around periodic solutions for many particles by tracking fluid element. This question is important because of fluid mixing problem.

- Investigation of other periodic motions, reported e. g. by [68, 74, 103] in Brinkman medium. These studies are currently in progress.

Experimental verification of the system dynamics presented and analysed, both theoretically and numerically, in this dissertation would be an interesting step. Similar experiments for different systems performing periodic motions have been already done, e. g. by J. Nowakowski and M. L. Ekiel-Jeżewska [6] and by group of M. Shelley [77].

Appendix

A Fluid motion: additional analysis

Appendix A presents streamlines around periodic solutions for the system of 2 and 4 rings in the Stokes fluid. The plots presented here provide additional information to those discussed in Sections 4, 7, 8.3. They include analysis of fluid velocity during the period and analysis for different numbers of particles with respect to the main text. Additionally, more detailed picture of streamlines in the centre of the cluster is given for the 1st and 2nd solution in the 4-rings system.

A.1 The system of 2 rings in a viscous fluid

In Section 4 we observed, that for larger numbers of particles and particle radius $a_p = a_{p,max}/2$ fluid moves much slower than particles. Therefore very small amount of fluid is dragged with particles. We also observed that there are no closed streamlines in the centre of mass reference frame for larger numbers of particles (see Fig. 4.3). Here we show how it is in case of a smaller number of particles and a larger particle radius $a_p = a_{p,max}$. We also present how the streamlines change during the period.

In Figure 1 fluid motion around the cluster is shown for a quarter of the period. Streamlines are drawn in reference frame comoving with centre of mass of the cluster for the case where particles radius a_p is set to maximal possible value, $a_p = a_{p,max}$. Inside the area coloured in cyan fluid moves down faster than particles. Positions of particles are denoted with blue circles, drawn to scale. It can be observed that size of the droplet (the region of closed streamlines in the central part of the cluster, see definition in Sec. 7) is changing during the period. For $M = 8$ and $M = 16$, but not for $M = 32$, a drop of fluid is visible in all snapshots. Increasing the number of particles the drop of fluid cannot be recognised.
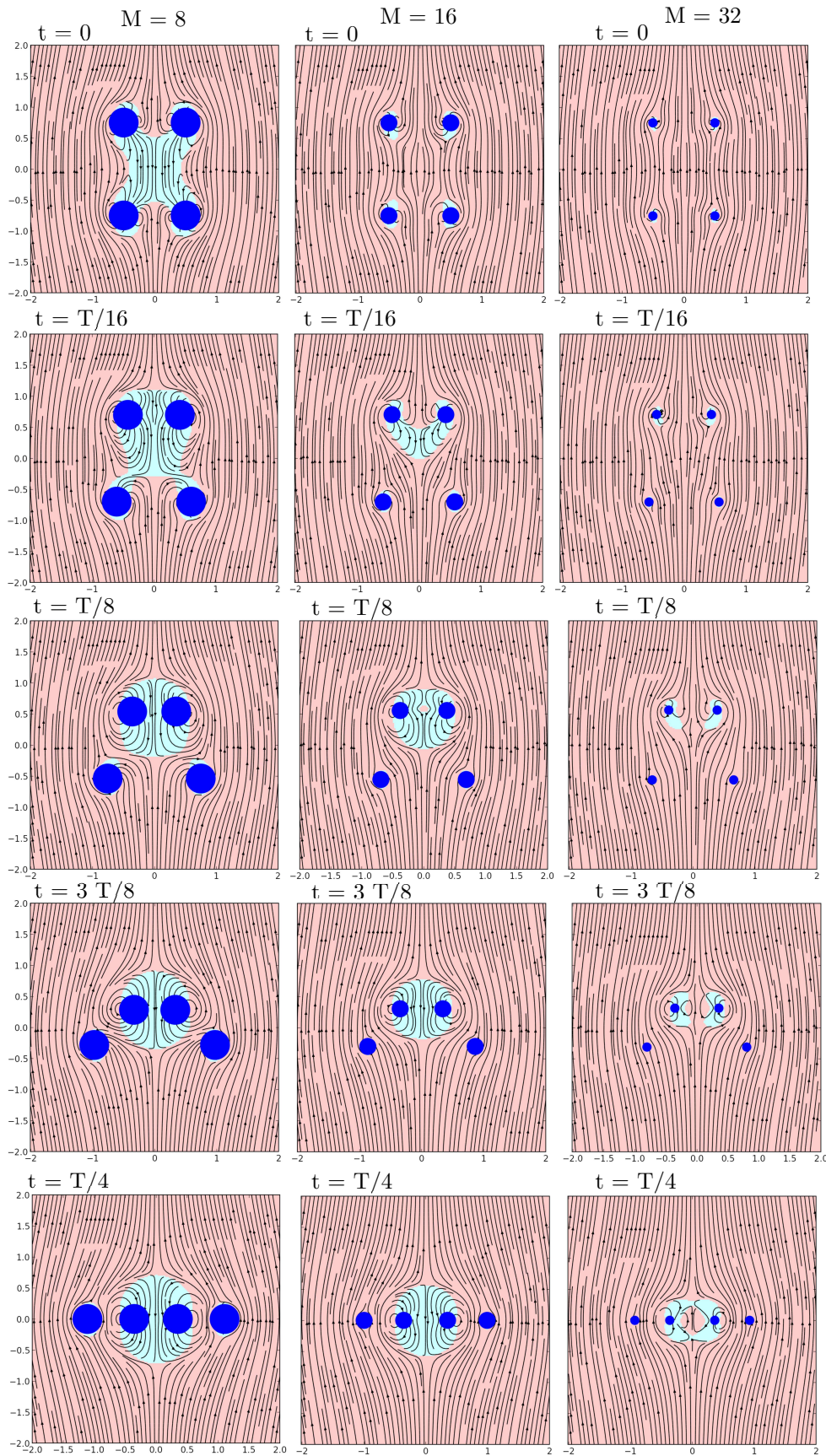
Figure 1: Streamlines around the cluster made of M particles plotted in chosen moments during the period, for $M = 8$, $M = 16$ and $M = 32$. Regions where fluid moves down faster than particles are coloured in light blue, and where situation is the opposite - in light red. The streamlines are shown in plane $y = 0$. Positions of particles are denoted with blue dots (drawn to scale), $C = 1.5$, $a_p = a_{p,max}$.

A.2 The system of 4 rings in a viscous fluid

In Section 7 fluid motion around the cluster of 4 rings was analysed. Here some additional information, namely streamlines in various moments during the period and for different numbers of particles are presented. We also show enlargement of streamlines in the central part of the cluster in a few cases, which were identified as having more complex streamlines pattern.

Results for streamlines are presented in a way analogous as it was done for 2 rings in Fig.1. In Figure 2 fluid motion around the $M = 256$ particles during representative part of the period is shown ($T/4$ in case of 1st type of solution and $T/3$ for 2nd and 3rd type). In Fig.2 and Fig.3 three different types of periodic solutions are presented. In can be observed that for $M = 256$ small amount of fluid is dragged with particles. Torus-shaped drops are not observed during whole period around the same given ring. The drops are formed around each ring repeatedly at different time instances during the period. For periodic solutions type 1 and 2 volume of the droplet is the largest when particles are at the initial configuration and at $t = T/4$ or $t = T/3$ respectively. In case of 3rd type of periodic solution the drop is the largest for $t = T/6$.

For $M = 32$ (Fig.3) the drop exists during the whole period for 1st and 3rd periodic solution. The amount of fluid dragged with particles is larger in case of 3rd solution. Situation is different for 2nd periodic solution where drop is visible during a part of the period only and its size is the smallest in comparison to other two types of periodic solutions.

In Fig. 2 it can be seen that pattern of streamlines in the central part of the cluster is complex. To analyse this structure we present more detailed picture of fluid motion inside the cluster for periodic solutions types 1st and 2nd at $t = 0$ in Figure 4. For the first periodic solution it can be observed that fluid streams up through the middle of the cluster, but this happens only for narrow region in the central part of the cluster (the drop has a toroidal shape). Most of the fluid streams around the drop. In case of second periodic solution shape of the drop is oblate spheroid. In the centre of the drop there is a spherical region inside which the fluid circulates in the direction opposite to the rest of the drop.
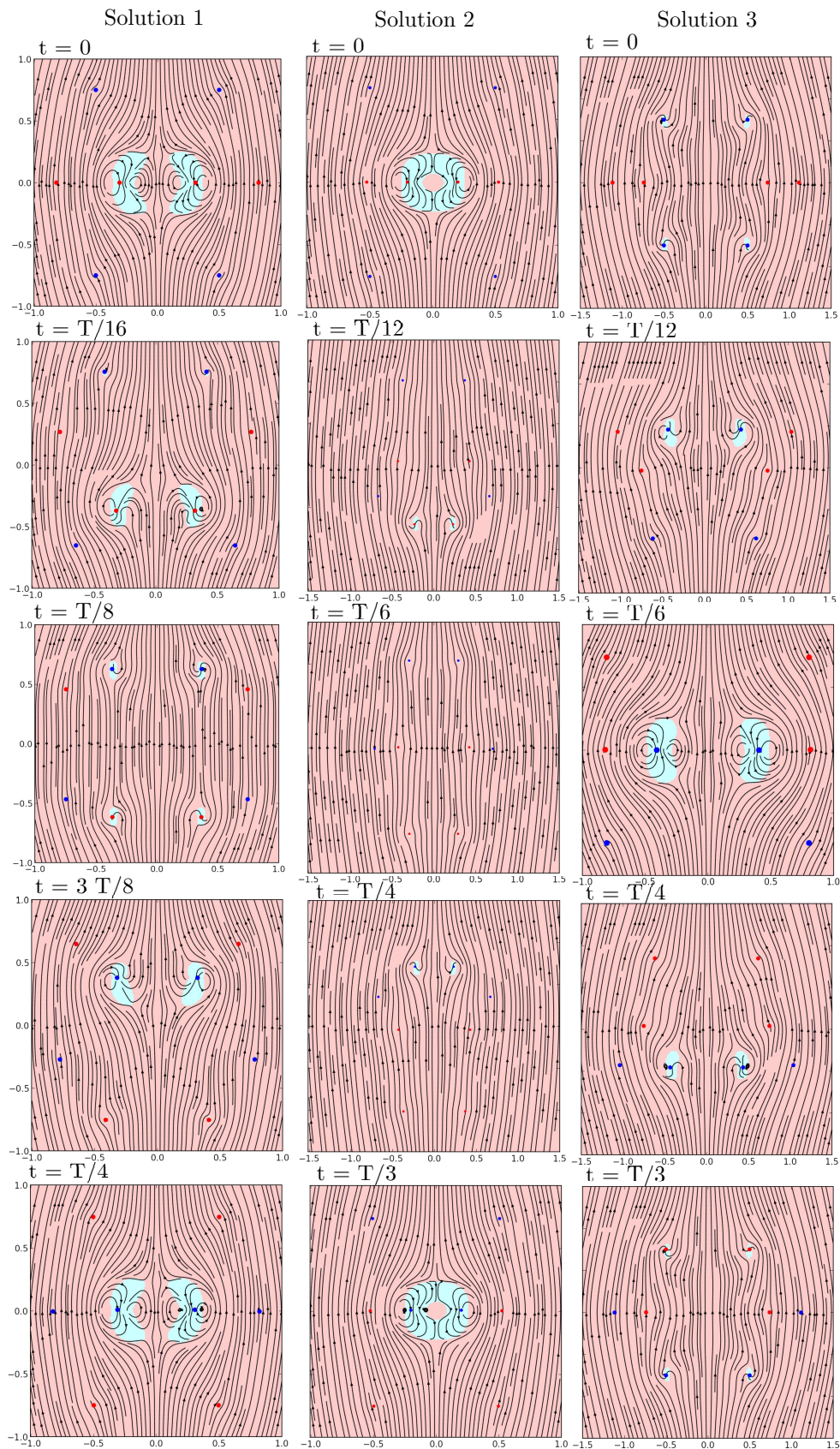
Figure 2: Streamlines in the system of 4 rings in Stokes fluid during $T/4, T/3, T/3$ for 1st, 2nd and 3rd periodic solution respectively. Positions of particles are denoted with blue dots (in plane $y = 0$) and with red ones (plane $y = pi/64$). $C = 1.5$, $M = 256$.
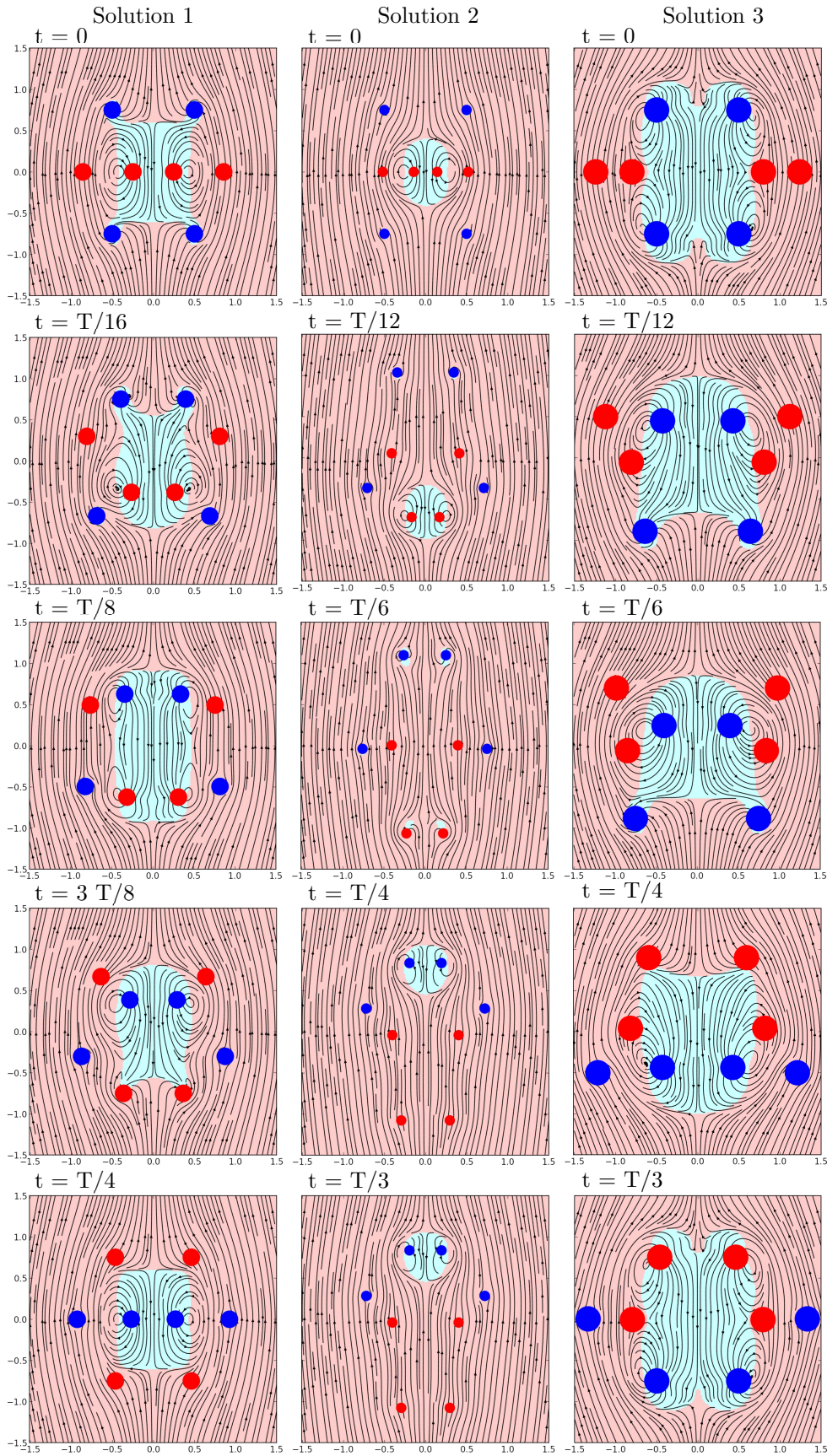
Figure 3: Streamlines in the system of 4 rings in Stokes fluid during $T/4, T/3, T/3$ for 1st, 2nd and 3rd periodic solution respectively. Positions of particles are denoted with blue dots (in plane $y = 0$) and with red ones (plane $y = pi/8$). $C = 1.5$, $M = 32$.
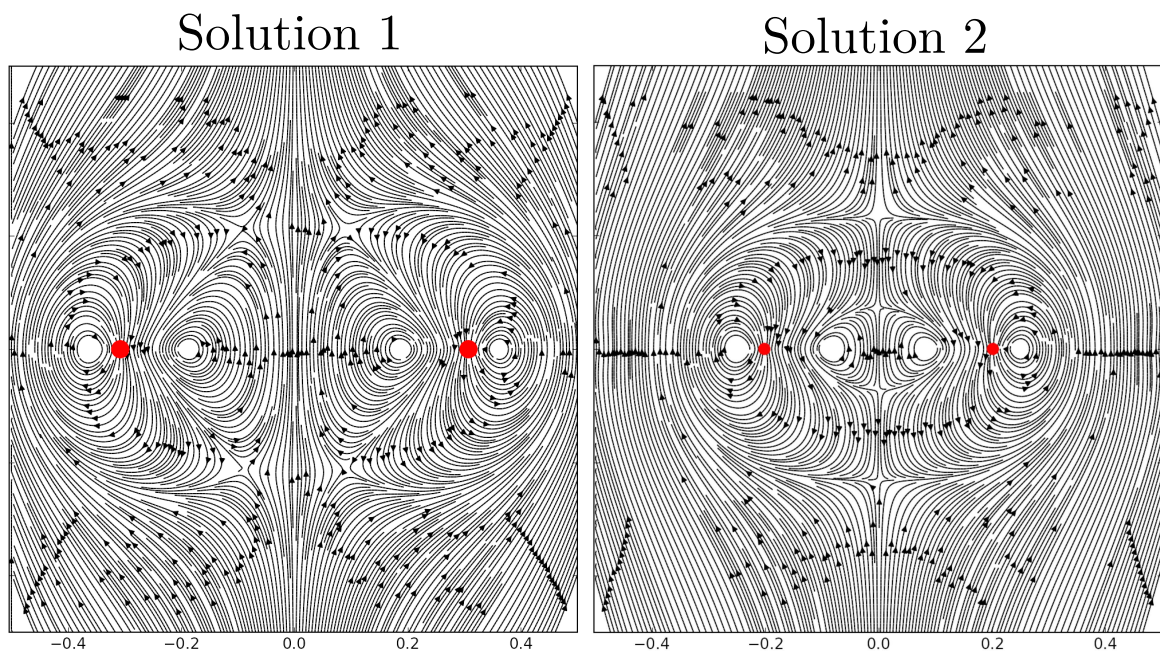
Figure 4: Enlargement of two plots in top row in Fig. 2- streamlines in the central part of the cluster for 1st and 2nd periodic solution. Only particles from the second ring are visible - the rest is outside the plotted area, $M = 256$.

A.3   The system of 4 rings in permeable medium

The aim of this section is to give supplementary information about fluid motion around cluster of 4 rings in permeable medium (analysed in Section 8.3). For the system of $M = 256$ particles evolution of streamlines during representative part of the period is presented. We show also plots of settling velocities and streamlines for smaller number of particles ($M = 32$, $M = 64$) than it was done in the main text.

In Figure 5 the dynamics of fluid during the period is shown for permeable medium with $\kappa = 0.6$. It may be compared with analogous results for Stokes fluid, presented in Fig. 2. Here, the amount of fluid dragged with particles is much lower than for $\kappa = 0$, what is visible during the whole period.

Figures 6 and 7 show fluid velocity and settling velocities of particles during the period for 32 and 64 particles, respectively (analogous to Fig. 8.5). Colour code is the same as in Figure 8.5 in the main text: blue line represents fluid velocity in the centre of the cluster, dashed line is the interaction term of particles settling velocity and black and grey lines correspond to settling velocity of particles with $a_p = a_{p,max}/2$ and $a_p = a_{p,max}$ respectively. In less permeable medium (higher kappa) fluid velocity is lower with respect to velocity of particles. For smaller values of κ the opposite situation is observed: fluid moves down faster than particles what allows for formation of a drop.

Streamlines around clusters in permeable media are presented in Figures 8 and 9 for $M = 32$ and $M = 64$, respectively. As before (Figures 1, 2) they show results for $a_p = a_{p,max}$. Comparing streamlines for different number of particles it is clear that drops are larger for clusters consisting of less particles. The same dependence was observed in the Stokes fluid: the larger number of particles is, the smaller amount of fluid is dragged. In general in less permeable media particles drag less fluid, albeit this effect is weak for low values of κ.
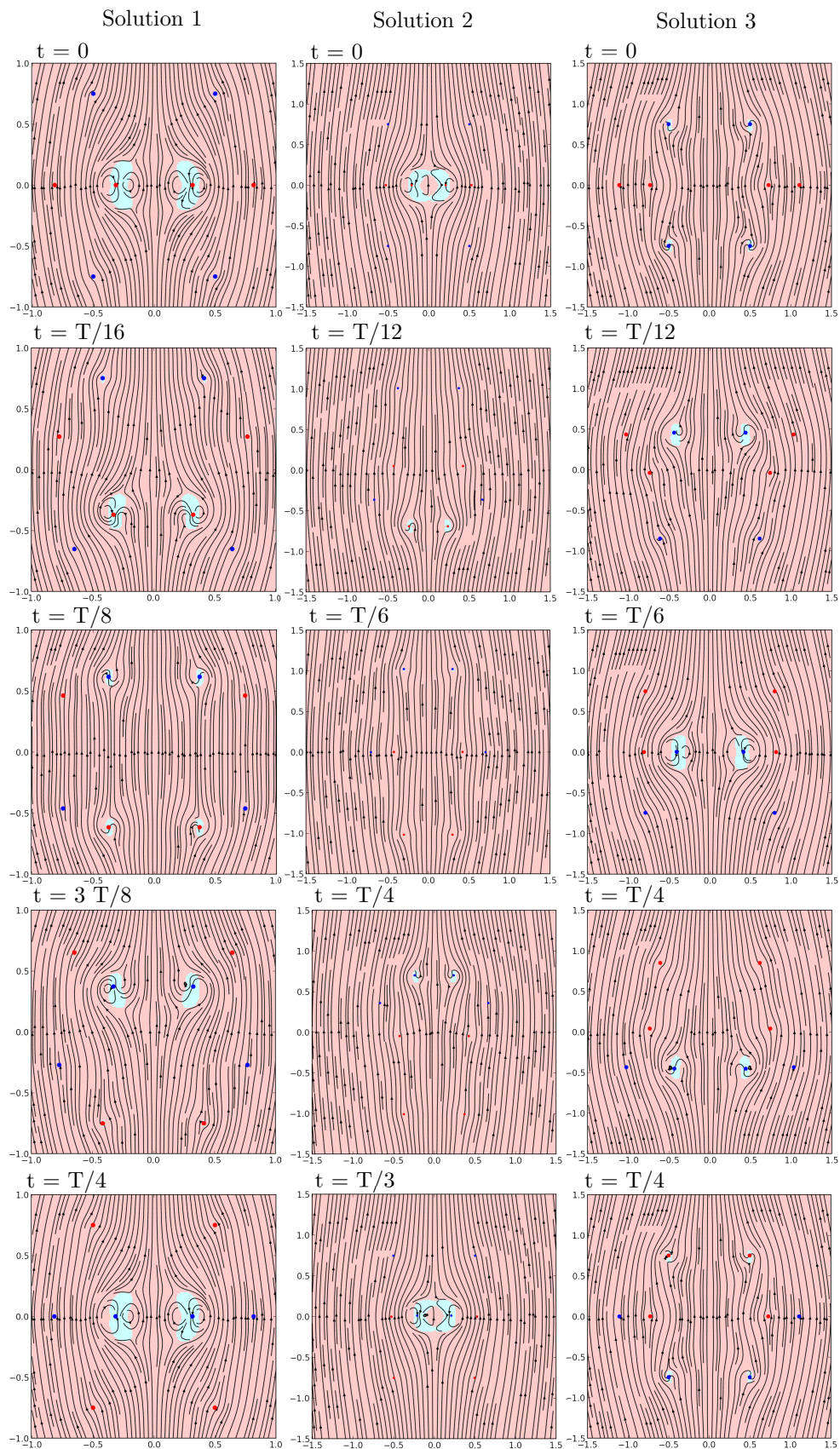
Figure 5: Evolution of streamlines in the system of 4 rings in permeable medium for the 1st, 2nd and 3rd periodic solutions, respectively. $C = 1.5$, $M = 256$ and $\kappa = 0.6$.
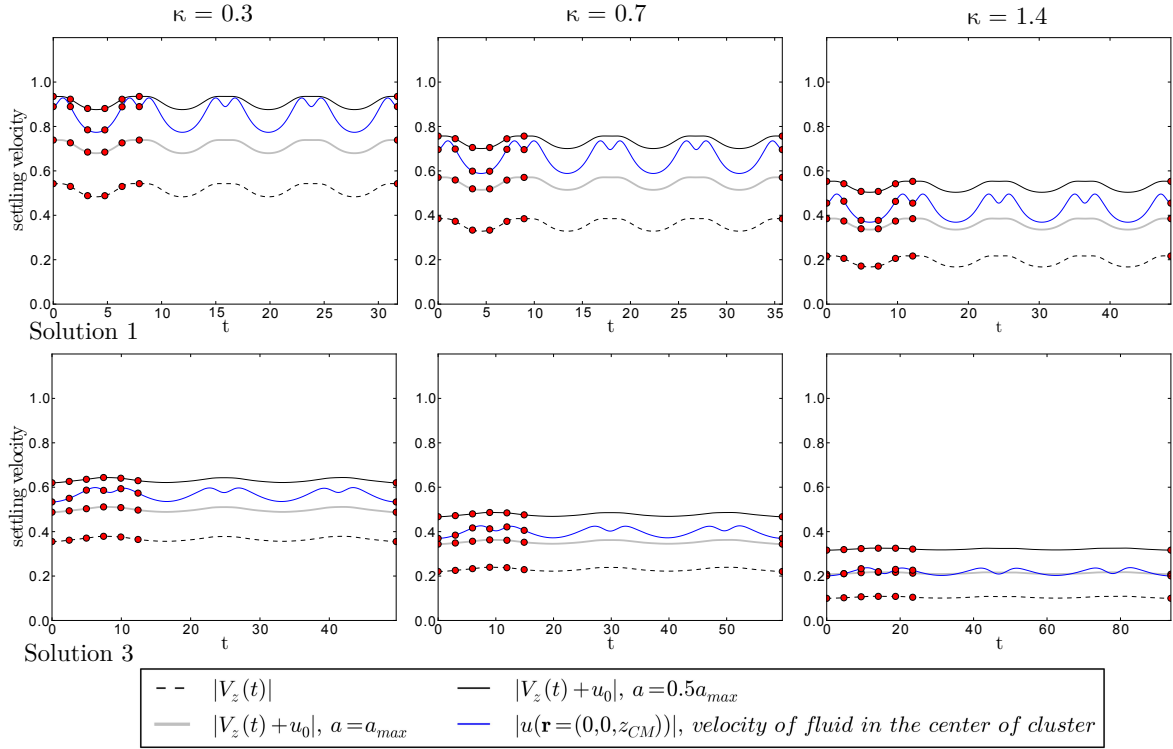
Figure 6: Velocity of the fluid $|u(\boldsymbol{r} = (0, 0, z_{CM}))|$ (blue line) at the centre of the cluster, velocity of the particles $|V_z(t)|$ without self-term u_0 (dashed line) and velocity of the particles $|V_z(t) + u_0|$ for two different radii: $a = a_{max}$ (grey line) and $a = a_{max}/2$ (black solid line); plots for different values of κ, for three different periodic solutions. Red dots denote time points: $t = 0$, $t = T/20$, $t = T/10$, $t = 3T/20$, $t = T/5$, $t = T/4$ and $t = T$. $C = 1.5$, $M = 32$.
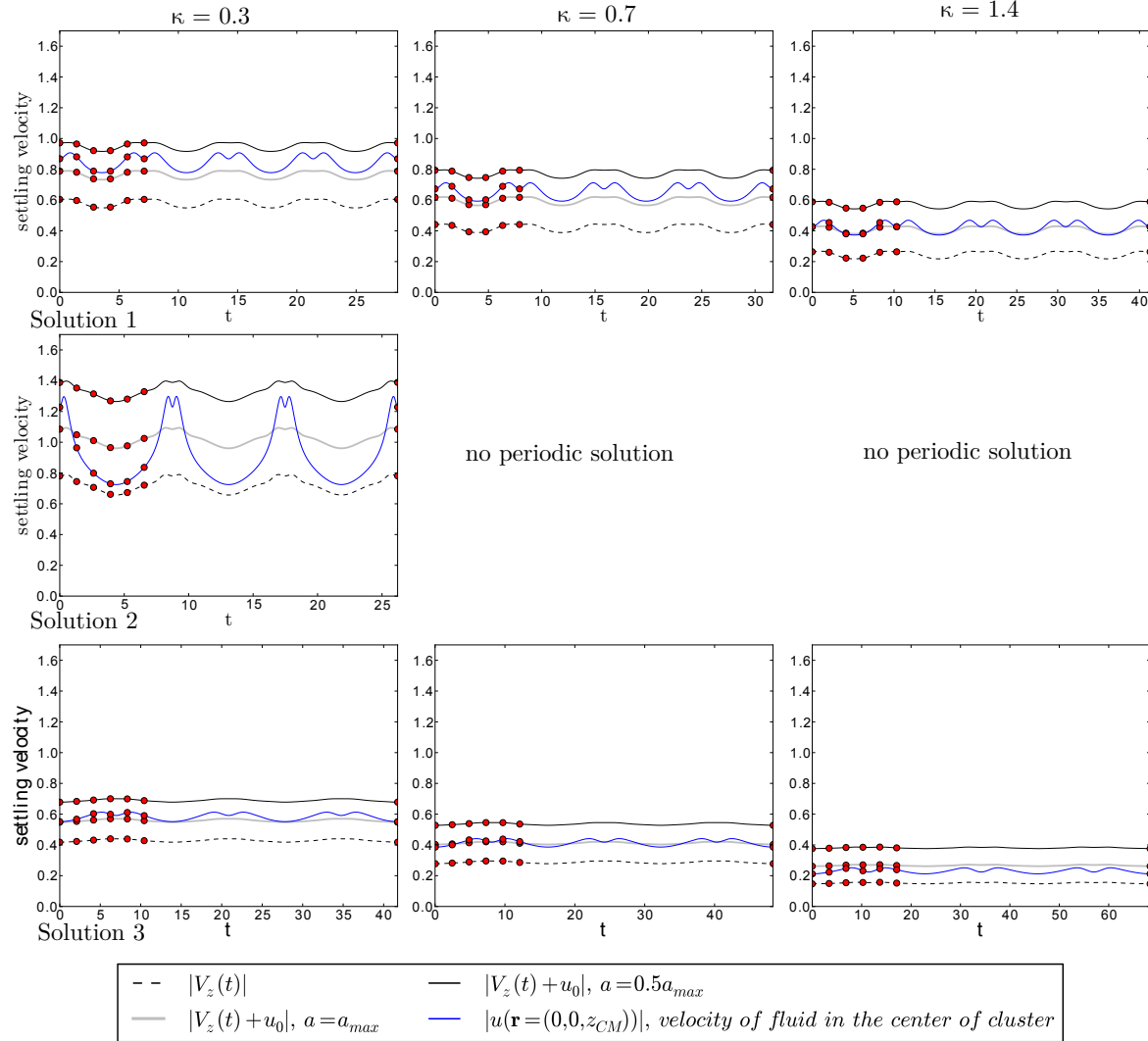
Figure 7: Velocity of the fluid $|u(\boldsymbol{r} = (0,0,z_{CM}))|$ (blue line), velocity of the particles $|V_z(t)|$ without self-term u_0 (dashed line) and velocity of the particles $|V_z(t) + u_0|$ for two different radii: $a = a_{max}$ (grey line) and $a = a_{max}/2$ (black solid line); plots for different values of κ, for three different periodic solutions. Red dots denote time points: $t = 0$, $t = T/20$, $t = T/10$, $t = 3T/20$, $t = T/5$, $t = T/4$ and $t = T$. $C = 1.5$, $M = 64$.
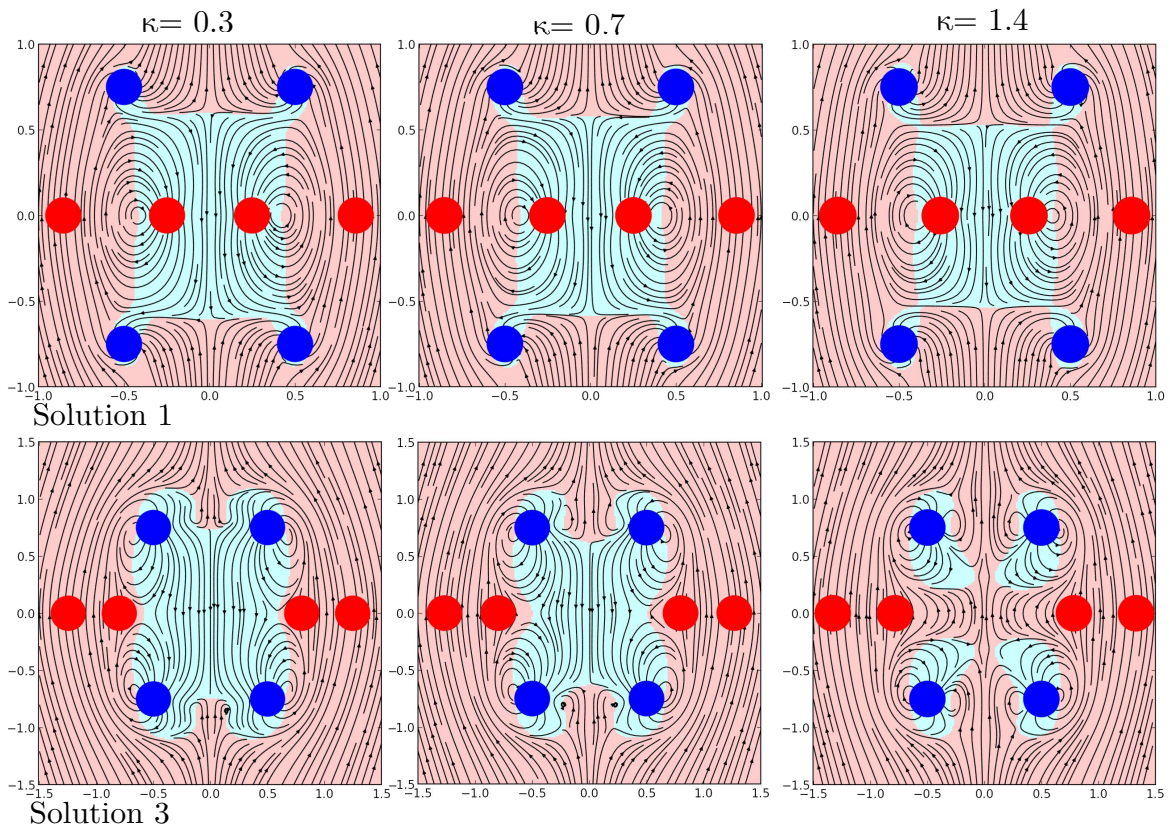
Figure 8: Streamlines in the system of 4 rings in permeable medium for 2 periodic solutions and different values of κ at $t = 0$. 2nd solution does not exist for this number of particles, $M = 32, C = 1.5$. The particle size drawn to scale.
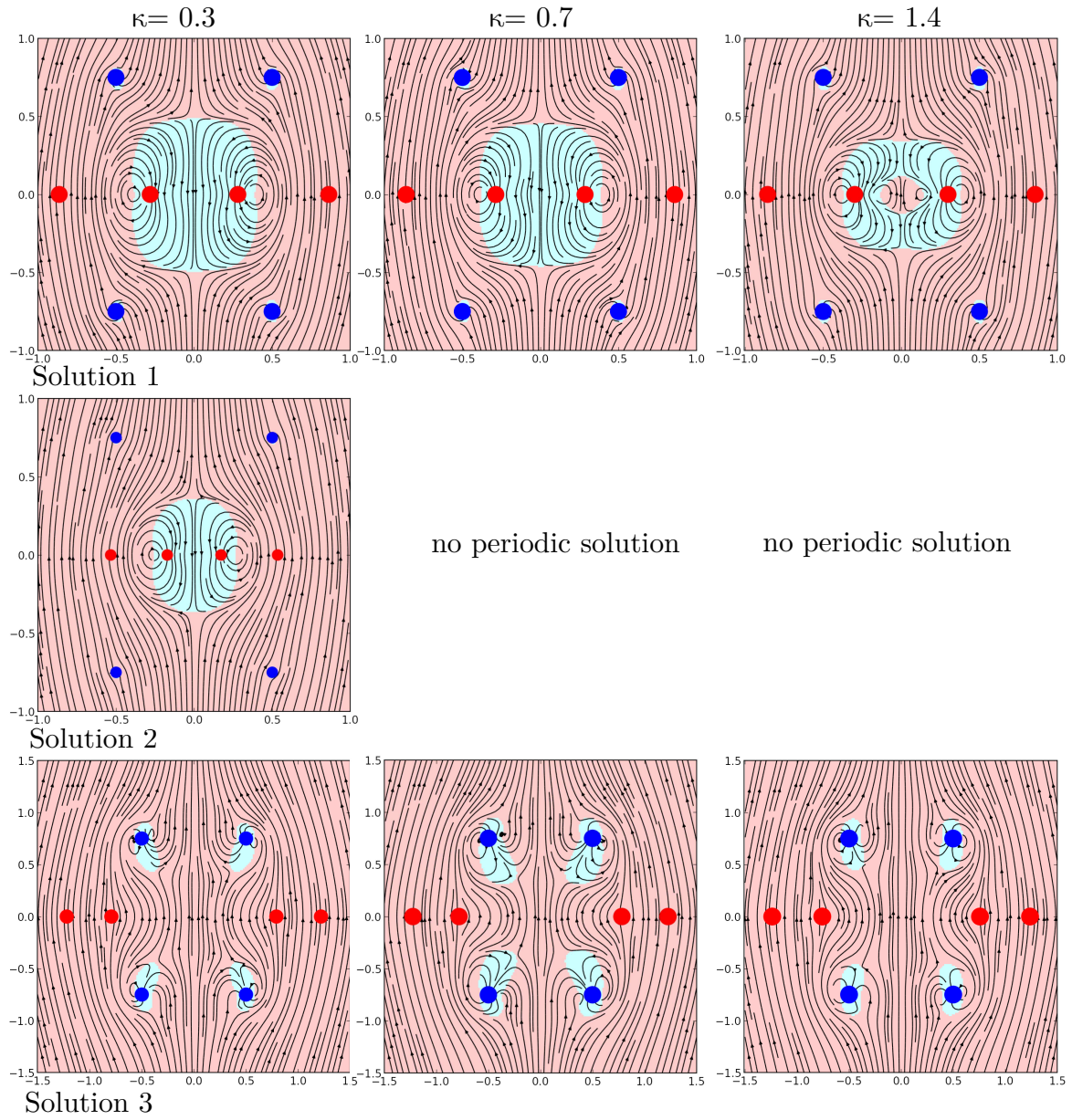
Figure 9: Streamlines in the system of 4 rings in permeable medium for 3 periodic solutions and different values of κ at $t = 0$. $M = 64, C = 1.5$.

B   Complex periodic trajectories in 4-rings system

Appendix B presents examples of some complex periodic and quasi-periodic trajectories in 4-rings system. Apart from three main types of periodic solutions, discussed in Section 6, other periodic trajectories, with more complex shapes, can be found. As mentioned in Section 6.6 some of them exist for small M or C parameters for which no periodic solutions of three main types can be found. Examples of such complex trajectories for small M or C are shown in Figure 10A-C. These trajectories were found in the procedure described in Section 6.6, but differ from main three periodic solutions. R_2 and R_4 parameters of these complex trajectories in Figure 6.20 would locate in extensions of marked curves.

Trajectory presented in Figure 10D can be considered as an example of separate case. It was found for $M = 256$ and $C = 1.5$ and is not similar to any of three main types of periodic solutions. Particles from each ring follow the same trajectory which is much longer among periodic motions observed in analysed system. It may be related to period doubling and chaotic behaviour in such a system and it will be subject of future studies.
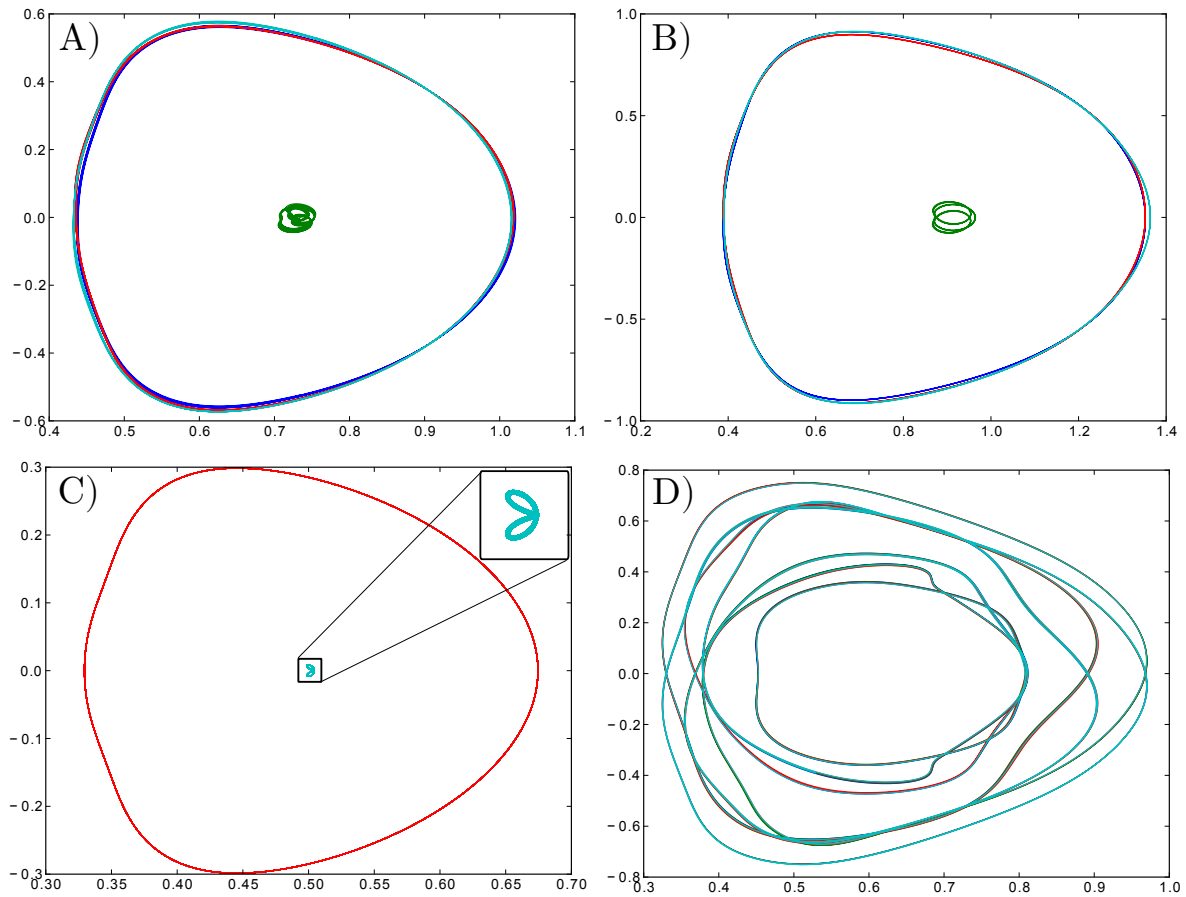
Figure 10: Periodic trajectories for parameters: A) $M = 256, C = 0.92$, trajectory similar to 3rd type of periodic solution B) $M = 28, C = 1.5$, trajectory similar to 3rd type of periodic solution, C) $M = 256, C = 0.57$, trajectory similar to 2nd type of periodic solution, D) $M = 256, C = 1.5$, an example of periodic motion with complex trajectory.

C   Non-symmetrized dynamics

In Section 9 it was shown how symmetrization affects the dynamics of 2- and 4-rings system for smaller numbers of particles. The natural question is whether for larger numbers of particles the system breaks up almost immediately, or periodic motions still can be observed, what requires that destabilisation does not occur till $T/2$ in case of 2 rings, and till $T/4$ or $T/3$ in the system of 4 rings.

Appendix C presents comparison between symmetrized and non-symmetrized dynamics in the system of 2 and 4 rings in the Stokes fluid for larger numbers of particles as it was shown in Section 9. Results are shown in frame of reference comoving with a settling velocity of a single particle.
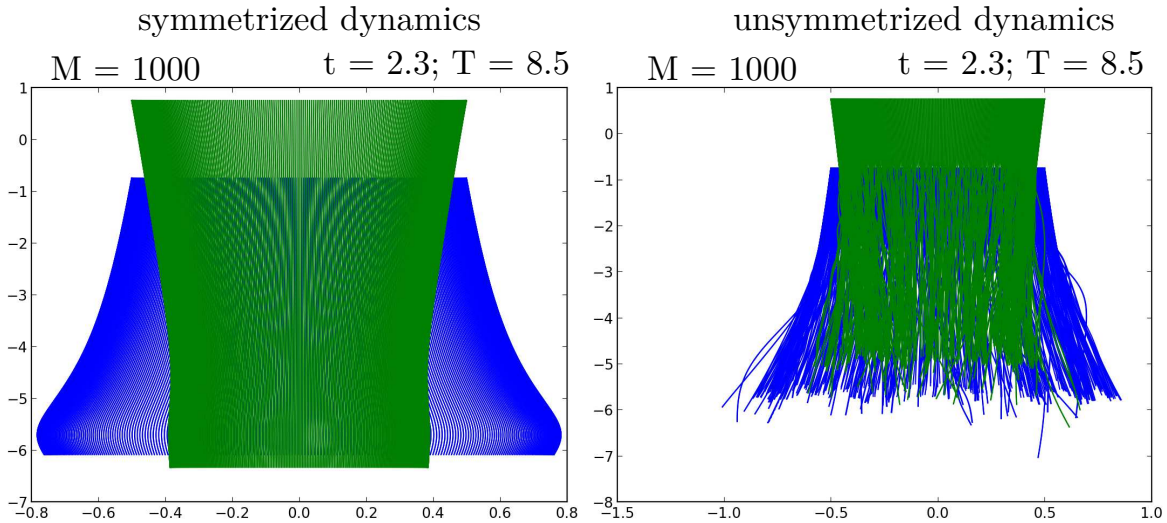

Figure 11: Comparison between trajectories in symmetrized (left column) and non-symmetrized (right) dynamics in the system of two rings. Plot for $M = 1000$ in reference frame moving down with settling velocity of an isolated particle, u_0. Trajectories are shown up to time $t = 2.3$ in order to show the process of destabilization. $C = 1.5$

In Fig.11 trajectories of particles in system of 2 rings are shown for $M = 1000$ particles. Let us remind that for $M = 256$ cluster breaks down after roughly quarter of the period (Fig. 9.1); here, in case of $M = 1000$ the destabilisation occurs almost immediately. As a result periodic motions could not be observed because destabilisation time is much shorter than $T/2$.

Results for the system of 4 rings are presented in Figures 12 and 13 for $M = 256$ and $M = 1024$, respectively. In all cases destabilisation time is shorter than the period. However, for $M = 256$, periodic motions can be observed at the beginning of

Figure 12: Comparison between trajectories in symmetrized (left column) and non-symmetrized (right) dynamics in the system of four rings. Plot for three periodic solutions for parameters $M = 256$ and $C = 1.5$, in laboratory reference frame moving down with settling velocity of an isolated particle, u_0.

simulations because decay of the cluster occurs after $T/4$ for first periodic solution and $T/3$ for second and third periodic solutions. For larger number of particles, $M = 1024$, cluster breaks up almost immediately.

Results presented here show that for larger number of particles it is difficult, or even
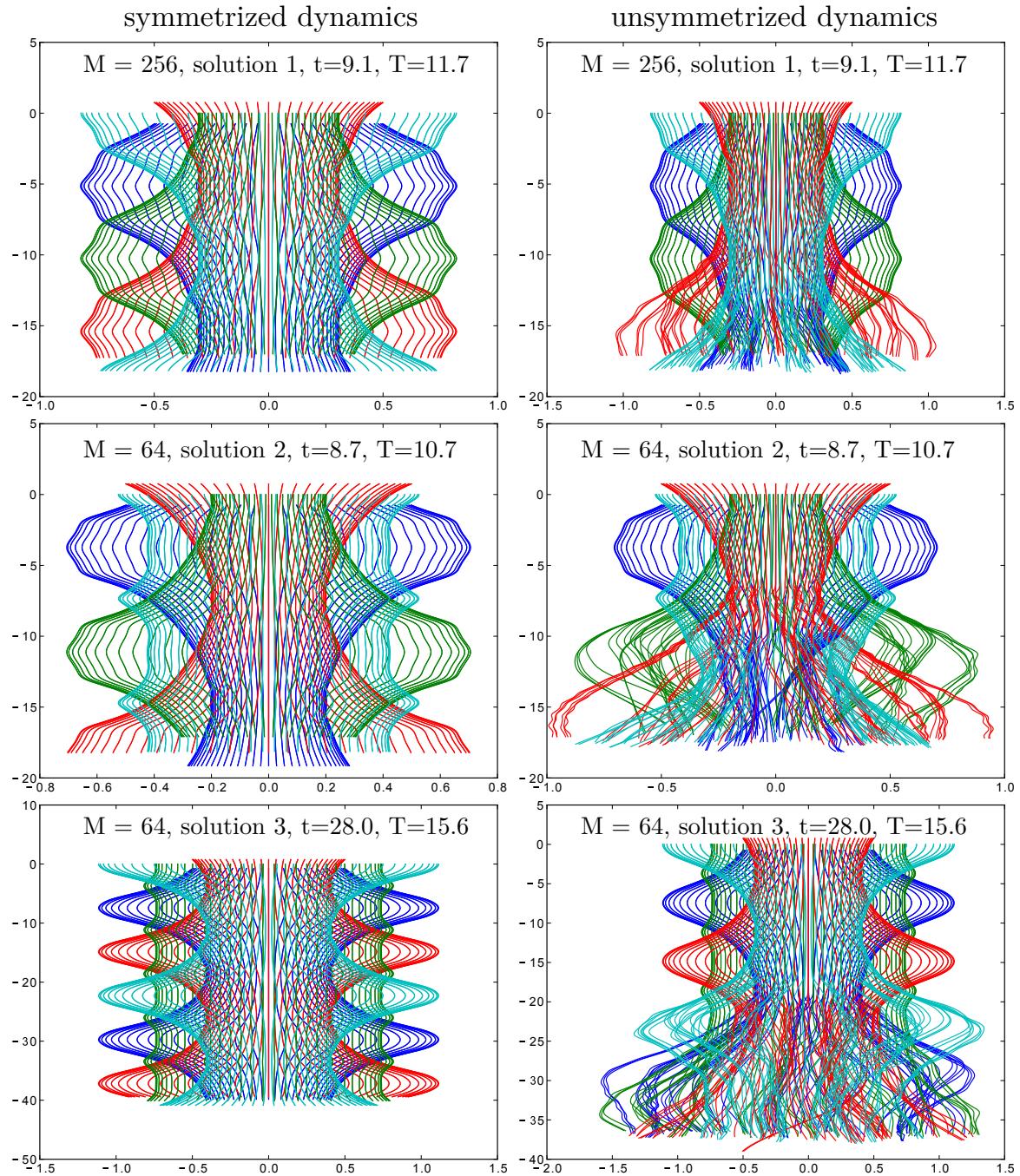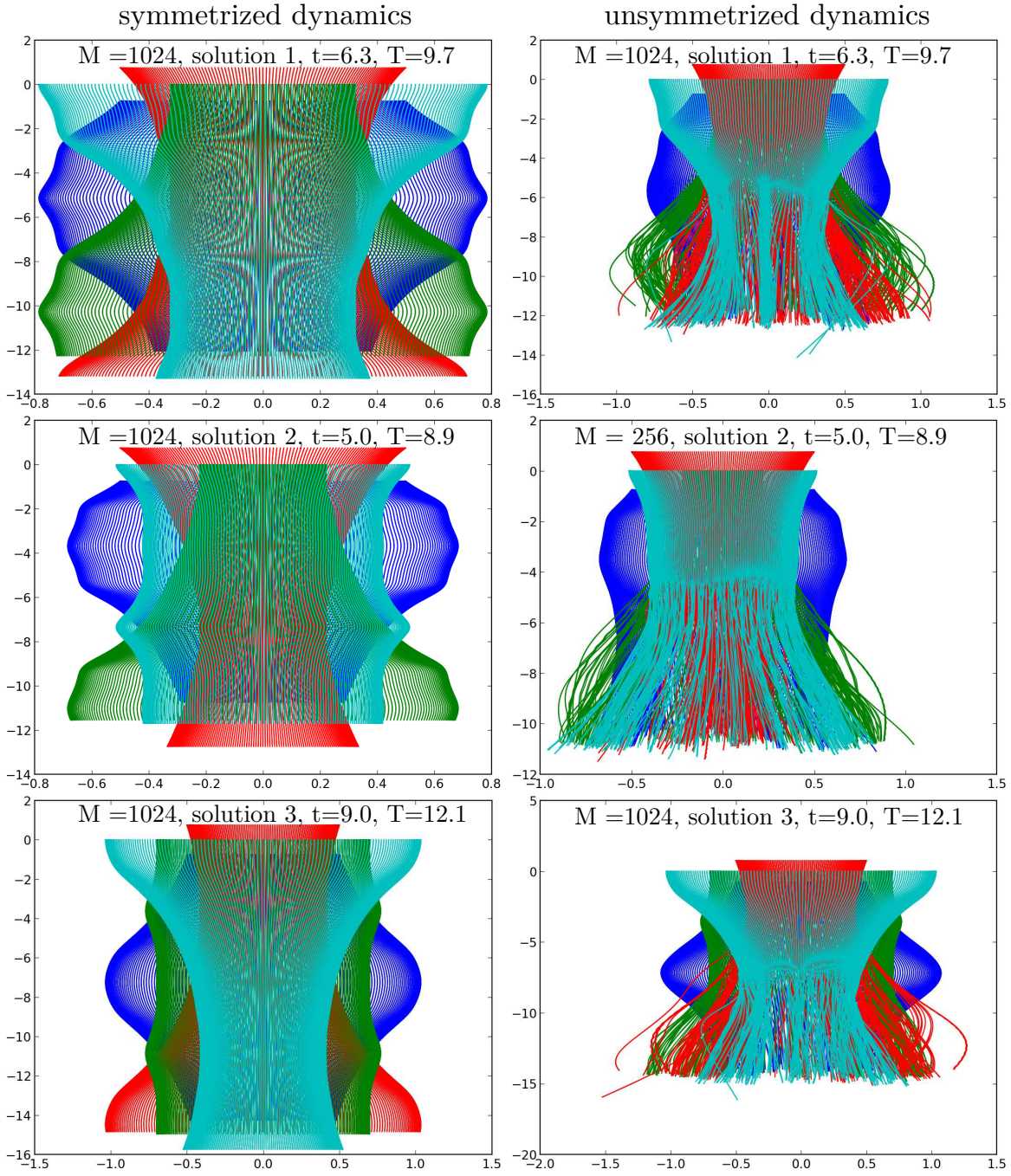
Figure 13: Comparison between trajectories in symmetrized (left column) and non-symmetrized (right) dynamics in the system of four rings. Plot for three periodic solutions for parameters $M = 1024$ and $C = 1.5$, in laboratory reference frame moving down with settling velocity of an isolated particle, u_0.

impossible, to observe periodic motions. This fact, alongside with longer computation time for non-symmetrized dynamics, was the reason for using symmetrized model in the main part of analysis presented in this dissertation. Apart from this observation it is visible that the system of 2 rings destabilises faster than system of 4 rings - similar

observation was made for smaller number of particles in Section 9.

Bibliography

[1] L. D. Landau and J. M. Lifszyc, *Hydrodynamika*. PWN, 2009.

[2] G. K. Batchelor, *An introduction to fluid dynamics*. Cambridge University Press, 2000.

[3] S. Kim and S. J. Karrila, *Microhydrodynamics: principles and selected applications*. Courier Corporation, 2013.

[4] M. Manga and H. Stone, "Interactions between bubbles in magmas and lavas: effects of bubble deformation," *Journal of Volcanology and Geothermal Research*, vol. 63, no. 3, pp. 267–279, 1994.

[5] M. Manga and H. Stone, "Collective hydrodynamics of deformable drops and bubbles in dilute low Reynolds number suspensions," *Journal of Fluid Mechanics*, vol. 300, pp. 231–263, 1995.

[6] J. Nowakowski and M. L. Ekiel-Jeżewska. (2014). Experiments with heavy particles in a viscous fluid: amazing oscillations. 67th Annual Meeting of the APS Division of Fluid Dynamics, Ed., [Online]. Available: `http://gfm.aps.org/meetings/dfd-2014/54174e7869702d585c240300`.

[7] S. Alabrudziński, M. L. Ekiel-Jeżewska, D. Chehata-Gómez, and T. A. Kowalewski, "Particle clusters settling under gravity in a viscous fluid," *Physics of Fluids (1994-present)*, vol. 21, no. 7, p. 073 302, 2009.

[8] H. N. Schulz and B. B. Jørgensen, "Big bacteria," *Annual Reviews in Microbiology*, vol. 55, no. 1, pp. 105–137, 2001.

[9] E. Lauga and T. R. Powers, "The hydrodynamics of swimming microorganisms," *Reports on Progress in Physics*, vol. 72, no. 9, p. 096 601, 2009.

[10] A. Grimm and H. Stark, "Hydrodynamic interactions enhance the performance of Brownian ratchets," *Soft Matter*, vol. 7, no. 7, pp. 3219–3227, 2011.

[11] T. Ando and J. Skolnick, "Crowding and hydrodynamic interactions likely dominate in vivo macromolecular motion," *Proceedings of the National Academy of Sciences*, vol. 107, no. 43, pp. 18 457–18 462, 2010.

[12] T. Frembgen-Kesner and A. H. Elcock, "Striking effects of hydrodynamic interactions on the simulated diffusion and folding of proteins," *Journal of chemical theory and computation*, vol. 5, no. 2, pp. 242–256, 2009.

[13] P. Szymczak and M. Cieplak, "Hydrodynamic effects in proteins," *Journal of Physics: Condensed Matter*, vol. 23, no. 3, p. 033 102, 2010.

[14] A. J. Ladd, "Sedimentation of homogeneous suspensions of non-Brownian spheres," *Physics of Fluids (1994-present)*, vol. 9, no. 3, pp. 491–499, 1997.

[15] E. Guazzelli and J. Hinch, "Fluctuations and instability in sedimentation," *Annual review of fluid mechanics*, vol. 43, pp. 97–116, 2011.

[16] F Bülow, H Nirschl, and W Dörfler, "On the settling behaviour of polydisperse particle clouds in viscous fluids," *European Journal of Mechanics-B/Fluids*, vol. 50, pp. 19–26, 2015.

[17] E. Boomsma and L. J. Pyrak-Nolte, "Particle swarms in fractures," *Fluid Dynamics in Complex Fractured-Porous Systems*, vol. 210, p. 65, 2015.

[18] T. L. Fabry, "Mechanism of erythrocyte aggregation and sedimentation," *Blood*, vol. 70, no. 5, pp. 1572–1576, 1987.

[19] M Hadjinicolaou, G Kamvyssas, and E Protopapas, "Stokes flow applied to the sedimentation of a red blood cell," *Quarterly of Applied Mathematics*, vol. 73, no. 3, pp. 511–523, 2015.

[20] M. Peltomäki and G. Gompper, "Sedimentation of single red blood cells," *Soft Matter*, vol. 9, no. 34, pp. 8346–8358, 2013.

[21] D. Legendre, J. Magnaudet, and G. Mougin, "Hydrodynamic interactions between two spherical bubbles rising side by side in a viscous liquid," *Journal of Fluid Mechanics*, vol. 497, pp. 133–166, 2003.

[22] M Hriberšek, B Žajdela, A Hribernik, and M Zadravec, "Experimental and numerical investigations of sedimentation of porous wastewater sludge flocs," *Water research*, vol. 45, no. 4, pp. 1729–1735, 2011.

[23] M. Bargieł and E. M. Tory, "A particle-based approach to sedimentation and fluidization," *Leading-Edge Applied Mathematical Modeling Research*, p. 19, 2008.

[24]   A. M. Laganapan, M. Mouas, A. Videcoq, M. Cerbelaud, M. Bienia, P. Bowen, and R. Ferrando, "How colloid–colloid interactions and hydrodynamic effects influence the percolation threshold: A simulation study in alumina suspensions," *Journal of colloid and interface science*, vol. 458, pp. 241–246, 2015.

[25]   J. Werth, M Linsenbühler, S. Dammer, Z Farkas, H Hinrichsen, K.-E. Wirth, and D. Wolf, "Agglomeration of charged nanopowders in suspensions," *Powder Technology*, vol. 133, no. 1, pp. 106–112, 2003.

[26]   U. H. Thygesen and T. Kiørboe, "Diffusive transport in Stokeslet flow and its application to plankton ecology," *Journal of mathematical biology*, vol. 53, no. 1, pp. 1–14, 2006.

[27]   K. Drescher, K. C. Leptos, I. Tuval, T. Ishikawa, T. J. Pedley, and R. E. Goldstein, "Dancing volvox: hydrodynamic bound states of swimming algae," *Physical Review Letters*, vol. 102, no. 16, p. 168 101, 2009.

[28]   R. E. Goldstein, "Green algae as model organisms for biological fluid dynamics," *Annual review of fluid mechanics*, vol. 47, p. 343, 2015.

[29]   E Mollo-Christensen, M. Chalufour, C. R. Conn, B. A. Egan, A. Pesetsky, and K. Smith, *Flow instabilities*. Encyclopaedia Britannica Educational Corporation, 1988.

[30]   J. Nitsche and G. Batchelor, "Break-up of a falling drop containing dispersed particles," *Journal of Fluid Mechanics*, vol. 340, pp. 161–175, 1997.

[31]   G. Machu, W. Meile, L. C. Nitsche, and U. Schaflinger, "Coalescence, torus formation and breakup of sedimenting drops: experiments and computer simulations," *Journal of Fluid Mechanics*, vol. 447, pp. 299–336, 2001.

[32]   M. Ekiel-Jeżewska, B Metzger, and E Guazzelli, "Spherical cloud of point particles falling in a viscous fluid," *Physics of Fluids (1994-present)*, vol. 18, no. 3, p. 038 104, 2006.

[33]   B. Metzger, M. Nicolas, and E. Guazzelli, "Falling clouds of particles in viscous fluids," *Journal of Fluid Mechanics*, vol. 580, pp. 283–301, 2007.

[34]   K. Jayaweera, B. Mason, and G. Slack, "The behaviour of clusters of spheres falling in a viscous fluid Part 1. Experiment," *Journal of Fluid Mechanics*, vol. 20, no. 01, pp. 121–128, 1964.

[35]   F. Pignatel, M. Nicolas, and E. Guazzelli, "A falling cloud of particles at a small but finite Reynolds number," *Journal of Fluid Mechanics*, vol. 671, pp. 34–51, 2011.

[36] Y. Rosenstein and A. M. Leshansky, "The Oseen problem for a finite collection of spheres settling in a viscous liquid," *European Journal of Mechanics-B/Fluids*, vol. 31, pp. 71–79, 2012.

[37] A. Myłyk, W. Meile, G. Brenn, and M. L. Ekiel-Jeżewska, "Break-up of suspension drops settling under gravity in a viscous fluid close to a vertical wall," *Physics of Fluids (1994-present)*, vol. 23, no. 6, p. 063 302, 2011.

[38] M. L. Ekiel-Jeżewska, "Class of periodic and quasiperiodic trajectories of particles settling under gravity in a viscous fluid," *Physical Review E*, vol. 90, no. 4, p. 043 007, 2014.

[39] I. M. Jánosi, T. Tél, D. E. Wolf, and J. A. Gallas, "Chaotic particle dynamics in viscous flows: The three-particle Stokeslet problem," *Physical Review E*, vol. 56, no. 3, p. 2858, 1997.

[40] M. Reichert and H. Stark, "Circling particles and drafting in optical vortices," *Journal of Physics: Condensed Matter*, vol. 16, no. 38, S4085, 2004.

[41] Y. Roichman, D. G. Grier, and G. Zaslavsky, "Anomalous collective dynamics in optically driven colloidal rings," *Physical Review E*, vol. 75, no. 2, p. 020 401, 2007.

[42] S. E. Spagnolie, *Flapping, ratcheting, bursting, and tumbling: A selection of problems in fluid-body interaction dynamics*. ProQuest, 2008.

[43] K. Sadlej, E. Wajnryb, and M. L. Ekiel-Jeżewska, "Hydrodynamic interactions suppress deformation of suspension drops in Poiseuille flow," *The Journal of chemical physics*, vol. 133, no. 5, p. 054 901, 2010.

[44] W. E. Uspal and P. S. Doyle, "Scattering and nonlinear bound states of hydrodynamically coupled particles in a narrow channel," *Physical Review E*, vol. 85, no. 1, p. 016 325, 2012.

[45] Y. Sassa, S. Shibata, Y. Iwashita, and Y. Kimura, "Hydrodynamically induced rhythmic motion of optically driven colloidal particles on a ring," *Physical Review E*, vol. 85, no. 6, p. 061 402, 2012.

[46] K. Thøgersen, M. Dabrowski, and A. Malthe-Sørenssen, "Transient cluster formation in sheared non-Brownian suspensions," *Physical Review E*, vol. 93, no. 2, p. 022 611, 2016.

[47] T Tél and H. Bai-Lin, "Directions in chaos," *Vol. 3World Scientific, Singapore*, pp. 149–211, 1990.

[48] G. B. Jeffery, "The motion of ellipsoidal particles immersed in a viscous fluid," in *Proceedings of the Royal Society of London A: Mathematical, Physical and Engineering Sciences*, The Royal Society, vol. 102, 1922, pp. 161–179.

[49] F. P. Bretherton, "The motion of rigid particles in a shear flow at low Reynolds number," *Journal of Fluid Mechanics*, vol. 14, no. 02, pp. 284–304, 1962.

[50] E. Hinch and L. Leal, "Rotation of small non-axisymmetric particles in a simple shear flow," *Journal of Fluid Mechanics*, vol. 92, no. 03, pp. 591–607, 1979.

[51] A. Yarin, O Gottlieb, and I. Roisman, "Chaotic rotation of triaxial ellipsoids in simple shear flow," *Journal of Fluid Mechanics*, vol. 340, pp. 83–100, 1997.

[52] J Einarsson, B. Mihiretie, A Laas, S Ankardal, J. Angilella, D Hanstorp, and B Mehlig, "Tumbling of asymmetric microrods in a microchannel flow," *Physics of Fluids (1994-present)*, vol. 28, no. 1, p. 013 302, 2016.

[53] J. Wang, E. J. Tozzi, M. D. Graham, and D. J. Klingenberg, "Flipping, scooping, and spinning: drift of rigid curved nonchiral fibers in simple shear flow," *Physics of Fluids (1994-present)*, vol. 24, no. 12, p. 123 304, 2012.

[54] E. S. Shaqfeh, "The dynamics of single-molecule dna in flow," *Journal of Non-Newtonian Fluid Mechanics*, vol. 130, no. 1, pp. 1–28, 2005.

[55] C. Aust, S. Hess, and M. Kröger, "Rotation and deformation of a finitely extendable flexible polymer molecule in a steady shear flow," *Macromolecules*, vol. 35, no. 22, pp. 8621–8630, 2002.

[56] K Sadlej, E Wajnryb, M. Ekiel-Jeżewska, D Lamparska, and T. Kowalewski, "Dynamics of nanofibres conveyed by low Reynolds number flow in a microchannel," *International Journal of Heat and Fluid Flow*, vol. 31, no. 6, pp. 996–1004, 2010.

[57] A. M. Słowicka, M. L. Ekiel-Jeżewska, K. Sadlej, and E. Wajnryb, "Dynamics of fibers in a wide microchannel," *The Journal of chemical physics*, vol. 136, no. 4, p. 044 904, 2012.

[58] A. M. Słowicka, E. Wajnryb, and M. L. Ekiel-Jeżewska, "Lateral migration of flexible fibers in Poiseuille flow between two parallel planar solid walls," *The European Physical Journal E*, vol. 36, no. 3, pp. 1–12, 2013.

[59] A. M. Słowicka, E. Wajnryb, and M. L. Ekiel-Jeżewska, "Dynamics of flexible fibers in shear flow," *The Journal of chemical physics*, vol. 143, no. 12, p. 124 904, 2015.

[60] D. Erickson and D. Li, "Integrated microfluidic devices," *Analytica Chimica Acta*, vol. 507, no. 1, pp. 11–26, 2004.

[61] P Sajeesh and A. K. Sen, "Particle separation and sorting in microfluidic devices: a review," *Microfluidics and nanofluidics*, vol. 17, no. 1, pp. 1–52, 2014.

[62] W. E. Uspal and P. S. Doyle, "Collective dynamics of small clusters of particles flowing in a quasi-two-dimensional microchannel," *Soft Matter*, vol. 8, no. 41, pp. 10 676–10 686, 2012.

[63] E. Lushi and P. M. Vlahovska, "Periodic and chaotic orbits of plane-confined micro-rotors in creeping flows," *Journal of Nonlinear Science*, vol. 25, no. 5, pp. 1111–1123, 2015.

[64] J. E. Davidheiser, P. Syers, P. Segrè, and E. R. Weeks, "Complex dynamics of three interacting spheres in a rotating drum," *Physics of Fluids (1994-present)*, vol. 22, no. 3, p. 033 305, 2010.

[65] V. Uskoković, "Theoretical and practical aspects of colloid science and self-assembly phenomena revisited," *Reviews in Chemical Engineering*, vol. 23, no. 5, pp. 301–372, 2007.

[66] Z. Nie, A. Petukhova, and E. Kumacheva, "Properties and emerging applications of self-assembled structures made from inorganic nanoparticles," *Nature nanotechnology*, vol. 5, no. 1, pp. 15–25, 2010.

[67] S. Whitelam, E. H. Feng, M. F. Hagan, and P. L. Geissler, "The role of collective motion in examples of coarsening and self-assembly," *Soft Matter*, vol. 5, no. 6, pp. 1251–1262, 2009.

[68] L. Hocking, "The behaviour of clusters of spheres falling in a viscous fluid Part 2. Slow motion theory," *Journal of Fluid Mechanics*, vol. 20, no. 01, pp. 129–139, 1964.

[69] R. E. Caflisch, C. Lim, J. H. Luke, and A. S. Sangani, "Periodic solutions for three sedimenting spheres," 1988.

[70] C. C. Lim and I.-H. McComb, "Stability of normal modes and subharmonic bifurcations in the 3-body Stokeslet problem," *Journal of differential equations*, vol. 121, no. 2, pp. 384–405, 1995.

[71] S. Alabrudziński, "Badania eksperymentalne i interpretacja teoretyczna bliskich oddziaływań hydrodynamicznych w układach wielociałowych w zakresie małych liczb Reynoldsa," PhD thesis, Politechnika Warszawska, 2006.

[72]   E. Tory, M. Kamel, and C. Tory, "Sedimentation of clusters of identical spheres iii. Periodic motion of four spheres," *Powder technology*, vol. 67, no. 1, pp. 71–82, 1991.

[73]   M. Bargieł, M. T. Kamel, and E. M. Tory, "Periodic motion of four spheres in a "kite" configuration," *Powder technology*, vol. 214, no. 1, pp. 14–20, 2011.

[74]   M. Bargieł and E. M. Tory, "Effect of higher-order and lubrication terms on the stability of polygonal arrangements of sedimenting spheres," *Powder Technology*, vol. 264, pp. 519–526, 2014.

[75]   I.-H. McCombtt and C. C. Limt, "Stability of equilibria for a class of time-reversible, d_n*o(2)-symmetric homogeneous vector fields," *SIAM journal on mathematical analysis*, vol. 24, no. 4, pp. 1009–1029, 1993.

[76]   L Durlofsky and J. Brady, "Analysis of the Brinkman equation as a model for flow in porous media," *Physics of Fluids*, vol. 30, no. 11, pp. 3329–3341, 1987.

[77]   S. Jung, S. Spagnolie, K Parikh, M Shelley, and A.-K. Tornberg, "Periodic sedimentation in a Stokesian fluid," *Physical Review E*, vol. 74, no. 3, p. 035 302, 2006.

[78]   M. Golubitsky, M. Krupa, and C. Lim, "Time-reversibility and particle sedimentation," *SIAM Journal on Applied Mathematics*, vol. 51, no. 1, pp. 49–72, 1991.

[79]   R. Phillips, J. Brady, and G Bossis, "Hydrodynamic transport properties of hard-sphere dispersions. ii. Porous media," *Physics of Fluids (1958-1988)*, vol. 31, no. 12, pp. 3473–3479, 1988.

[80]   S. Schwarzer, "Sedimentation and flow through porous media: Simulating dynamically coupled discrete and continuum phases," *Physical Review E*, vol. 52, no. 6, p. 6461, 1995.

[81]   B. Cichocki and M. L. Ekiel-Jeżewska, "Self-diffusion of a sphere in an effective medium of rods," *The Journal of chemical physics*, vol. 130, no. 21, p. 214 902, 2009.

[82]   M. Sahimi and A. Imdakm, "Hydrodynamics of particulate motion in porous media," *Physical review letters*, vol. 66, no. 9, p. 1169, 1991.

[83]   R. Cortez, B. Cummins, K. Leiderman, and D. Varela, "Computation of three-dimensional Brinkman flows using regularized methods," *Journal of Computational Physics*, vol. 229, no. 20, pp. 7609–7624, 2010.

[84] K. Leiderman and S. D. Olson, "Swimming in a two-dimensional Brinkman fluid: Computational modeling and regularized solutions," *Physics of Fluids (1994-present)*, vol. 28, no. 2, p. 021 902, 2016.

[85] H. Brinkman, "Calculations on the flow of heterogeneous mixtures through porous media," *Applied Scientific Research*, vol. 1, no. 1, pp. 333–346, 1949.

[86] M. Gruca, M. Bukowicki, and M. L. Ekiel-Jeżewska, "Periodic and quasiperiodic motions of many particles falling in a viscous fluid," *Physical Review E*, vol. 92, no. 2, p. 023 026, 2015.

[87] B. Felderhof, "Many-body hydrodynamic interactions in suspensions," *Physica A: Statistical Mechanics and its Applications*, vol. 151, no. 1, pp. 1–16, 1988.

[88] B Cichocki, B. Felderhof, K Hinsen, E Wajnryb, J Bl, *et al.*, "Friction and mobility of many spheres in Stokes flow," *The Journal of chemical physics*, vol. 100, no. 5, pp. 3780–3790, 1994.

[89] B Cichocki, M. Ekiel-Jeżewska, and E Wajnryb, "Lubrication corrections for three-particle contribution to short-time self-diffusion coefficients in colloidal dispersions," *The Journal of chemical physics*, vol. 111, no. 7, pp. 3265–3273, 1999.

[90] A. J. Ladd, "Hydrodynamic transport coefficients of random dispersions of hard spheres," *The Journal of Chemical Physics*, vol. 93, no. 5, pp. 3484–3494, 1990.

[91] M. Ekiel-Jeżewska and E Wajnryb, "Precise multipole method for calculating hydrodynamic interactions between spherical particles in the Stokes flow," *Theoretical Methods for Micro Scale Viscous Flows*, pp. 127–172, 2009.

[92] J. Rotne and S. Prager, "Variational treatment of hydrodynamic interaction in polymers," *The Journal of Chemical Physics*, vol. 50, no. 11, pp. 4831–4837, 1969.

[93] M. L. Ekiel-Jeżewska and E. Wajnryb, "Hydrodynamic orienting of asymmetric microobjects under gravity," *Journal of Physics: Condensed Matter*, vol. 21, no. 20, p. 204 102, 2009.

[94] M. L. Ekiel-Jeżewska, T. Gubiec, and P Szymczak, "Stokesian dynamics of close particles," *Physics of Fluids (1994-present)*, vol. 20, no. 6, p. 063 102, 2008.

[95] M. L. Ekiel-Jeżewska and E. Wajnryb, "Equilibria for the relative motion of three heavy spheres in Stokes fluid flow," *Physical Review E*, vol. 73, no. 4, p. 046 309, 2006.

[96]   C.-M. Tchen, "Motion of small particles in skew shape suspended in a viscous liquid," *Journal of Applied Physics*, vol. 25, no. 4, pp. 463–473, 1954.

[97]   Z. Adamczyk, K. Sadlej, E. Wajnryb, M. L. Ekiel-Jeżewska, and P. Warszyński, "Hydrodynamic radii and diffusion coefficients of particle aggregates derived from the bead model," *Journal of colloid and interface science*, vol. 347, no. 2, pp. 192–201, 2010.

[98]   M. L. Ekiel-Jeżewska and E. Wajnryb, "Lifetime of a cluster of spheres settling under gravity in Stokes flow," *Physical Review E*, vol. 83, no. 6, p. 067 301, 2011.

[99]   M. Müller, *Information retrieval for music and motion*. Springer, 2007, vol. 2.

[100] B. Lin and J. Su, "One way distance: For shape based similarity search of moving object trajectories," *Geoinformatica*, vol. 12, no. 2, pp. 117–142, 2008.

[101] A. J. Ladd, "Hydrodynamic interactions in a suspension of spherical particles," *The Journal of chemical physics*, vol. 88, no. 8, pp. 5051–5063, 1988.

[102] L. Durlofsky, J. F. Brady, and G. Bossis, "Dynamic simulation of hydrodynamically interacting particles," *Journal of fluid mechanics*, vol. 180, pp. 21–49, 1987.

[103] E. M. Tory and M. T. Kamel, "A note on the periodic motion of four spheres," *Powder technology*, vol. 73, no. 1, pp. 95–96, 1992.

[104] M. Kamel and E. Tory, "Sedimentation of clusters of identical spheres ii. periodic motion of three spheres," *Powder technology*, vol. 63, no. 2, pp. 187–195, 1990.

[105] M. Ekiel-Jezewska, "Periodic orbits of Stokesian dynamics," in *CDROM Proceedings of the XXII International Congress of Theoretical and Applied Mechanics, edited by J. Denier, MD Find and T. Mattner*, 2008.

[106] M. Bukowicki, M. Gruca, and M. L. Ekiel-Jeżewska, "Dynamics of elastic dumbbells sedimenting in a viscous fluid: oscillations and hydrodynamic repulsion," *Journal of Fluid Mechanics*, vol. 767, pp. 95–108, 2015.